CCMS-85-10
VPI-E-85-21

VIRGINIA TECH

CENTER FOR COMPOSITE MATERIALS AND STRUCTURES

Thermoplastic Matrix Composite Processing Model

Philip H. Dara
Alfred C. Loos

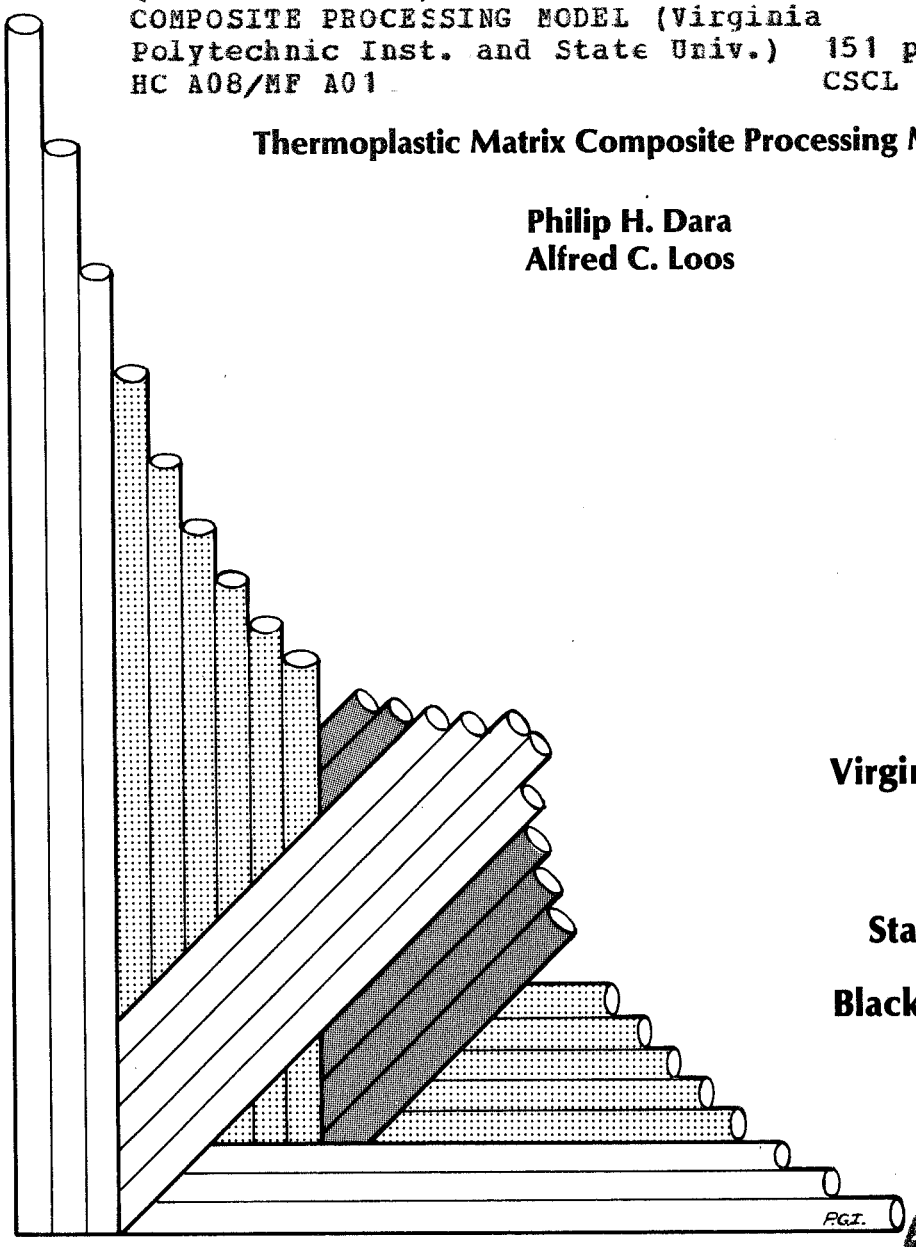

Virginia Polytechnic Institute and State University

Blacksburg, Virginia 24061

College of Engineering
Virginia Polytechnic Institute and State University
Blacksburg, Virginia 24061

CCMS-85-10
VPI-E-85-21

September 1985

Thermoplastic Matrix Composite Processing Model

Philip H. Dara[1]

Alfred C. Loos[2]

Department of Engineering Science & Mechanics

Interim Report 57
The NASA-Virginia Tech Composites Program
NASA Cooperative Agreement NAG-1-343

Prepared for: W. T. Freeman, Jr.
Polymeric Materials Branch
National Aeronautics and Space Administration
Langley Research Center
Hampton, VA 23665

[1]Graduate Student, Department of Engineering Science & Mechanics

[2]Assistant Professor, Department of Engineering Science & Mechanics

THERMOPLASTIC MATRIX COMPOSITE PROCESSING MODEL

(ABSTRACT)

The effects the processing parameters pressure, temperature, and time have on the quality of continuous graphite fiber (AS4) reinforced thermoplastic matrix (UDEL® P1700) composites have been quantitatively accessed by defining the extent to which intimate contact and bond formation has occurred at successive ply interfaces. Two models are presented predicting the extents to which the ply interfaces have achieved intimate contact and cohesive strength. The models are based on experimental observation of compression molded laminates and neat resin conditions, respectively. Identified as the mechanism explaining the phenomenon by which the plies bond to themselves is the theory of autohesion (or self diffusion). Theoretical predictions from the "Reptation Theory" between autohesive strength and contact time are used to explain the effects of the processing parameters on the observed experimental strengths. The application of a time-temperature relationship, in the WLF manner, for autohesive strength predictions is evaluated. A viscoelastic compression molding model of a tow was developed to explain the phenomenon by which the prepreg ply interfaces develop intimate contact. The intimate contact model contains sub-models defining the degree of nonuniformity of tow heights across the width of a prepreg, viscoelastic mechanics model simulating the response of tows to a compressive load, and an empirical relationship of the influence of fibers on the neat resin viscosity.

Acknowledgements

The authors would like to express thanks for support of this work from the NASA-Virginia Tech Composites Program through NASA Grant NAG1-343, and the faculty and students of the program.

Table of Contents

Table of Contents (continued)

Table of Contents (continued)

List of Figures

List of Figures (continued)

List of Figures (continued)

List of Figures (continued)

List of Tables

1.0 Introduction

Increased damage tolerance and decreased cost are the main drivers behind the interest in development of thermoplastic matrix composites over thermosetting matrix composites. However, currently, no processing theory exists that would assure the quality of a composite for a given set of the processing parameters pressure, temperature, and time. To eliminate the trial and error approach taken to date, this study attempts to; 1) understand the phenomena occurring during processing; 2) identify the mechanisms explaining the phenomena; and 3) relate the processing parameters with the mechanisms to define the state of some properties that define a known quality.

The type of thermoplastic matrix composite under study was made of a prepreg material composed of a thermoplastic resin (matrix material) reinforced with a high percentage of continuous unidirectional fibers. The methods commonly used to process the prepreg material into a composite uses either a matched metal die press or an autoclave. In both methods the prepreg sheets are orientated, shaped, and processed under an applied pressure and elevated temperature condition for a given length of time, called the processing cycle. The applied pressure is the driving force causing the prepreg ply interfaces to coalesce. The elevated temperature controls the rate at which the ply interfaces bond together by influencing the mobility of the molecular chains of the polymer. The molecular chain mobility influences the material properties of viscosity and self diffusion. The magnitude of the applied

temperatures and pressures significantly affect the performance of the finished part.

In the making of prepregs, a solvent must be introduced to the thermoplastic matrix material to allow the resin to wet out the fibers. In general, the lowest attainable thermoplastic viscosity (> 10^4 poise), already exceeds the gel point of an epoxy resin (i.e. gel point is where epoxy resin solidifies). The lower viscosity allows the fibers to be thoroughly wetted with resin and evenly distributed. However, the solvent must be bled from the prepreg prior to processing so that good mechanical properties can be attained.

The motivation for using thermoplastic matrix composites in lieu of thermosetting matrix composites is the potential for increasing the toughness of composites in order to improve damage tolerance, and for lowering the fabrication cost by reducing processing time and allowing for high speed production. Other advantages are: its abilities to be postformed and reformed making use of metal forming techniques; reduced storage cost by eliminating refrigeration; reduced scrappage; and it is easily weldable and repairable. The interested reader is referred to the industrial reports listed as references 1-5.

The motivation for studying thermoplastic matrix composites is the desire to define a processing state (i.e. interfacial contact area, degree of cure for thermosets, etc.) through the processing parameters pressure, P, temperature, T, and time, t, from a scientific approach and not the presently used empirical method. At the present time no model exists that relates the interfacial bonding, and

interfacial deformation phenomena that occur during processing of thermoplastic matrix composites. In an analogous fashion just as the steam tables are to the thermodynamicist, so should the thermoplastic matrix composite model be to the processing engineer (i.e. given any two processing parameters (P, T, t) the third parameter is automatically defined, as well as, all the processing states.)

In studying the processing of UDEL® P1700 Polysulphone/AS4 graphite fiber thermoplastic matrix composites, one must address four problem areas: 1) the solvent removal from the matrix material, 2) the strength of the fiber/matrix interface, 3) the bonding (consolidation) of the ply interfaces to one another, and 4) the formation of intimate contact (coalescence) at the laminate ply interfaces. The last two problem areas are addressed in this study.

The third problem mentioned, the bonding of ply interfaces to one another, is addressed in Section 2.0. The phenomenon was identified as autohesive bonding. The mechanism describing the autohesive phenonenon has been described by the "Reptation Theory" where molecular chain movement across the ply interface was related to time, depth of chain penetration, and resulting bond strength. An experimental investigation of neat resin interfacial strength was undertaken at temperature conditions above the glass transition temperature of the resin (Tg = 194°C (381.2°F)). Several interesting results occur as a result of performing strength tests at the elevated temperatures differing from most other studies.

The fourth problem, the formation of intimate contact at the laminate ply interfaces, is addressed in Section 3.0. A time

dependent model was formulated that simulates the viscoelastic response of a fiber bundle impregnated with resin (i.e. tow) subjected to uniform compressive loading normal to the top and bottom surfaces. This model was used as the basis for describing the flattening of nonuniform tow height distributions across the width of a prepreg. The model combines the viscoelastic properties of the fiber reinforced resin, the distribution of tow height nonuniformity, and the processing parameters pressure, temperature, and time to describe the degree of intimate contact. The model was verified experimentally, where $[0, 90, 0]_T$ cross-ply laminates were processed under several processing conditions and ultrasonically C-scanned for presence of spacial gaps at the two-ply interfaces.

In Section 4.0 an overall thermoplastic processing model is constructed by combining the autohesion model of Section 2.0 with the Intimate Contact model of Section 3.0.

Lastly, Section 5.0 presents the conclusions and recommendations for further study.

2.0 AUTOHESION-Au

2.1 Introduction-Au

In studying the processing of thermoplastic matrix composites it has been observed that individual prepreg plies consolidate into a laminate by bonding themselves to one another at the interfaces. The bond strength for thermoplastic matrix composites has been shown to be dependent upon the processing parameters pressure (P), temperature (T), and contact time (t_c). The degree at which bond formation has occurred at the interface, as a function of the processing parameters, is the subject of this section of the report. Thus, this study addresses only the neat resin at the interface in which bond formation occurs. It is assumed that strong bond formations on the neat resin will result in strong bond formations at the interface of a composite.

Before the bonding of the ply interfaces can be modelled, the mechanism explaining the phenomenon must be identified. A special type of bonding, called autohesion, has been identified as the mechanism by which neat thermoplastic resins bond to themselves.

Autohesion, or self diffusion, is the type of adhesion used to explain the phenomenon high polymers possess when two surfaces of the same material are placed in contact with each other, resulting in the formation of a strong bond at the interface [6]. The term self-diffusion implies the time dependency of the bond formation process and its eventual asymptotic convergence to some final state of bond strength. A requirement for autohesion is that the materials placed in contact be similar.

Autohesion is distinguishable from adhesion in that autohesive bond strength is the result of diffused chain segments across the interface. In the case of adhesion, bond strength is due to the chemical bonding of two dissimilar materials present at the interface (i.e. metal to high polymer.) Also, thermoplastic matrix composites distinguish themselves from thermosetting matrix composites in the manner by which the plies consolidate, even though the materials at the interface in both cases are identical (i.e. polysulfone/polysulfone and epoxy/epoxy, respectively.) Thermoplastic matrix composites rely strictly on the strong autohesive properties of the neat resin to consolidate the plies. Thermosetting matrix composites rely on the polymerization of the neat resin to bond the plies and not on its weaker autohesive strength properties.

It has largely been accepted in the field that the mechanism by which autohesion occurs is attributed to two characteristics of high polymers: 1) a random chain network consisting of entanglements, and 2) flexible macromolecules able to move within the bulk polymer [6].

Schematically outlined in Fig. 2.1 is the autohesion phenomenon for an amorphous polymer above its glass transition temperature, T_g. At the initial contact (Fig. 2.1a) of the two surfaces, localized deformation occurs so that macroscopic fitting of the surfaces takes place. At some intermediate time (Fig. 2.1b) partial diffusion has occurred across the interface. This is due to free chain movement, resulting from the increased molecular free volume at temperatures above the T_g. This is the stage at which the increased penetration depth of the diffusing chain occurs, resulting in increased

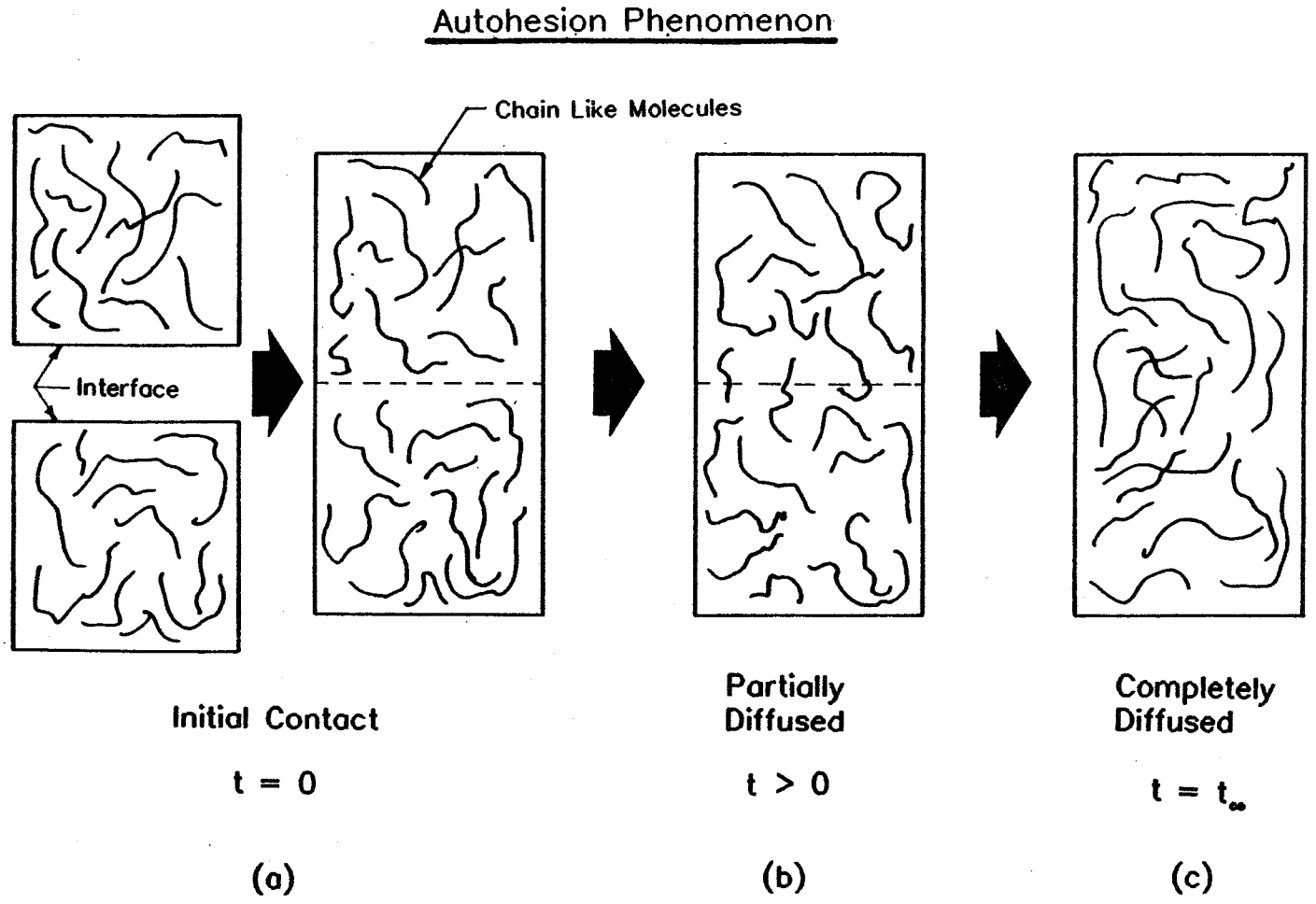

Figure 2.1 Physical Picture of Autohesion Phenomenon

entanglements, causing increased bond strength. At long contact times (Fig. 2.1c) the interfacial diffusion process has been completed and the interface can no longer be distinguished from the bulk material [7].

Experimental evidence has shown that autohesion is largely a time and temperature dependent problem. This is due to the diffusive and viscoelastic nature of the material. Also, the pressure required to achieve good contact at the interface of the neat resin is very much less than the pressure needed to process a fiber reinforced thermoplastic matrix composite. This is because macroscopic fitting of the smooth neat resin surfaces in the study of autohesion requires pressures much less than the pressures required to deform irregular fiber reinforced resin surfaces.

Two major approaches for quantifying the autohesion phenomenon have been cited in the literature: 1) mechanical strength testing of the polymer's interface, and 2) radioactive doping of the polymer chains and measurement of the rate at which the tracer progresses through the polymer. The present study of the autohesive bond formation made use of the mechanical strength approach.

The mechanical strength approach assumes a definite correlation exists between the contact (entanglement) time to form the bond and the disentanglement period required to cause failure. The entanglement process is the time required for molecular entanglements to form through increased penetration of diffused chain lengths across the interface. The disentanglement process is the time span during which the interface is loaded until failure. The failure mechanism

can either be chain pull-out or chain fracture depending upon the depth of penetration of molecular chains and the molecular free volume. Strain rate effects must be accounted for when comparing the absolute values of the autohesive strengths above the glass transition temperature because of the viscoelastic nature of the material.

2.2 Literature Review-Au

2.2.1 Mechanism Explaining the Autohesion Phenomenon

Molecular Dynamics of Random-Coil Chains

The "reptation theory" of Pierre-Gilles de Gennes [8,9] has been used to model the motions of individual linear random-coil chains in amorphous solid state bulk materials. The major points of the theory will be presented here. Wool gives a good summary of the reptation theory [10].

The premise of the reptation model is that the chain-like molecules can change shape and move, but cannot intersect each other. Thus, the chain is confined to an imaginary tube within which all motion takes place (Fig. 2.2a). The tube represents the constraints imposed by adjacent macromolecules preventing transverse motion. The chain moves in a snake-like motion within this tube but cannot go outside the tube boundary except at the ends. The local snake-like motion causes the molecular chain to slip out of the original tube over a period of time. Simultaneously, as the original tube length decreases a new tube of equal length is being formed.

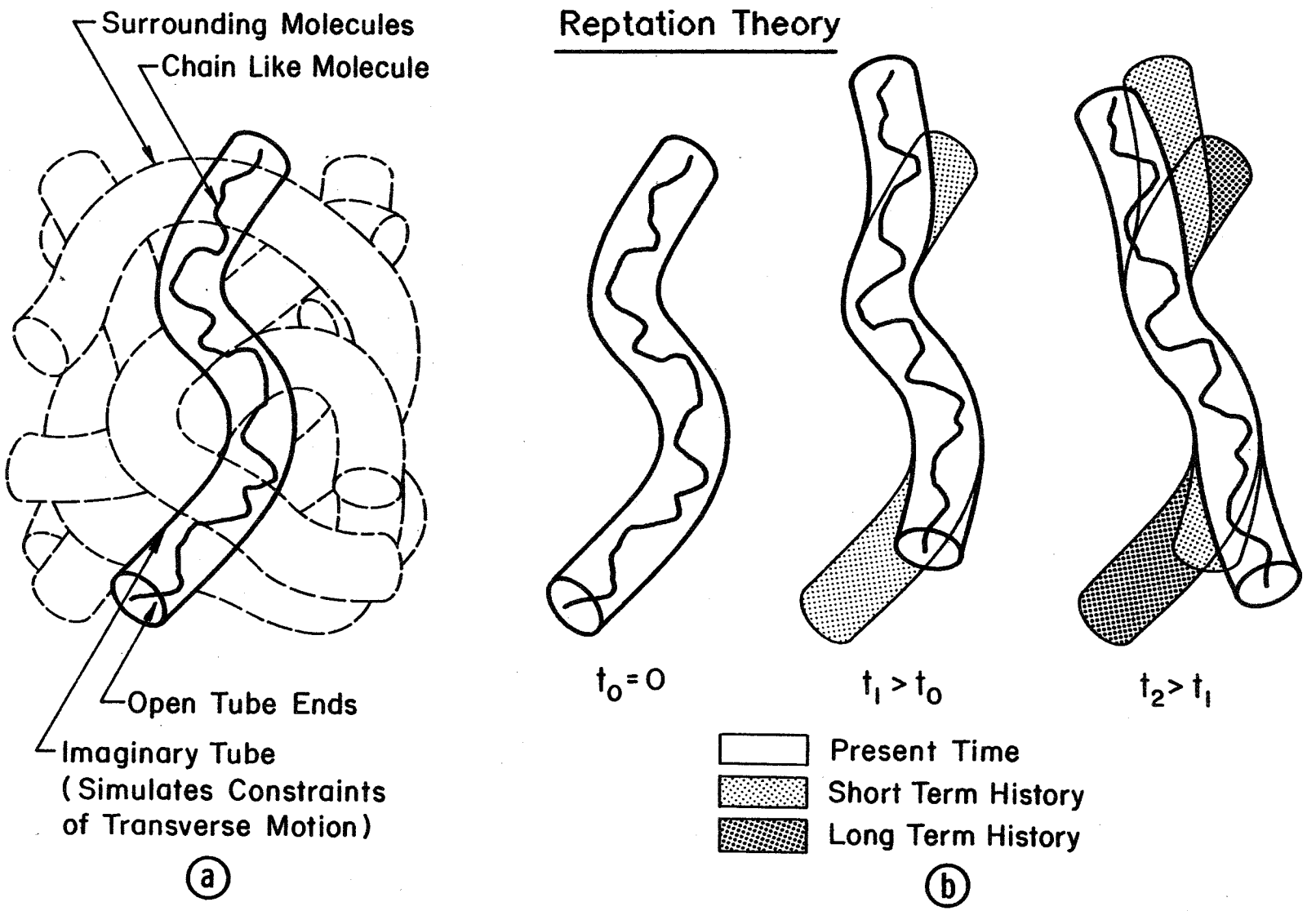

Figure 2.2 Reptation Model

Figure 2.2b schematically shows the transition from snake-like motion to macroscopic motion. It is this snake-like motion back and forth in the tube, coupled with the gradual loss of memory, that allows for the formation of new tube orientations and macromolecular motion. This apparent loss of memory by the polymer is characteristic of high polymers due to the viscoelastic nature of the material. Considering long time intervals, the details of the snake-like motion may be ignored and a macroscopic viewpoint may be taken. This macroscopic viewpoint entails the movement of the chain as a whole [8]. This macromolecular motion acts initially at the chain's ends and works towards the center of mass of the original chain where some memory has still been maintained [11].

With this physical model, de Gennes formulated relationships between chain length, chain-tube mobility, chain length diffused, and time. Of major importance in the study of autohesion is the relationship shown in Eq 2.1 between the 'random walk' (i.e. mean square path (< >)) of the chain length diffused $<\ell^2>$ and the depth of the resulting penetration of chain lengths across a plane within the bulk material $<\chi^2>$.

$$<\ell^2>^{1/2} \sim <\chi^2> \qquad (2.1)$$

Equation 2.1 describes the random progress of the chain's uncertain path to that resulting in a preferred direction on the average of many chains.

The relationship between χ and time (t) via a double random walk

process as proposed by de Gennes becomes:

$$x \sim t^{1/4} \qquad (2.2)$$

Where the introduction of time is made through the application of Einstein's diffusion equation $\langle \ell^2 \rangle = 2Dt$ to the motion of the chain within the tube, where D is the microscopic diffusion coefficient.

These relationships describing the polymer's chain motions in an entangled melt are the basis of Wool's [12] and Jud's [13] work addressing crack healing and welding of polymers.

Presented in the next section are the testing methods used by Wool and Jud for quantifying autohesion along with their extensions of the reptation model for autohesive strength predictions.

2.2.2 Experiment/Theory for Quantifying Autohesion

Several mechanical strength approaches for quantifying autohesion are presented here. Compact tension tests (CT) of thick films were used to study the welding time and crack healing times of like polymers. Peel and double cantilever beam tests were also used to study crack healing of like polymers. Wool et. al. [11] carried out welding and crack healing studies. Studies were carried out on neat resin, as well as continuous and short fiber reinforced resin coupons. No remarks concerning the influences of the reinforcement on autohesive strength were reported.

Jud et. al. [13] studied the autohesive strength properties through the use of the compact tension test. Razor edge cracks were

introduced into the exposed edges. The sample was then fractured in a tensile machine at room temperature. Smooth, clean fractured surfaces resulted. The fractured specimens were put back together under a light compression to assure good contact. The temperature of the sample was then raised above the T_g for the desired length of contacting time and then cooled to room temperature. The sample was then fractured again. The peak load at fracture defined the fracture toughness K_{Ic} (or autohesive strength (Au) [11]) resulting from the temperature and contact time conditions during autohesion. Jud [13] used the above CT test in the studying of welding. Smooth virgin surfaces were brought into contact at a given temperature (> glass transition temperature) and contact time in order for autohesion to occur. The sample was then returned to room temperature, notched with a razor's edge, and tested until fracture.

The theory presented by Jud relates a diffusion model similar to the reptation theory of de Gennes, where the number of physical links per unit area is proportional to the average depth of penetration of molecules. Jud assumes that the strength is proportional to the number of links and that the Einstein diffusion equation holds true $\langle \ell^2 \rangle = 2Dt$. Jud has shown good agreement between experiment and theory.

Jud observed in both studies a linear relationship between fracture toughness and the fourth root of time, $(t_c^{1/4})$ and that specimens healed or welded at a higher temperature required less time to achieve the same toughness. Also, welded specimens with polished surfaces required longer contact times in order to attain a given

fracture toughness than those observed in the crack healing study, where fractured surfaces were healed as is. This was attributed to the different initial conditons of molecular chain orientations at the interface.

Wool et. al. [10,11,12] studied the autohesion phenomenon in a similar fashion to Jud and observed similar relationships between autohesive strength, contact time, and temperature. In addition to the compact tension test Wool also added the double cantilever beam and peel test. These tests were also conducted at room temperature conditions in similar fashion to the CT test described above.

Wool extended de Gennes' reptation theory of macromolecular motion within the bulk of the polymer to that of macromolecular motion across a polymer-polymer surface (Fig. 2.3). Thus, Wool assumes that the molecular chain entanglement density near and at the interface has the same influence on chain motion as does the bulk's entanglement density.

Wool asserts that the autohesive strength (Au) is proportional to the square root of the average interpenetration length ℓ shown in Eq 2.3 and proportional to the average interpenetration depth, χ, given in Eq 2.4 and defined in the reptation theory by de Gennes.

$$Au \sim \sqrt{\ell} \tag{2.3}$$

$$Au \sim \chi \tag{2.4}$$

With this assumption, Wool used a strain energy approach to

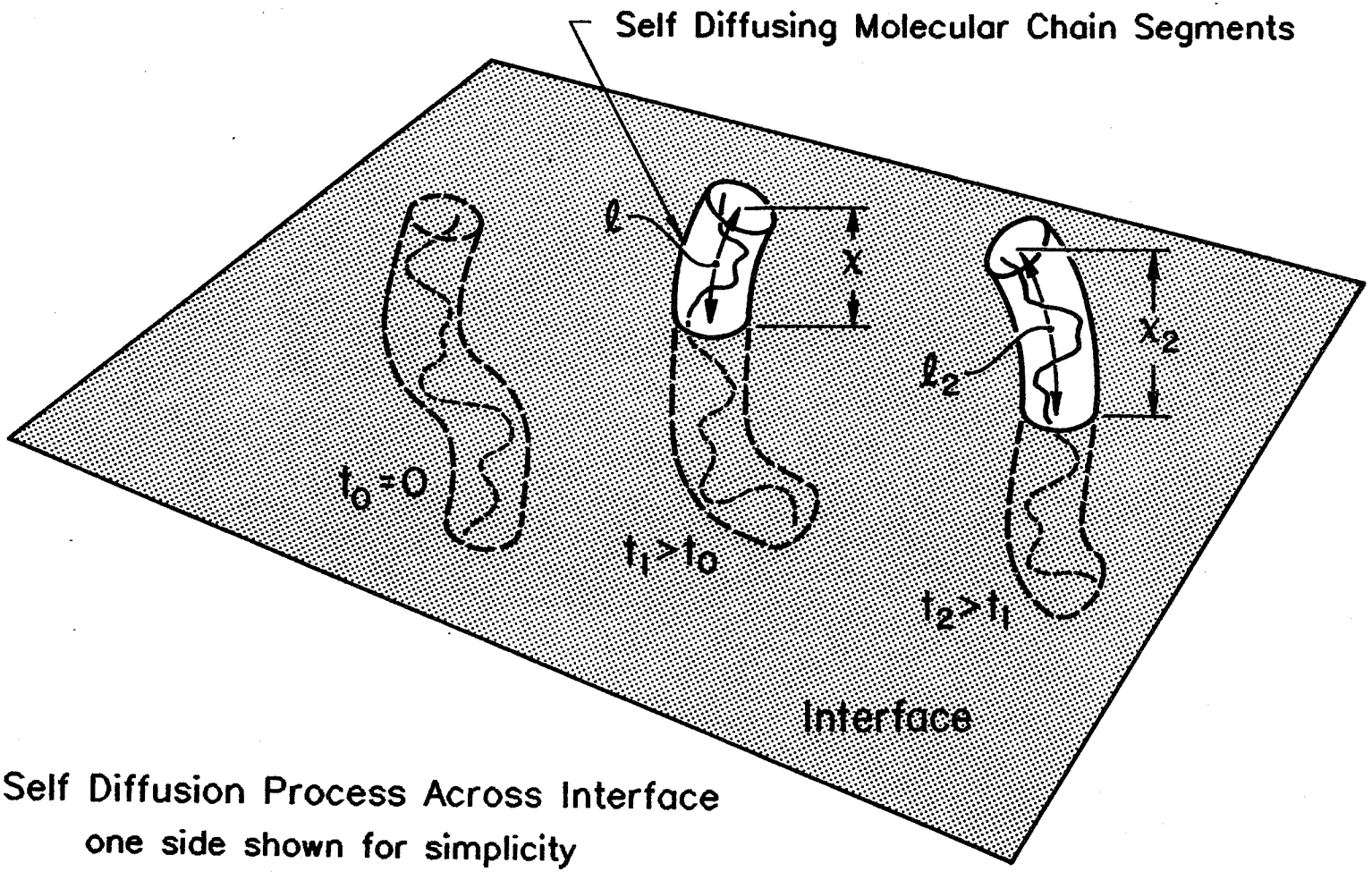

Figure 2.3 Reptation at an Interface

derive relationships between: 1) autohesive strength and contact time (Eq 2.5), 2) autohesive strength and strain rate for a chain pull-out failure mechanism (Eq 2.6), and 3) autohesive strength and strain rate for a chain fracture failure mechanism (Eq 2.7).

$$Au \sim t_c^{1/4} \tag{2.5}$$

$$Au \sim \dot{\varepsilon}^{1/2} \tag{2.6}$$

$$Au \sim \dot{\varepsilon}^{0} \tag{2.7}$$

These equations were also supported by experimental evidence [10-14]. The strain energy approach assumes a uniaxial stress is applied normal to the interface. A unit surface area contains a finite number of molecular chains intersecting the interface with various depths of penetration. The chain is assumed to be held within a tube by a molecular friction coefficient, resisting longitudinal loading (i.e. direction parallel to tube end.) The molecular friction coefficient similates the chain's entanglement with other chains. The stored strain energy resulting from a longitudinal load can either cause chain fracture or chain pull-out, depending upon the magnitude of the applied load, the strain rate, and the depth of the penetrating chains. Chain pull-out is favored for slow strain rates, high temperatures, short contact times, and shallow depths of penetration. As shown in Eq 2.5, Wool's study of polymer welding and crack healing predicts a linear relationship between Au and $t_c^{1/4}$ up to

the green strength (i.e. cohesive strength) after which the strength becomes independent of processing time. The green strength corresponds to that state within the polymer in which the interface has become indistinguishable from the surrounding bulk polymers. Wool assumes that the autohesive strength data approaches the green strength of the material linearly with the fourth root of time ($t_c^{1/4}$).

Wool [11] states that contact time-temperature relationships for the diffusion coefficients (D) may behave according to the theory of Williams, Landel, and Ferry (commonly referred to as WLF). Experimentally determined temperature-dependent self-diffusion coefficients become independent of strain rate provided the autohesive failure data results from chain pull-out and are normalized to the cohesive strength under identical temperature and strain rate conditions. This observation was supported by the following experimental work done by Hamed et. al. [15].

Hamed and Shieh [15] reported cohesive tear strength data versus peel rate at several constant temperatures above the Tg as shown in Fig. 2.4. The results support Wool's theoretical predictions of strain rate effects on autohesive strength for failure mechanisms of chain pull-out (Eq 2.6) and chain fracture (Eq 2.7). Three important observations of Fig. 2.4 are pointed out here which will be used in Section 2.4.1b. First, an increasing strain rate results in an increasing percentage (0 to 100%) of chain fracture failure, and that a decreasing strain rate results in an increasing percentage of chain pull-out failures. Second, at temperatures just above the T_g, chain

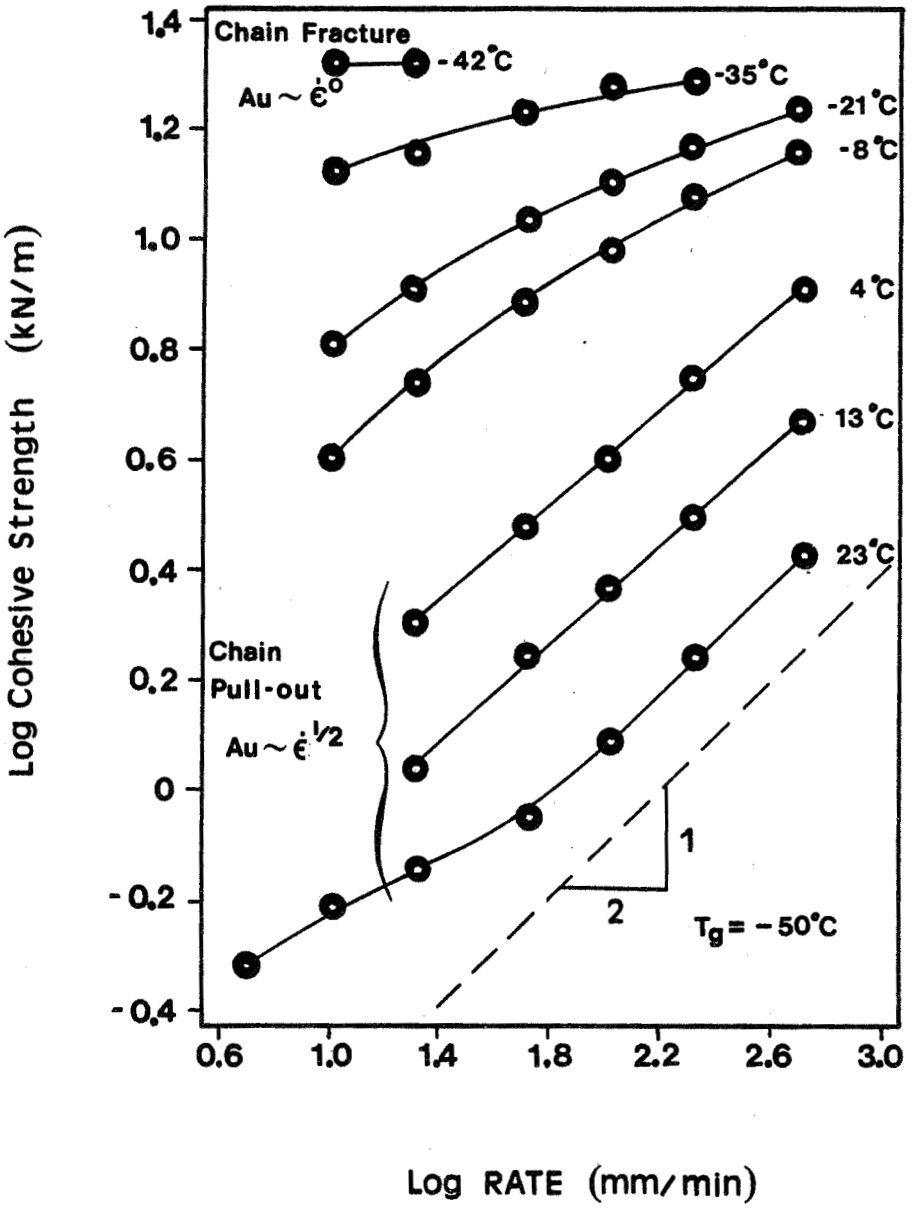

Figure 2.4 Cohesive Tear Strength as a Function of Pealing Rate at Several Constant Temperatures (Hamed and Shieh [15]). The dashed line shows a slope of 1/2 as predicted by Wool for chain pullout failure mechanism to occur [11]

failure due to fracture predominates over a large range of strain rates. Three, the curves exhibit a time-temperature relationship in a WLF manner for the disentanglement process.

The reason the above observations occur is that the molecular free volume increases with temperature; thus, shorter disentanglement times (i.e. faster strain rates) are required for chain fracture to occur at higher temperatures. Also, the slower the strain rate, the longer the time the chain entanglements have to untangle, and so the greater the occurrence of chain pull-out.

With these findings by Jud et al. and Wool et. al. a test program for quantifying autohesion for P1700 neat resin was undertaken with three goals: 1) to see if the linear relationship between Au and $t_c^{1/4}$ exists up to the cohesive strength of the material, 2) to reduce amount of scatter in the mechanical strength data as observed by Wool and Jud by conducting mechanical strength tests at the temperatures at which the autohesion phenomenon occurs, and 3) to determine if a contact time-temperature relationship for the diffusion coefficient exists in a WLF manner. The last goal would greatly reduce the number of tests by simulating the autohesion phenomenon at low temperatures above T_g requiring long contact times with the higher temperature test data requiring short contact times.

2.3 Experiment-Au

2.3.1 Description

Measuring the progress of the polymer's state of interfacial

diffusion has been qualitatively and quantitatively obtained using numerous approaches. Some of the strength approaches have been peel strength, tensile strength, and shear strength tests as reported in Section 2.2.2. The following experimental method for quantitatively assessing the effect of the processing parameters P, T, and t_c on autohesion is based on the premise that the distance of the diffused polymer chain across the interface is proportional to interfacial strength given in Eq 2.4. Processing is concerned with the time required to achieve a certain degree of autohesion D_{Au}, defined in Eq 2.8 as the ratio of the autohesive strength to cohesive strength.

$$D_{Au} = \frac{A_u(t_c,T)}{Au_\infty(t_\infty,T)} \tag{2.8}$$

Strength measurements were made on polysulfone (Union Carbide's UDEL® P1700) material. The measurements included the following: 1) effects of contact pressure on autohesion, 2) effects of material temperature on autohesion, and 3) the effects of contact time on autohesion. Table 2.1 lists the testing temperature and contact times during the autohesion phenomenon and the temperature conditions during the strength test.

To determine the degree of autohesive strength an interfacial tensile test approach at elevated processing temperatures above the T_g was used.

The reasons for the high temperature testing approach are threefold: 1) to reduce the inherent error caused by the temperature transitions of going from room temperature to processing temperature

Table 2.1 Autohesion Test Matrix

Autohesion Temperature °C/°F	t_c (sec)	Strength Test Temperature °C/°F
200/392	5.8	200/392
	12.5	
	15.5	
	30.1	
	45.0	
	60.0	
	90.0	
	120.0	
	180.0	
210/410	10.0	210/410
	29.0	
	52.0	
	210.0	
	363.0	
	720.0	
	1200.0	
220/428	10.0	220/428
	10.0	
	16.0	
	39.0	
	120.0	
	240.0	
	600.0	
230/446	6.7	230/446
	15.0	
	270.0	
	600.0	
240/464	10.6	240/464
	19.0	
	20.5	
	40.0	
	90.0	
	180.0	
	480.0	
	570.0	
250/482	8.0	250/482
	10.5	
	30.0	
	90.0	
260/500	6.0	260/500
	6.7	
	7.0	
	7.2	
	8.0	

and back down to room temperature for testing, 2) to devise a test method so that a standard test apparatus (Rheometrics System Four rheometer) common to most processing facilities could be used for evaluating autohesion properties, and 3) to evaluate the possibilites of expanding the data through time and temperature superposition.

As pointed out in Section 2.2.2 the failure mechanism is a function of both strain rate ($\dot{\varepsilon}$) and temperature. Thus, if high temperature testing is used, it becomes imperative that the failure mechanism be constant throughout the contacting time spectrum for each set of temperature data. It is also necessary that failure be due totally to chain pull-out throughout the temperature range for which time-temperature superposition is used [11]. The reason for these restrictions is that no additional influences caused by differences in the type of failure mechanism are allowed to affect the relationship between the failure load and the depth of penetrating chain lengths (i.e. testing/disentanglement time and contacting/entanglement time, respectively). The cause for a possible change in the failure mechanism is that as the penetrating chain length increases with increasing contacting time a higher probability of chain fracture results unless the disentanglement time (i.e. $\dot{\varepsilon}$) is sufficiently slow or temperature sufficiently high.

For the above reasons and the inability of the test apparatus to produce more than one strain rate, the useful temperature range is expected to have a lower bound above the T_g while the upper temperature is bounded by material limitations.

The evaulation of autohesion required the following capability:

1) an oven temperature range of 200 - 260°C (392-500°F),

2) a constant cross-head rate, and

3) monitoring of compressive and tensile loads as a function of time

The Rheometrics System Four rheometer (used for obtaining shear viscosity data for non-Newtonian fluids) meets the above requirements. The oven, servo motors and test fixtures (parallel plates) designed primarily for shearing flows are versatile enough to be used for the autohesion experiment. The instrument is very accurate in monitoring temperature, compressive and tensile normal loads, and is capable of storing data as a function of time. However, limitations of the test rig are having only one crosshead speed (2.2 mm/min. (.0215 in./min.)), and a maximum normal load capacity of 1000 grams.

A picture of the Rheometrics System Four is shown in Fig. 2.5 along with a close-up detailing the transducer and test fixture in Fig. 2.6.

2.3.2 Sample Preparation

Test samples were prepared in the following manner:

1) starting with UDEL® P1700 in bead form, beads were placed between .0762 mm (0.003 inch) thick Kapton films in a mold cavity with shims set at the desired specimen thickness, (Figure 2.7)

2) the mold was placed in a vacuum oven with enough dead load to assure adequate flow of beads during melt,

3) heat mold to 220°C (428°F) (T_g = 194°C (382°F)) while under a vacuum (heating above the T_g was required to ensure flow, and use of

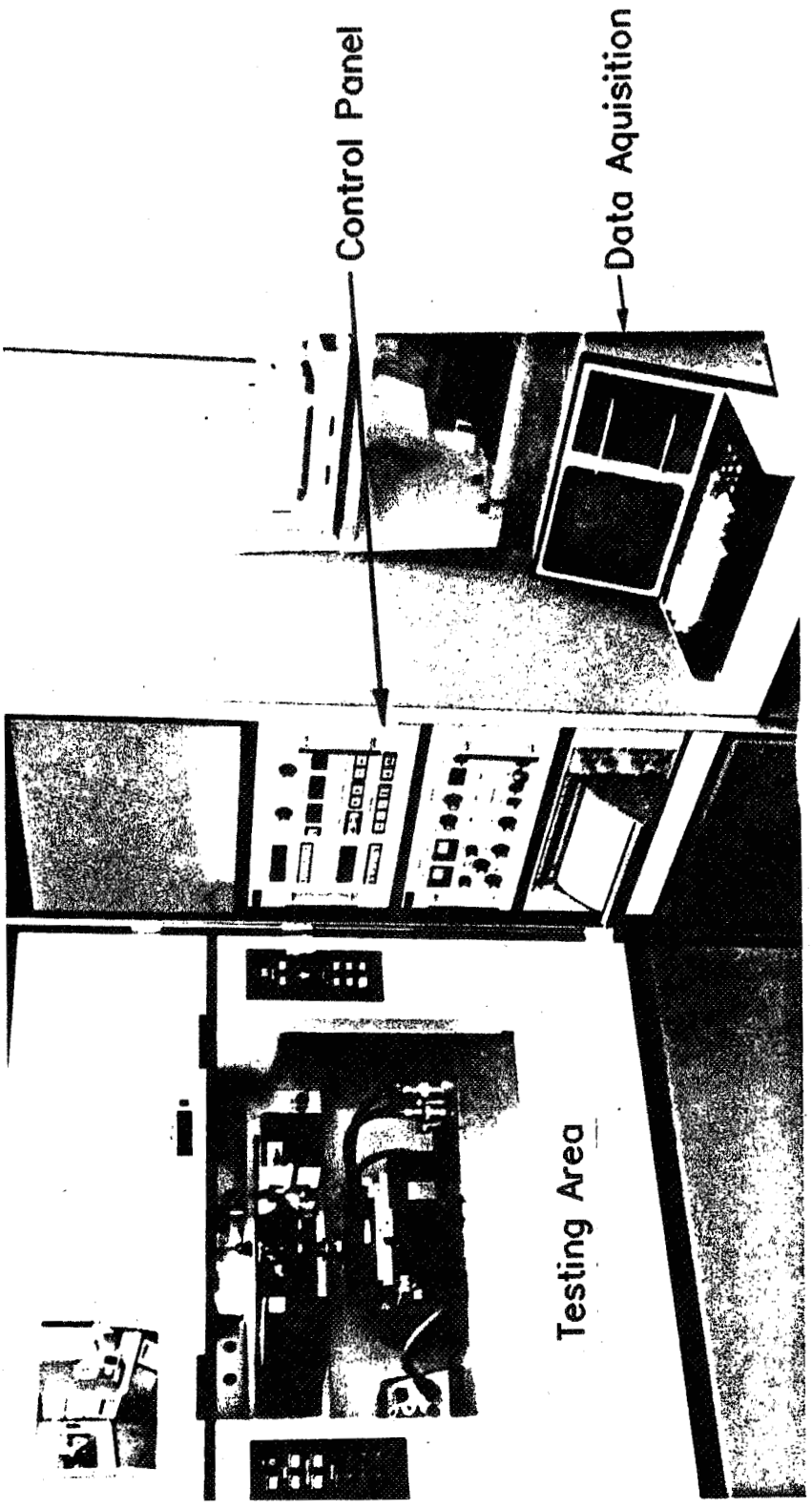

Figure 2.5 Testing Apparatus - Rheometrics Series Systems Four

(A) Top Parallel Plate
(B) Specimen (Kapton film not shown)
(C) Bottom Parallel Plate

Figure 2.6 Testing Fixture with Close-Up of Test Specimen

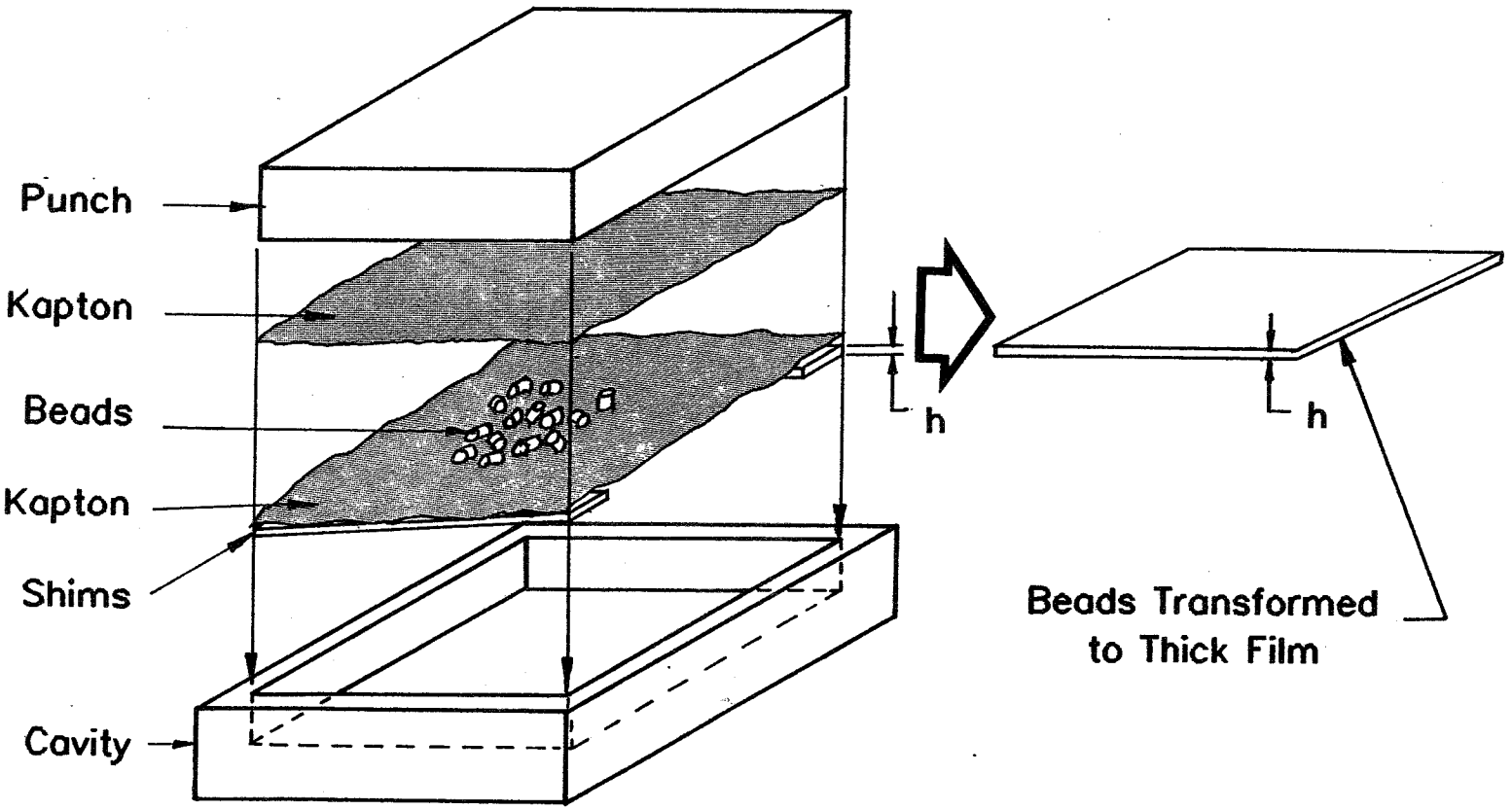

Figure 2.7 Sample Preparation - P1700 Bead to Thick Film Transformation

vacuum was required to reduce contamination,)

Note: The final temperature was approached very slowly (~6 hrs.) to allow moisture to diffuse out of the polysulfone beads before the onset of flow. Use of a higher heating rate during specimen preparation would cause the formation of bubbles.

4) cool sample down below T_g and remove from oven,

5) keep sample stored in vacuum desiccator heated to 100°C (212°F), and

6) remove Kapton film from samples just before testing.

2.3.3 Testing Program

The test program was divided into three sub-programs: 1) sizing the area of resin contact of the test specimen to the maximum load limits of the normal force transducer on the rheometer, 2) evaluating the effects of preloading the contact area (i.e. contact pressure) to assure intimate contact at the interface, and 3) evaluating the effects of contact time on the autohesive strength of the neat resin for various isothermal temperatures above the T_g.

Sizing the Specimen

The following procedure was used to determine the allowable area of resin contact of the specimen so as not to exceed the limit of the force transducer (1000 grams). The largest autohesive strength is expected to occur at the longest contact time (t_c = 1200 sec) and lowest test temperature (210°C (400°F)) expected to be tested. At these conditions the autohesive strength is expected to have the

maximum value because the depth of penetrating chains are at their maximum in addition to the molecular free volume being at its minimum.

Specimens 12.7 mm (0.5 in.) in diameter were punched from a flat sheet of P1700 thermoplastic resin. The protective Kapton films were then removed from the specimens surfaces. Holes were punched in the center of two 25.4 mm (1.0 in.) diameter Kapton films 2.54E-4 mm (0.001 inch) thick. The two identical Kapton films were placed between two P1700 specimens as shown in Fig. 2.8. Assembling the test specimens in this manner ensured that the load required for adhesive failure between the P1700 resin and the metallic parallel plate fixtures was greater than the load required to cause autohesive or cohesive failure of the P1700 resin at temperatures above the T_g. The test specimen was placed between the parallel plates of the rheometer and heated to 260°C (500°F) in a nitrogen purged atmosphere for over twenty minutes. The coupon was then placed under a compressive load of 750 grams to assure good adhesion between the metallic plate and the P1700 resin. The specimen was slowly cooled to 210°C (410°F) and pulled apart at the constant crosshead rate. The Kapton film hole diameter (5.08 mm (.20 in.)) was adjusted to ensure that the maximum load to cause failure would not exceed 1000 grams (the maximum load cell capacity.)

Effect of Pressure on Autohesive Strength

The first processing parameter that must be measured is the pressure (P_∞) required to achieve intimate contact for a particular temperature and contact time. The lowest temperature (210°C (410°F))

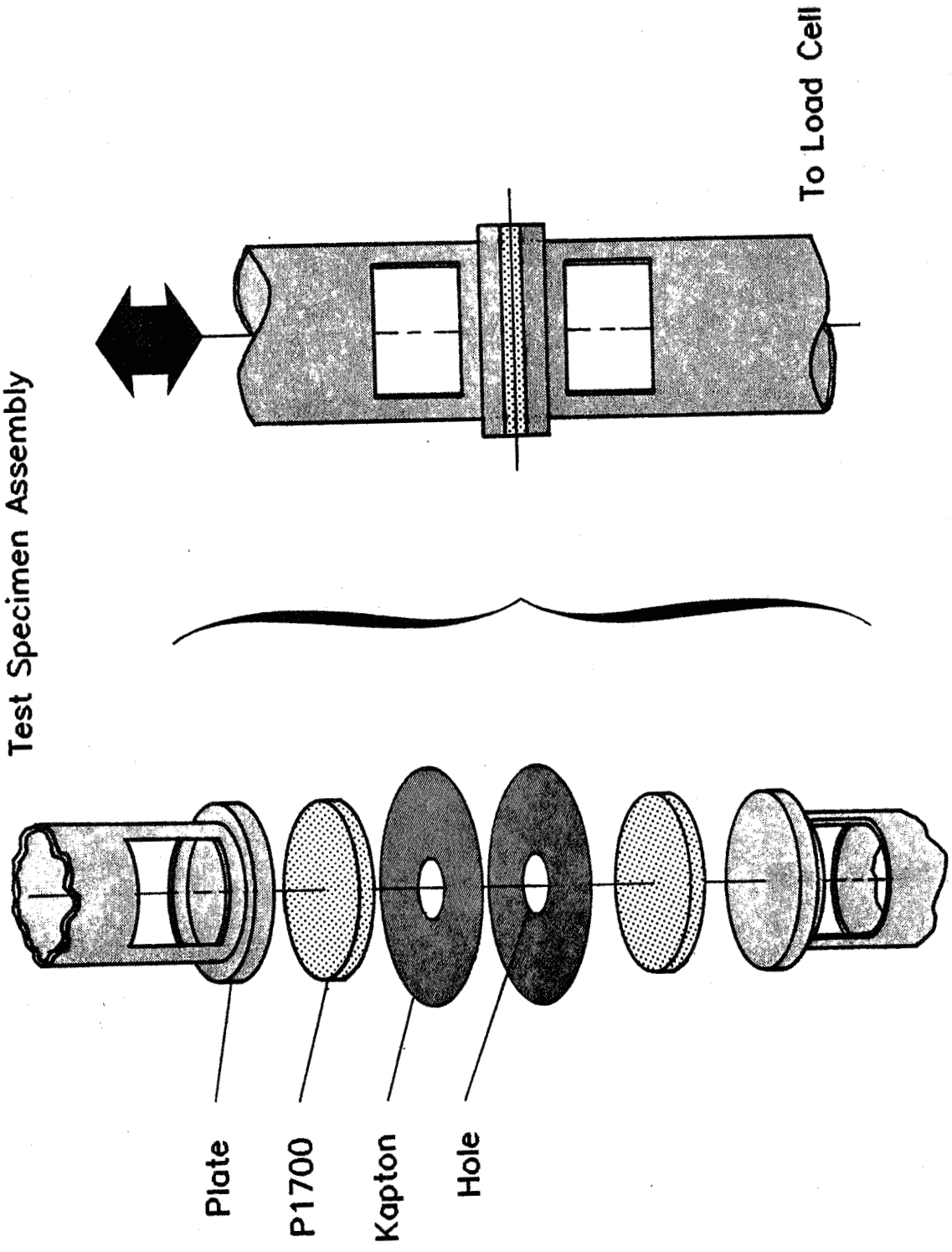

Figure 2.8 Test Specimen Preparation

and time (10 sec) expected to be measured were used in determining the saturation pressure. This would provide the largest P_∞ over the entire test spectrum. The contacting pressure was increased for successive tests and the resulting autohesive strength was recorded. The pressure corresponding to the maximum autohesive strength at a given T and t_c is the saturation pressure P_∞. This saturation pressure was used for all the tests listed in Table 2.1.

Effects of Contact Time and Temperature on Autohesive Strength

Table 2.1 lists the various temperatures and contact times tested for autohesive strength. The tests were conducted such that the entire contact time spectrum was run with one specimen for each isothermal temperature condition. Figure 2.9 shows the applied load as a function of time for a typical test run. The two piece specimen was allowed to reach the isothermal test temperature, and then brought into contact at the saturation contact pressure, P_∞, for the duration of the contacting time (t_c). The specimen was then put under tensile loading at the constant crosshead rate of the test apparatus. The maximum load was recorded and termed the autohesive load obtained for that T and t_c. Because the specimen's resin contact area was held constant for all tests, the autohesive loads for different tests can be compared directly to each other as if they were strength values. The specimen is then allowed to attain its initial conditions of chain entanglement density and orientations at the surface before contact was made again. This period of time is called the reentanglement time (t_r) shown in Fig. 2.9.

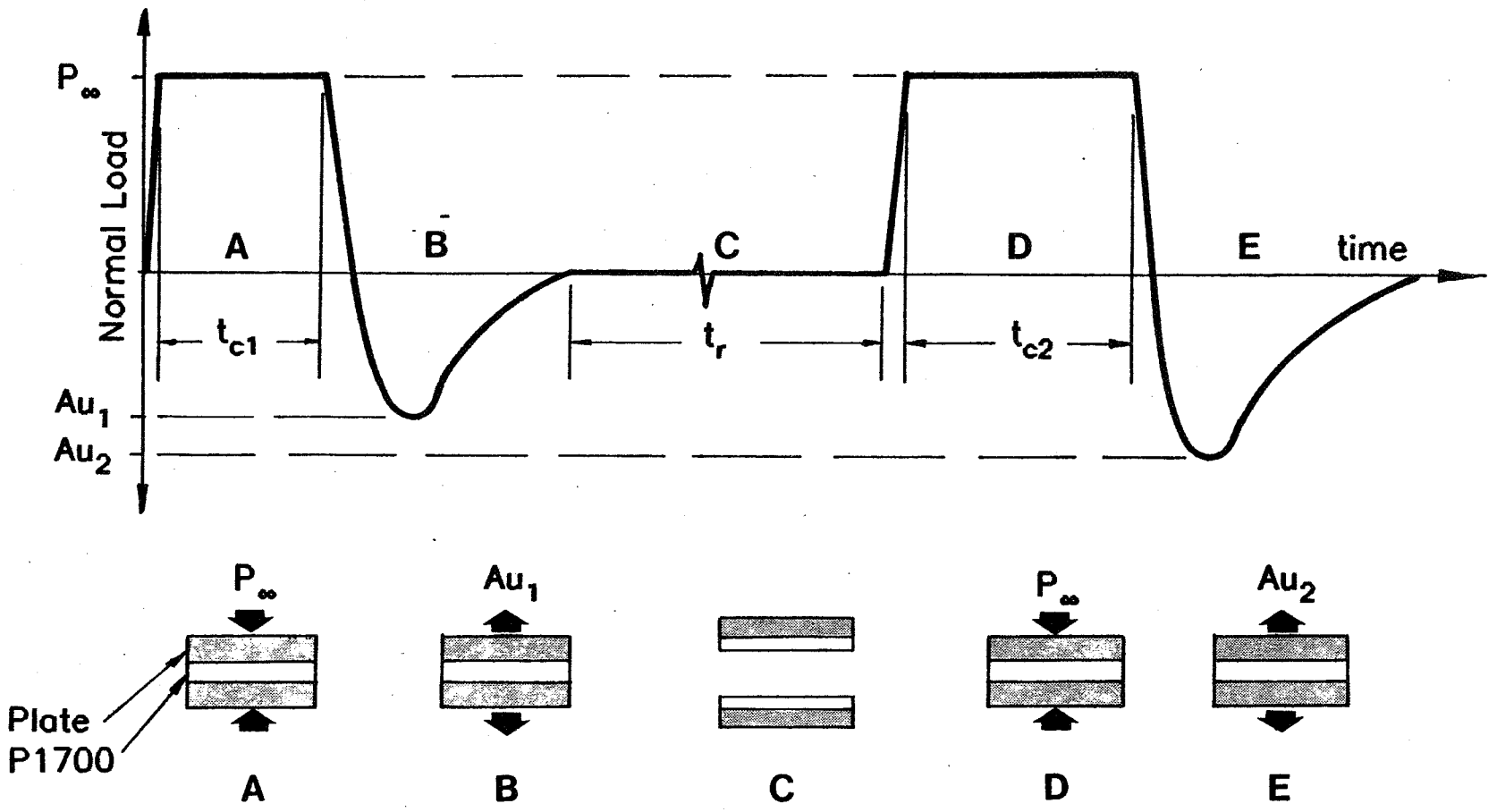

Figure 2.9 Typical Autohesive Strength Testing Format and Procedure

The reentanglement time was determined by repeating the above test at T = 210°C (410°F) and t_c = 1200 sec, and increasing t_r until the autohesive strengths were approximately equal on succesive runs. The t_r was found to be one hour and twenty minutes (1 hr. 20 min.) and was used for all other tests.

2.4 Results and Discussion-Au

The relationships between pressure, temperature, and contact time, and autohesive strength (Au) are discussed here. Autohesion is also a function of the elongational strain rate, sample geometry, molecular weight of the polymer (M), memory capability of the polymer, and the failure mechanism at the interface. Wool's and Jud's theoretical predictions (Section 2.2.2) between autohesive strength and contact time shown in Eq 2.5 are used to explain the effects of the processing parameters on the observed experimental strengths. Wool's assertion that the self-diffusion coefficient may be temperature dependent in a WLF manner is then evaluated. Lastly, a master curve defining the degree of autohesion as a function of contact time and temperature is derived. This was done by extending the data obtained at high temperatures, requiring short contact times to simulate the degree of autohesion obtained at the long contact times required for low temperature conditions. An explanation of the effects that the processing parameters have on the experimental results are discussed next. An application of the "free volume theory" to contact time and temperature data is used as its basis.

Autohesion strength data will be addressed in a relative sense. Recalling Eq 2.8, the degree of autohesion was defined as the ratio of autohesion strength at a given temperature and contact time to that of the maximum autohesive strength (i.e. cohesive strength) at the same temperature. This ratio compares the state at which interfacial diffusion has progressed relative to the state of cohesive strength (i.e. Au at t_∞, where t_∞ is the time required to achieve cohesive strength).

2.4.1 Original Data

This section presents a comparison between theory and experimental results obtained for the various processing parameter conditions listed in Table 2.1. First, the data used to evaluate P_∞ is presented. Second, the experimental data addressing effects of contact time on autohesive strength are compared to the autohesive strength theory. Third, the temperature effects on autohesive strength are discussed.

Because the area of contact was kept constant for all the tests, the autohesive load at failure is reported in lieu of its ultimate stress. Thus, the terms autohesive strength are used interchangeably with autohesive load.

2.4.1a Effects of Contact Pressure on Autohesion

Figure 2.10 shows that autohesion increases in an asymptotic fashion up to a saturation pressure where autohesion becomes a maximum. Thus, autohesion is invariant with contact pressures above

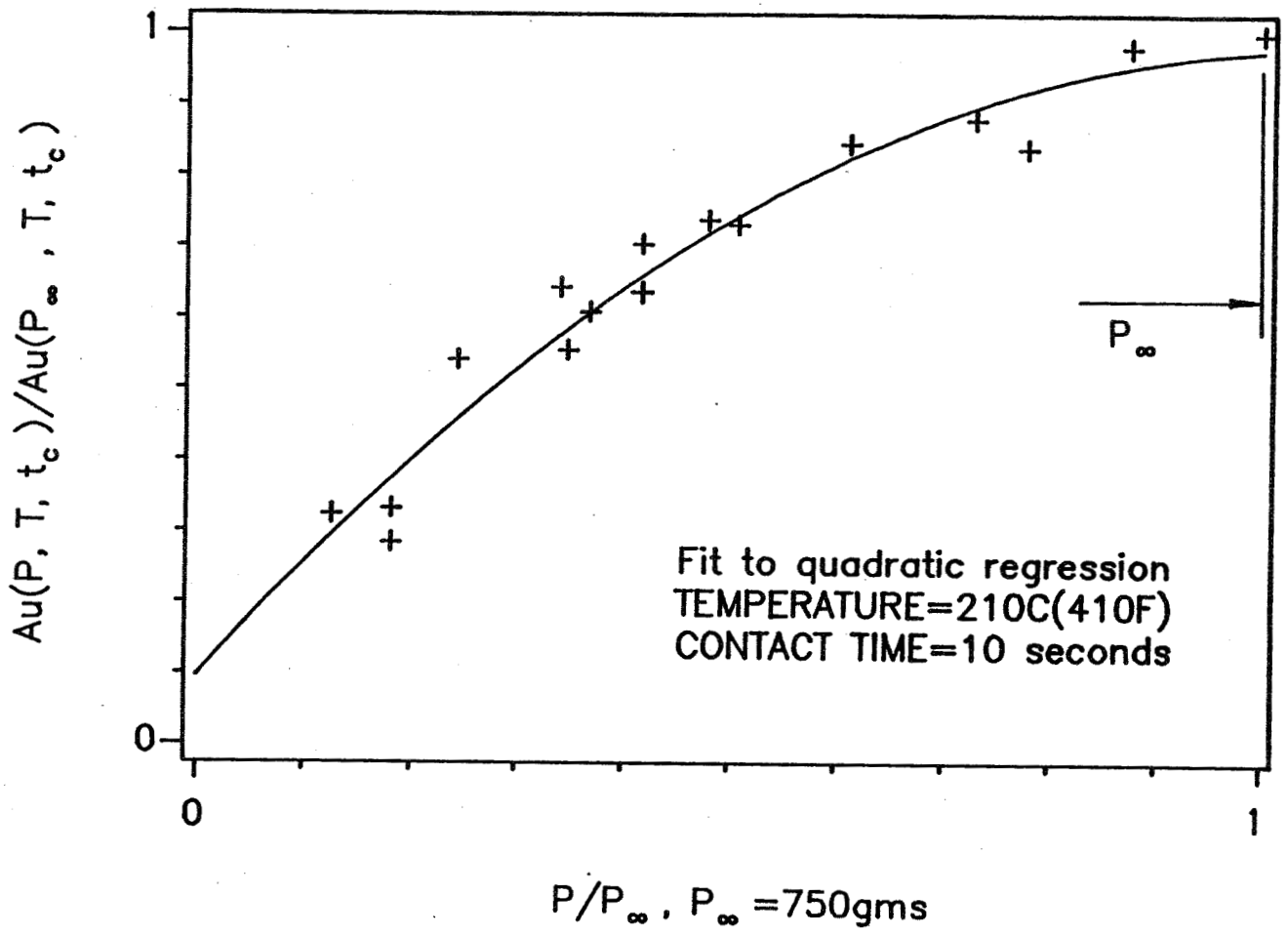

Figure 2.10 Evaluation of P_∞, and Effects of Contact Pressure on the Autohesive Strength

the saturation pressure. This fact has previously been noted by Wool [11] and Voyutskii [6]. As previously mentioned, this behavior is due to the area of contact at the interface increasing with increasing pressure until full intimate contact is achieved. Initially the surface must rearrange and deform as full intimate contact is approached.

Because P_∞ is very small compared to the pressures normally used in processing, its importance lies only in the autohesion testing procedure where intimate contact must be assured for all tests.

The value for P_∞ given in Fig. 2.10 corresponds to the lowest temperature and the shortest contact time in the test matrix. It can therefore be expected that intimate contact on the neat resin is achieved at all the temperature and contact time conditions tested as explained in Section 2.3.

2.4.1b Effects of Contact Time on Autohesion

Wool and Jud have derived theoretically and shown experimentally that autohesive strength increases in proportion with the fourth root of contact time ($t_c^{1/4}$). Thus, on a plot of autohesive strength versus the fourth root of contact time, the experimental data should fall on a straight line. Figures 2.11 and 2.12 show the experimentally measured autohesive strength data in comparison with the theory of Wool and Jud for the various temperature conditions listed in Table 2.1. The constant of proportionality relating Au and $t_c^{1/4}$ was determined by a linear regression curve fit. The cohesive strength region was not always achieved at the lower temperatures because of

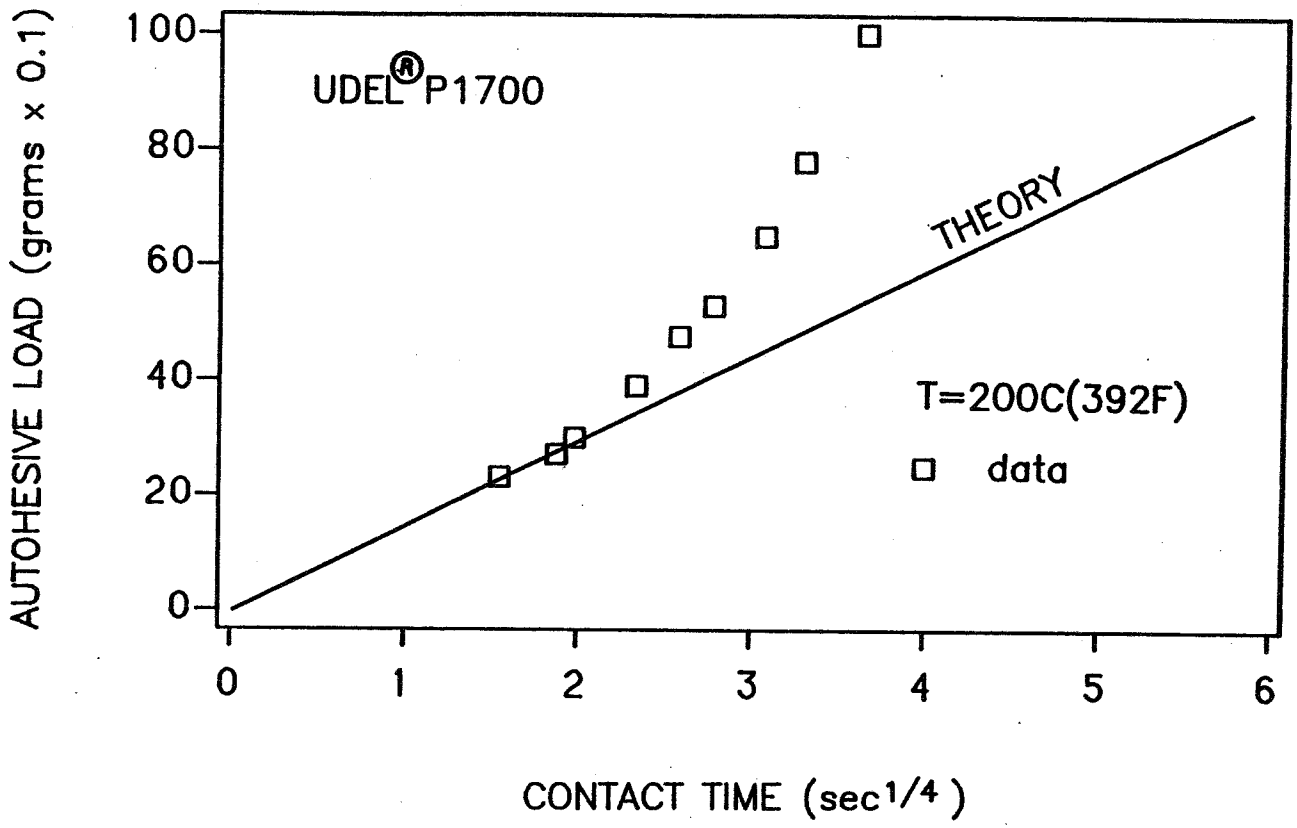

Figure 2.11 Autohesive Load versus Fourth Root of Contact Time at T = 200°C (392°F), and P = P_∞

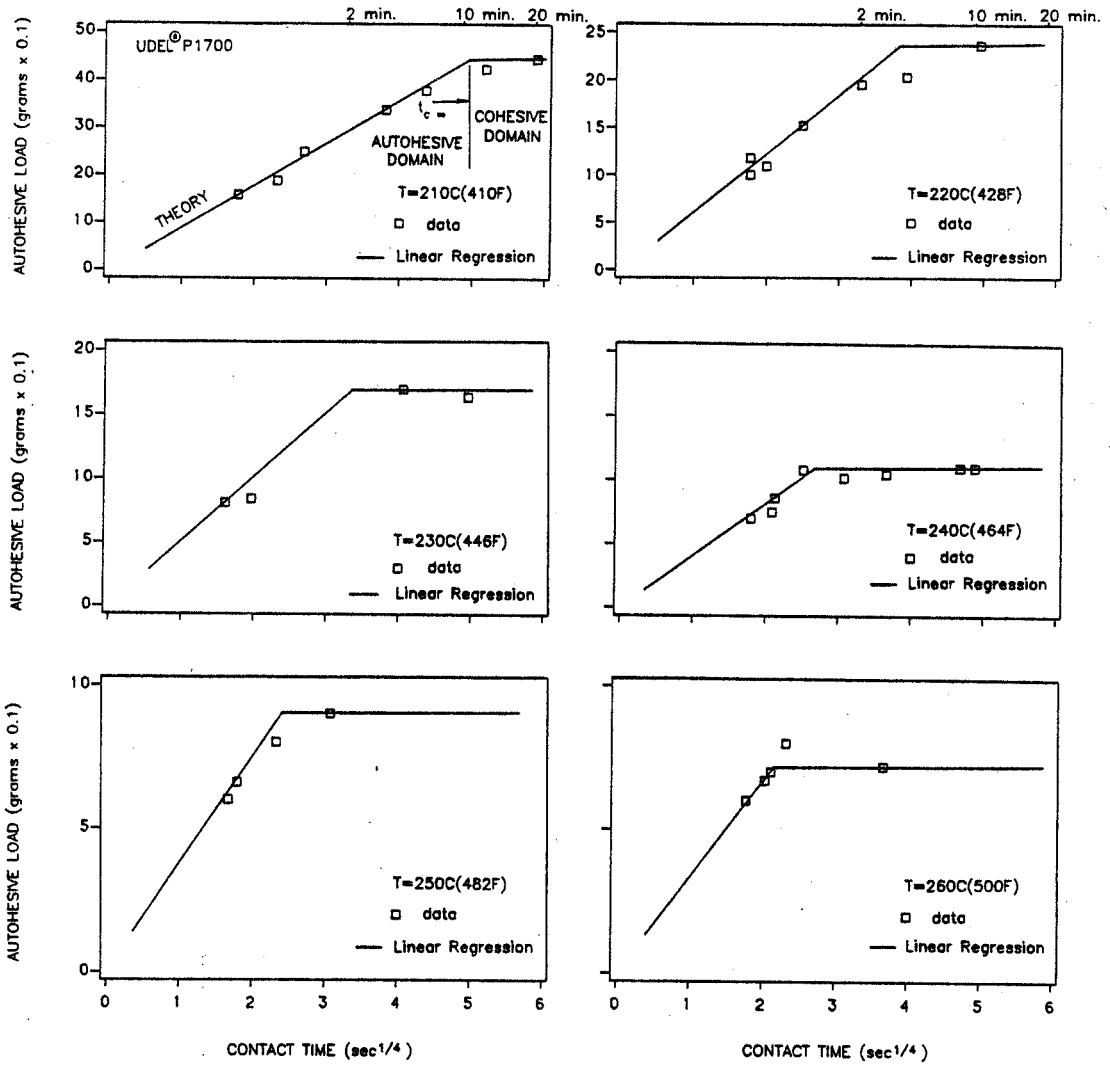

Figure 2.12 Autohesive Load versus Fourth Root of Contact Time at T = 210°C (410°F), 220°C (428°F), 230°C (446°F), 240°C (464°F), 250°C (482°F), 260°C (500°F), and $P = P_\infty$

insufficient durations of contact time. The acquisition of autohesive strength data at high temperatures was limited by the human capability to test for autohesion strength at short contact times. An explanation of each one follows.

Figure 2.11 shows that at T = 200°C (392°F) (T_g+5°C (10°F)) the autohesive data deviates increasingly with $t_c^{1/4}$ from the prediction by theory. It can also be seen that the theory is conservative in the prediction of autohesive strength. The cause of this disagreement between theory and experiment is that for the given strain rate (too high) and temperature (too low) condition an increasing proportion of chain failures due to fracture are occurring. Failure due to chain fracture corresponds to a higher failure load, and so the net effect is an increase in autohesive load for longer contact times. This increased incidence of chain fracture is due to an increased chain penetration depth at longer contact times. The theory requires that the fracture mechanism be constant throughout the test (i.e. the same proportion between fractured chains and pulled out chains). Thus, the 200°C (392°F) temperature cannot be used to evaluate the degree of autohesion and is placed as the lower limit for the test matrix. If lower temperatures are to be used for evaluating the degree of autohesion then a slower stain rate must be used to produce the desired failure by chain pull-out.

In Fig. 2.12 the T = 210°C (410°F) data shows good correlation between theoretical response and experiment for the autohesive region. However, the comparison between theory and experiment is inconclusive in determining the transition from the autohesive region

to the cohesive region. The slight deviation of the two data points at the largest contact times may be attributed to either experimental error in the transition to cohesive failure or to error resulting from the test conditions being so close to the conditions at which the reentanglement time (t_r) was determined, thus, causing different initial conditions of the molecular structure and affecting the diffusion mechanism and disentanglement period. The T = 220°C (428°F) data shows good correlation between theoretical response and experiment for the autohesive and cohesive strength regions. The last data point is indicating the plateau of cohesive strength. The T = 230°C (446°F) data shows fair correlation between theoretical response and experiment when comparing the theoretical response with the next higher and lower temperature data results. The T = 240°C (464°F) data shows good correlation between theoretical response and experiment for both regions of failure. The apparent curvature of data in the knee section separating the autohesive and cohesive regions, may be attributed to error in the experiment. The T = 250°C (482°F) and 260°C (500°F) data show good correlation between theoretical response and experiment for both regions of failure.

Figure 2.13 shows the degree of autohesion versus $t_c^{1/4}$ for the same processing temperature conditions of Fig. 2.12. The solid line indicates the theoretical response (autohesion region fit by linear regression) of the autohesive and cohesive regions of failure.

Figure 2.14 summarizes the effects between contact time and the degree of autohesion where the theoretical responses (autohesion region fit by linear regression) and the data from Fig. 2.13 are

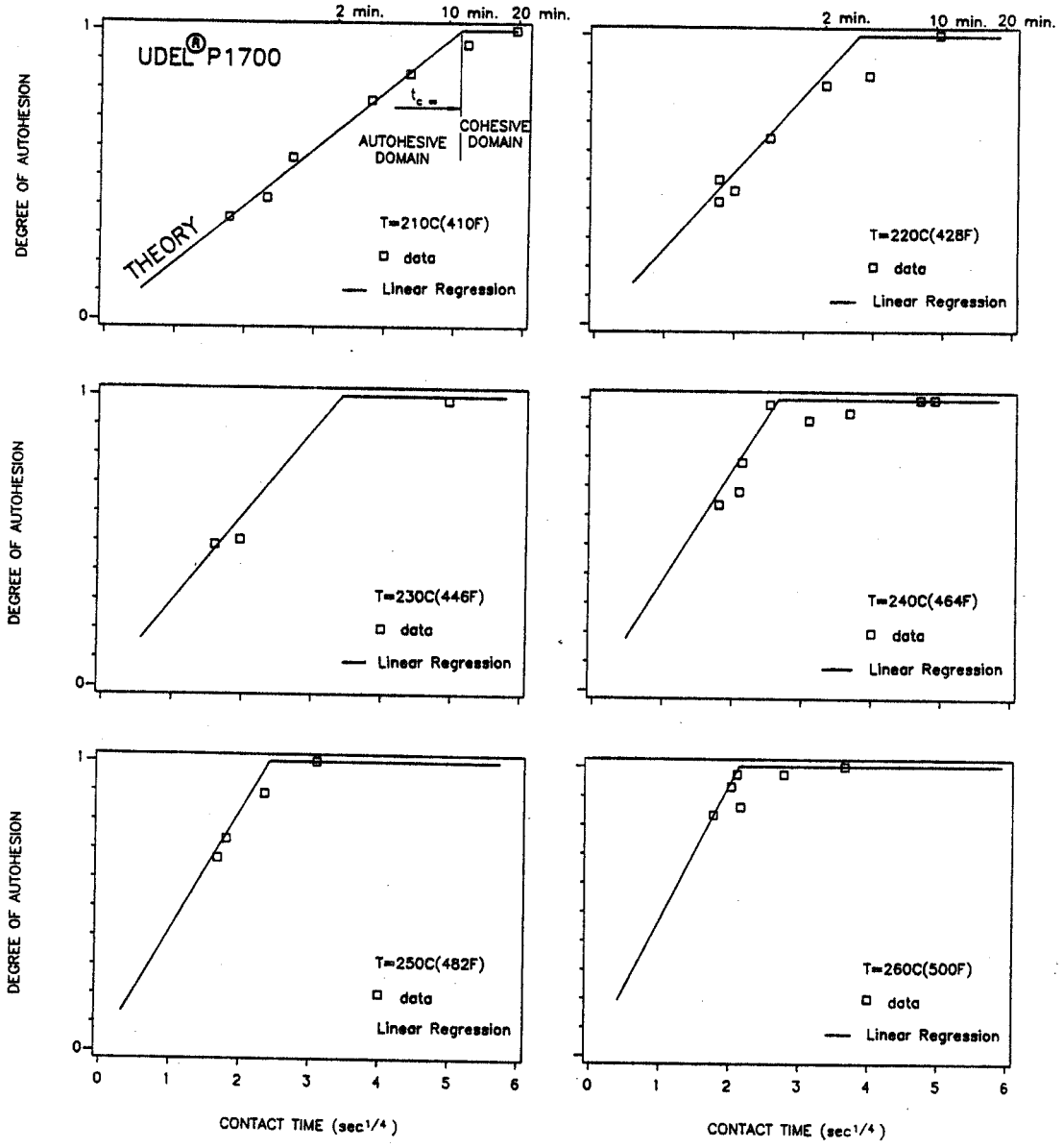

Figure 2.13 Degree of Autohesion Versus Fourth Root of Contact Time at T = 210°C (410°F), 220°C (428°F), 230°C (446°F), 250°C (482°F), 260°C (500°F), and P = P_∞

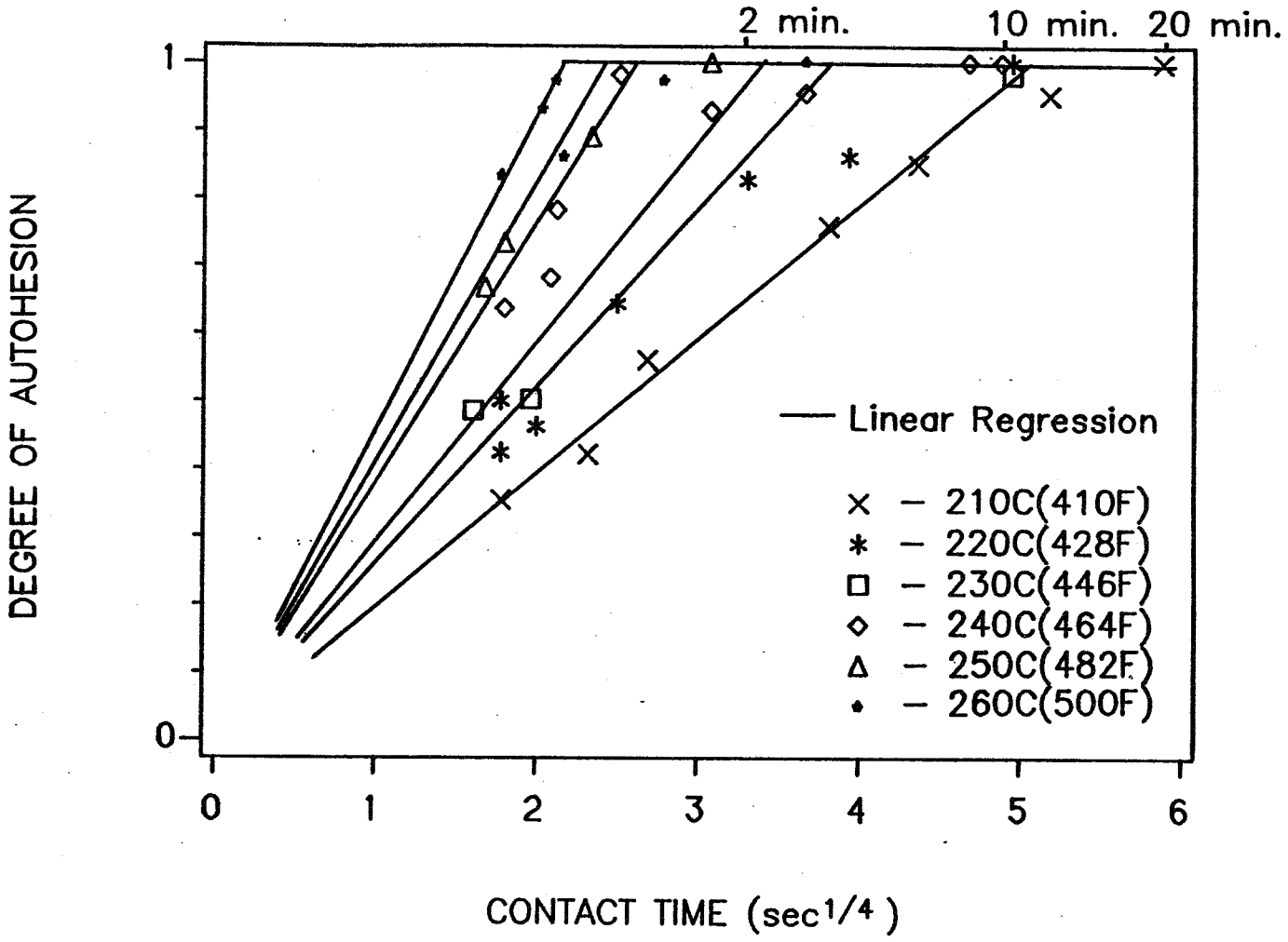

Figure 2.14 Summary Plot of Degree of Autohesion versus Fourth Root of Contact Time

shown. It is observed that as temperature increases, a greater degree of autohesion can be achieved for a given contact time.

Jud [13] observed that the experimentally determined macroscopic diffusion coefficients (D), proportional to the slopes of the strength versus fourth-root of time curves for various temperatures, can be represented by an Arrhenius law shown in Eq 2.9:

$$D(T) = D_o \exp\left[-\frac{E_a}{kT}\right] \tag{2.9}$$

where E_a is the activation energy, k is the Boltzmann constant, T is the absolute temperature, and D_o is a constant with the units of meters square per second (in^2/sec).

Thus, from the Fig. 2.14 the degree of autohesion can be written as:

$$D_{Au} = D_{Au_o} + K(T) \cdot t_c^{1/4} \tag{2.10}$$

where D_{Au_o} is the initial degree of autohesion at t = 0 (zero in this study) and K(T) is a temperature dependent parameter with dimensions of D_{Au}. K(T) is defined as that product of a proportionality constant times the self diffusion coefficient. The Arrhenius law has been rewritten as:

$$K(T) = K_o \exp\left[-\frac{E_a}{kT}\right] \tag{2.11}$$

The parameters K_o and E_a (Eq 2.11) are determined by plotting the natural log (Ln) of the slopes of the curves in Fig. 2.14 versus 1/T as shown in Fig. 2.15. The slope determines the value of E_a while the intercept determines the value of K_o. The constants were found to be; K_o = 1922 (dimensionless), and E_a = 6.0902E-20 Joules (5.7772E-23 BTU). The value of E_a is used strictly in an empirical manner.

With the use of Eq 2.11, the validity of Eq 2.10 can be compared to the experimental results. Shown in Fig. 2.16 are the experimental data while the solid lines are those curves obtained from Eq 2.11.

Fair agreement between the empirical formulation given by Eq 2.10 using the Arrhenius law (Eq 2.11) and the experimental data is observed. The empirical formulation overpredicts the time required to achieve a given degree of autohesion at the higher temperatures. However, the contact times observed at the higher temperature data are very short and may be, in reality shifted to longer or shorter contact times because of experimental procedure.

Thus, Eqs 2.10 and 2.11 describe completely the degree of autohesion as a function of temperature and contact time up to the cohesive state.

2.4.1c Effects of Temperature on Autohesion

Figure 2.17a is a plot of Au versus temperature at the saturation contact pressure and several contact times. It has been observed that on an absolute scale the autohesive strength at any one time is greater at the lower temperature condition than at the higher temperature condition. However, in the relative sense, it has been

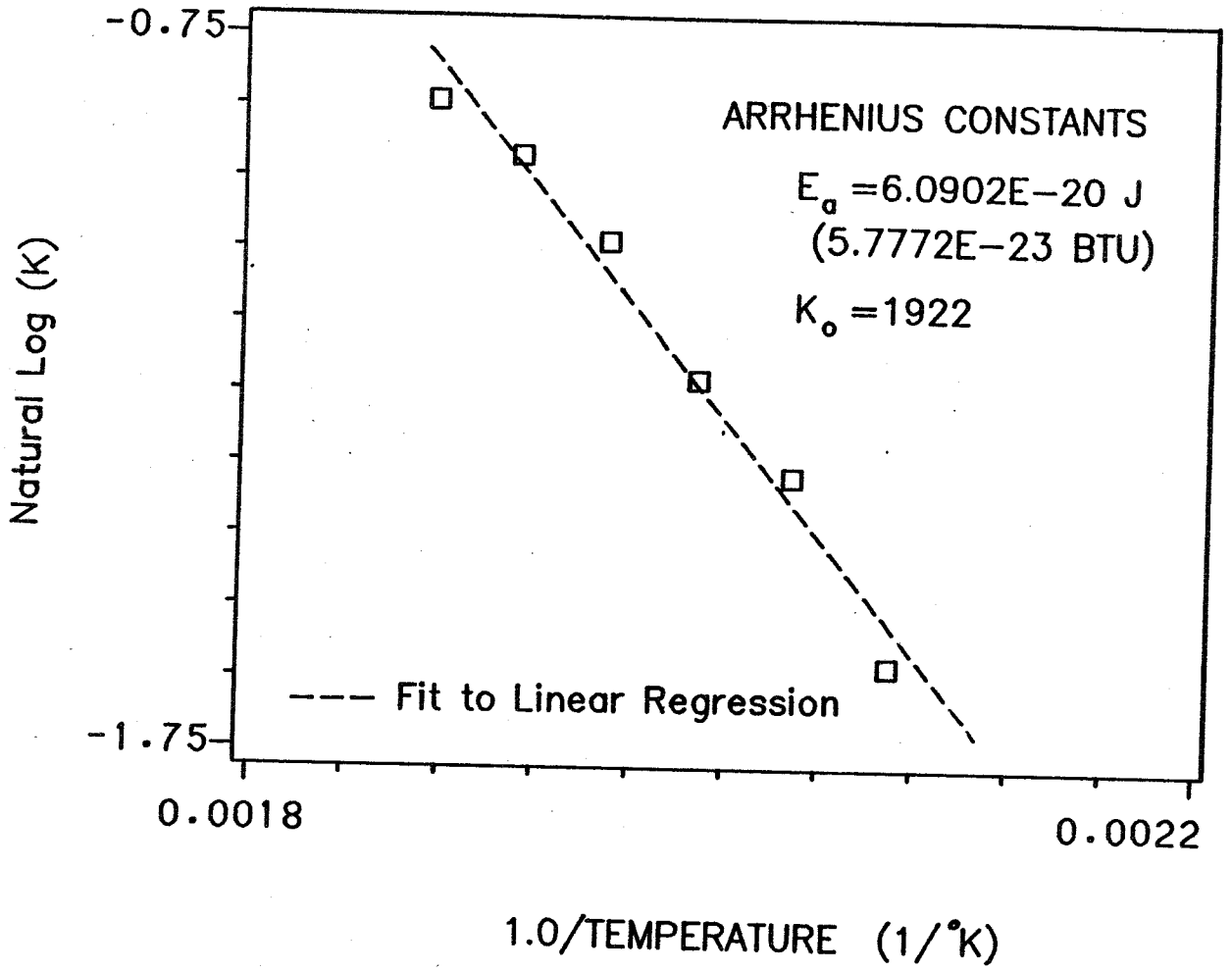

Figure 2.15 Evaluation of Arrhenius Constants for Autohesion Temperature Dependency

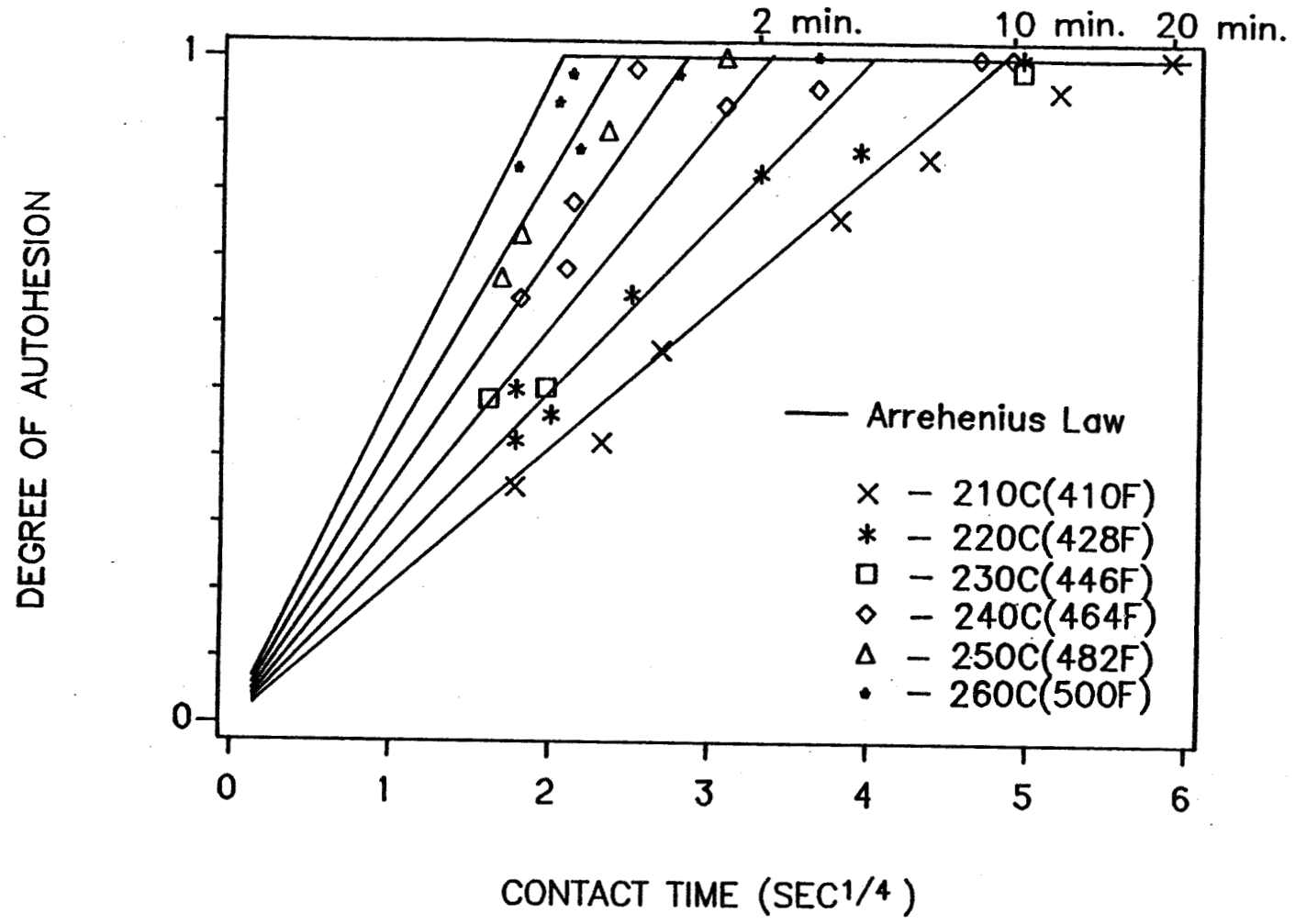

Figure 2.16 Comparison Between Arrhenius Law and the Degree of Autohesion Test Data for Evaluation of Temperature Relationship

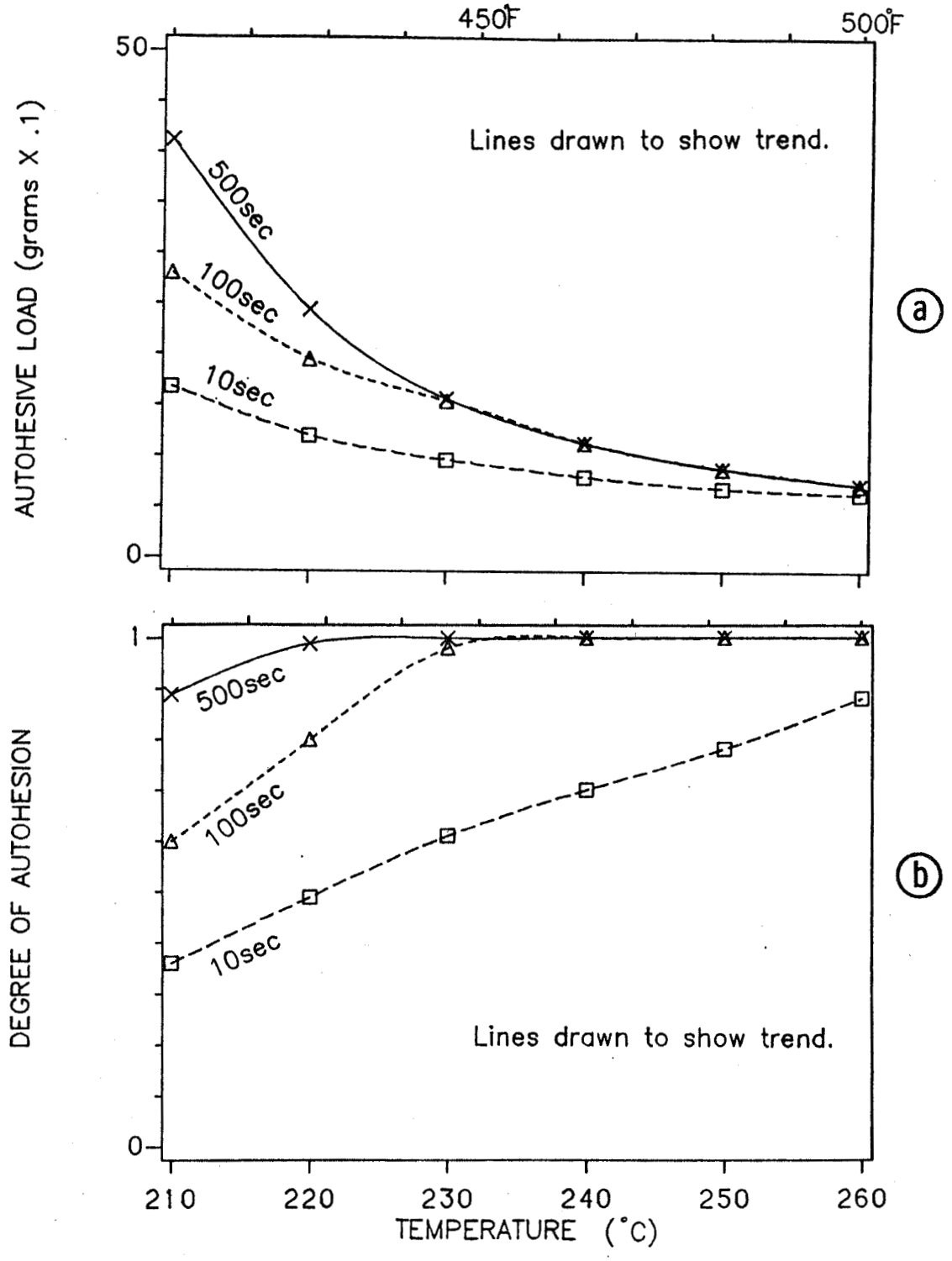

Figure 2.17 Parametric Study Between Temperature and Contact Time (a) Autohesive Load versus Temperature at Contact Times of 10, 100, and 500 Seconds (b) Degree of Autohesion versus Temperature at Contact Times of 10, 100, and 500 Seconds

observed that the degree of autohesion at any time less than t_∞ is greater at the higher temperature condition than at the lower temperature condition. This occurs because of the increased molecular mobility at higher temperatures allowing greater self diffusion for a given length of time. One must remember that just as it is easier for molecules to penetrate across the interface, the higher the temperature, it is just as easy to pull them out. Thus, one must use the definition of the degree of autohesion (Eq 2.8) to observe the effects of temperature on autohesion. Figure 2.17b is a plot of D_{Au} versus T.

2.4.1d Interrelationship Between Contact Time and Temperature on Autohesion

Wool [11] has suggested that the autohesion phenomenon may exhibit a time-temperature relationship provided that the failure mechanism is due to chain pull-out as stated in Section 2.2.2. Observation of the data in Fig. 2.12 has shown this to be true. However, the 200°C (392°F) temperature data shown in Fig. 2.11 has been shown to exhibit a combined failure mode of chain pull-out and chain fracture. With this stated, a brief explanation of the WLF theory is made, followed by its application as a contact time-temperature relationship for the degree of autohesion.

It is widely accepted that temperature affects self diffusion because of its effects on the molecular free volume [6,7,11]. As T increases so does the molecular mobility. The premise of the molecular free volume as proposed by William, Landel and Ferry is that

a given state a polymer possesses at T_1 and t_1 is not necessarily unique. There are a range of corresponding temperatures and times having an identical state of some physical property u (e.g. modulus, viscosity, etc.). This concept is written mathematically in Eq 2.12, and has been shown true for a wide choice of polymers.

$$u(t_1,T_1) = u(t_2,T_2) = \ldots \tag{2.12}$$

Replotting Fig. 2.14 on a log-log scale, shown in Fig. 2.18a, it has been observed that the slopes of the autohesive region are all 0.25 as predicted by the theory shown in Eq 2.5. Also from Fig. 2.18a, it was observed that for a given degree of autohesion (Au) at T_1 and t_1 the same degree of autohesion could be achieved at a shorter contact time if the temperature is increased. The contrary is also true. A longer contact time would be needed to achieve the same degree of autohesion if processed at a lower temperature.

The following mathematical observation was made of Fig. 2.18a:

$$\log_{10} t_c - \log_{10} t_{c_{ref}} = a_T \tag{2.13}$$

where; t_c is any contact time, $t_{c_{ref}}$ is the contact time at some reference temperature (T_{ref}), and a_T is the shift factor and is a function of temperature.

Equation 2.13 is the basis of the WLF theory and can be written in the WLF form shown in Eq 2.14:

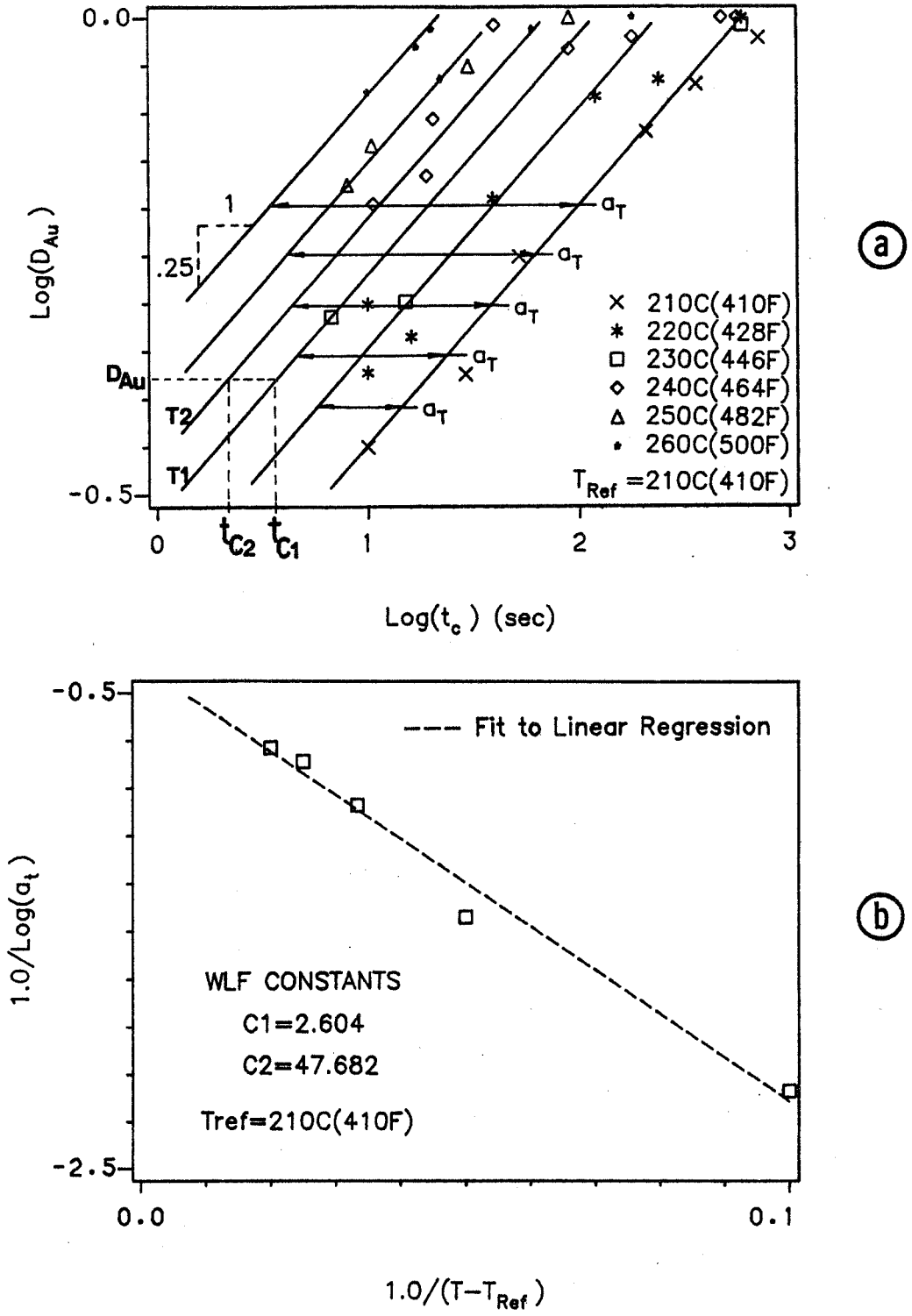

Figure 2.18 WLF Theory, (a) Shift of Original Data at Respective Temperature to the Reference Temperature, (b) Evaluation of WLF Constants

$$t_c = a_T \, t_{c_{ref}} \tag{2.14a}$$

where;

$$a_T = \frac{-C1(T - T_{ref})}{C2 + (T - T_{ref})} \tag{2.14b}$$

The constants C1 and C2 were determined by the shifts required to superimpose all the temperature data to one master curve. The constants have significance concerning the molecular free volume; however, no further interest other than those previously implied are made here for this study. Figure 2.18b plots the shifts as a function of temperature in such a way that the constants C_1 and C_2 were evaluated to be 2.604 and 47.682, respectively, for the reference temperature of 210°C (410°F).

With the WLF Eq 2.14, Eq 2.10 can be written as:

$$D_{Au} = K_o' \cdot [a_T \, t_{c\ ref}]^{1/4} \tag{2.15}$$

where; $K_o' = 0.1953\ sec^{-1/4}$ is the slope of the curve in Fig. 2.14 at 210°C (410°F). Figure 2.19 shows fair correlation over the entire temperature test spectrum between the experimental data and the time-temperature relationship evaluated in the WLF manner. The increasing apparent error in the high temperature results may be attributed to either, an error in estimating the actual time autohesion has occurred during the very short time intervals, or error in the assumed cohesive strengths of the low temperature tests. In both cases a shift in the

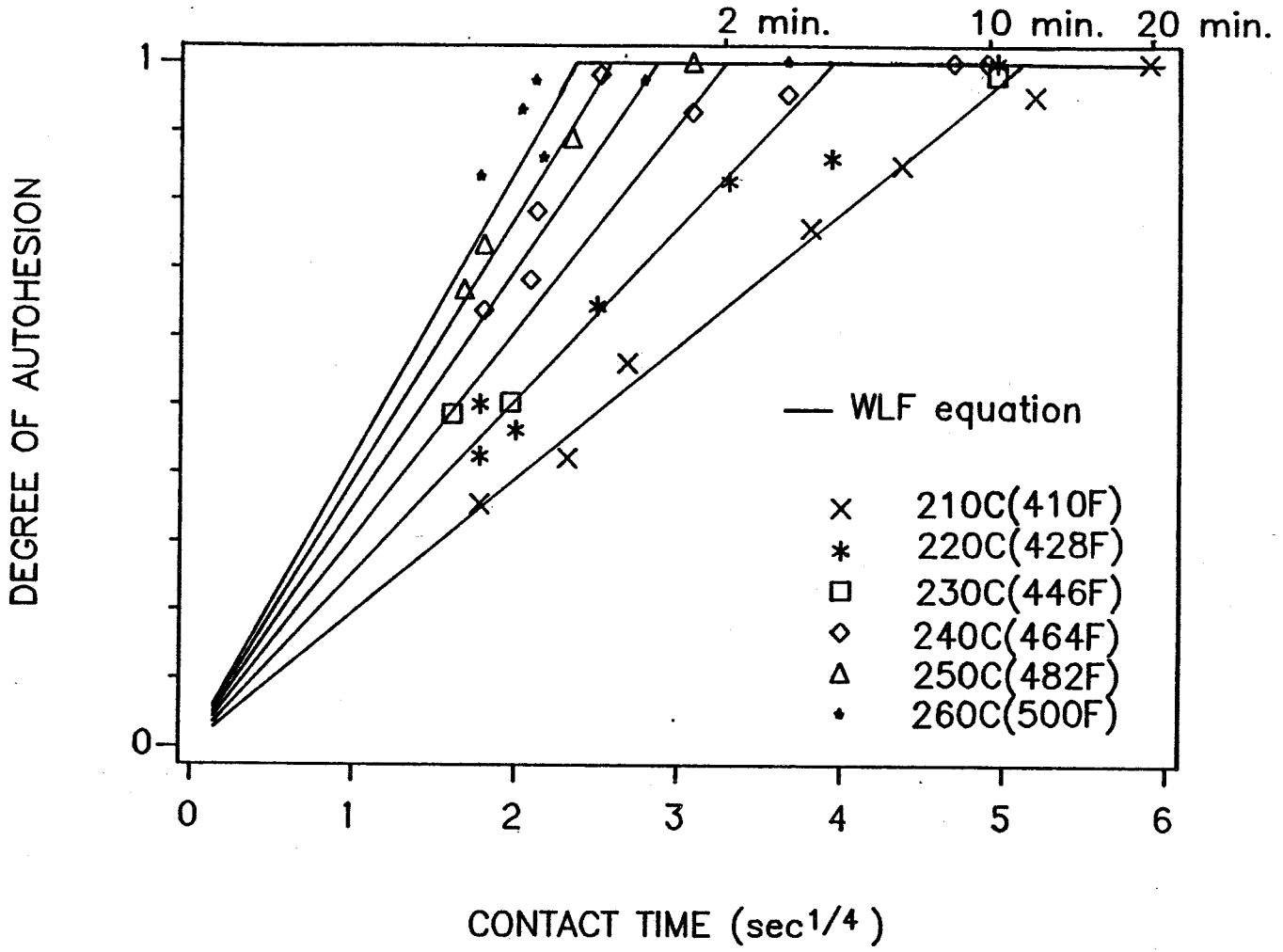

Figure 2.19 Comparison between the WLF Time-Temperature Relationship, and the Degree of Autohesion Test Data

data would result. It was uncertain whether the high temperature/short contact times or low temperature/long contact times tests produce the largest error. Thus, the well defined cohesive regions of the higher temperature data can be used to help evaluate the cohesive regions at lower temperatures requiring long contact times. One equation now describes the degree of intimate contact for any contact time and temperature.

3.0 Intimate Contact-IC

3.1 Introduction-IC

In the previous section, the mechanism by which a thermoplastic matrix composite consolidates to form a laminate was attributed to autohesive bond formation between plies. However, the autohesion phenomenon can only occur after the two surfaces have coalesced (i.e. are physically in intimate contact). Macromolecules cannot diffuse across spacial gaps at the interface. The study in this section identifies the mechanisms by which the interfaces of a thermoplastic prepreg coalesce (not to be confused with consolidate) resulting in intimate contact. The effect of the various processing parameters on the degree of intimate contact is discussed.

The presence of spacial gaps between prepreg plies prior to processing is evident in both thermosetting and thermoplastic matrix composites. Unlike thermosetting epoxy matrix composites, which rely on low viscosity flow and wetting ability of the resin to coalesce the ply interfaces, thermoplastic matrix composites must be physically deformed to cause coalescence. The viscosity of epoxy decreases substantially when heated, resulting in its ability to wet out the interface even with the presence of fibers. However, the neat thermoplastic matrix resin, when heated, still maintains a zero shear rate viscosity greater than the viscosity of the epoxy at its gel point (i.e. when the epoxy begins to set). The amount of wetting which occurs during the processing of a thermoplastic matrix composite is therefore minimal.

It has been visually observed that spacial gaps between the laminate ply can be present before, during, and after the processing cycle. The extent of these spacial gaps will depend on the processing parameters: pressure (P), temperature (T), and contact time (t_c). A brief explanation follows as to the nature of the prepreg's geometric non-uniformity of tow heights across the width of the prepreg sheet, and how the effect of this nonuniformity can be minimized through the judicious choice of the processing parameters.

A prepreg is made up of single tows laid side by side. The tows have constant cross-sectional areas and fiber/matrix fractions. However, the tow thickness varies across the width of the prepreg. Thus, when the prepreg plies are stacked on top of each other, spacial gaps are present.

It has been observed during processing that specific combinations of pressure, temperature and contact time result in varying degrees of intimate contact at the laminate ply interfaces. However, these processing conditions are not unique. The same degree of contact can be obtained for different processing parameter combinations. The present study will attempt to quantify the relationships between the processing parameters and the degree of contact at the ply interfaces.

Surface mechanicians have shown experimentally that increasing areas of contact can be achieved by increasing the applied load across the interface [16,17]. Local elastic and plastic deformations of surface irregularities are attributed to the cause of increasing areas of contact. Thus, one would also expect an increase in the processing pressure to increase contact area. However, because of the

viscoelastic nature of the matrix, some time dependency can also be expected. Also, the temperature of the material during processing will greatly influence the rate at which the area of contact increases because of its influence on the properties of the matrix.

If viscoelastic effects are present during the processing of the composite then intuitively the following can be said:

1) surface contact area will increase with increasing pressure (P) for a constant T and t_c,
2) surface area will increase with increasing temperature (T) for a constant P and t_c, and
3) surface area will increase with increasing time (t_c) for a constant P and T.

Based upon these observations, an intimate contact (IC) model is presented which simulates the phenomenon by which the interfaces of the stacked plies coalesce. The model incorporates the viscoelastic properties of the material. However, certain engineering material properties were not obtainable to allow absolute verification of the model. Thus, the proposed mechanistic approach must be reduced to an empirical one, until these properties can be obtained. Nevertheless, the empirical constants used to fit the data show the expected viscoelastic responses of the physical material properties they have replaced.

The following are presented below: 1) experimental procedure and test matrix, 2) the data reduction scheme, 3) sub-model formulation, 4) IC model formulation, 5) theory and experiment correlation, 6) parametric study of processing parameters and the prepreg's geometric

non-uniformity, and 7) viscoelastic observations of the model and empirical constants.

3.2 Experiment-IC

3.2.1 Description

The purpose of studying intimate contact is to determine the relationships between the contact area at the ply interfaces to the processing parameters. Reported here are the experimental approach, procedure, and data reduction scheme for accomplishing this task.

It is desired to determine a certain combination of P, T, and t_c which will provide maximum ply interfacial contact. Thus, given any two processing parameters the third parameter can be defined for any desired state of ply interface contact (usually 100%).

Towards this end, laminates were fabricated using various combinations of the processing conditions. Several means of defining the area of contact at the ply interfaces are currently in use. They are: 1) C-scan, 2) thermal diffusivity, 3) ultrasonics, and 4) dielectric analysis. Only the first of these methods was used for the current study. The latter three methods are current ongoing research projects being pursued at NASA-Langley.

The C-scan approach has been well established, however, it is not without difficulties. The true area of contact observed by the C-scan is subject to the threshold chosen for the relative attenuation values. The threshold chosen for this investigation was based on experience gained in locating cracks after mechanical loading and

spacial gaps after processing in graphite/epoxy laminates. It is necessary to assume that damage detected by the C-scan represents a lack of coalescence at the ply interfaces and not damage within the plies. Because the laminates are not subject to any loading before being C-scanned, this appears to be a reasonable assumption. Figure 3.1 shows the use of the C-scan technique used to locate the areas of spacial gaps in unidirectional graphite/epoxy laminates shown as black areas. These areas were sectioned and photomicrographed to show validity of the approach.

3.2.2 Sample Preparation

The test samples used in evaluating intimate contact were laminates with ply orientations of $[0,90,0]_T$. The crossply laminate provides a worst case situation in that no nesting of tows occurs as in the case of unidirectional laminae. The presence of two interfaces creates a need for a statistical interpretation of the data. This will be discussed in detail in Section 3.3.1.

The reinforcement material used in this study was AS-4 graphite fiber, manufactured by Hercules Inc. The matrix material used was polysulfone polymer UDEL® P1700 (beadform) manufactured by Union Carbide Corporation. The U.S. Polymeric division of Hitco was chosen to prepreg the AS-4 graphite fiber with the P1700 resin. The prepreging process required the use of a solvent to allow impregnation and wetting of the resin onto the graphite fibers surfaces. The solvent used was cyclohexanone. The prepreg received required the removal of the solvent before the processing study was undertaken.

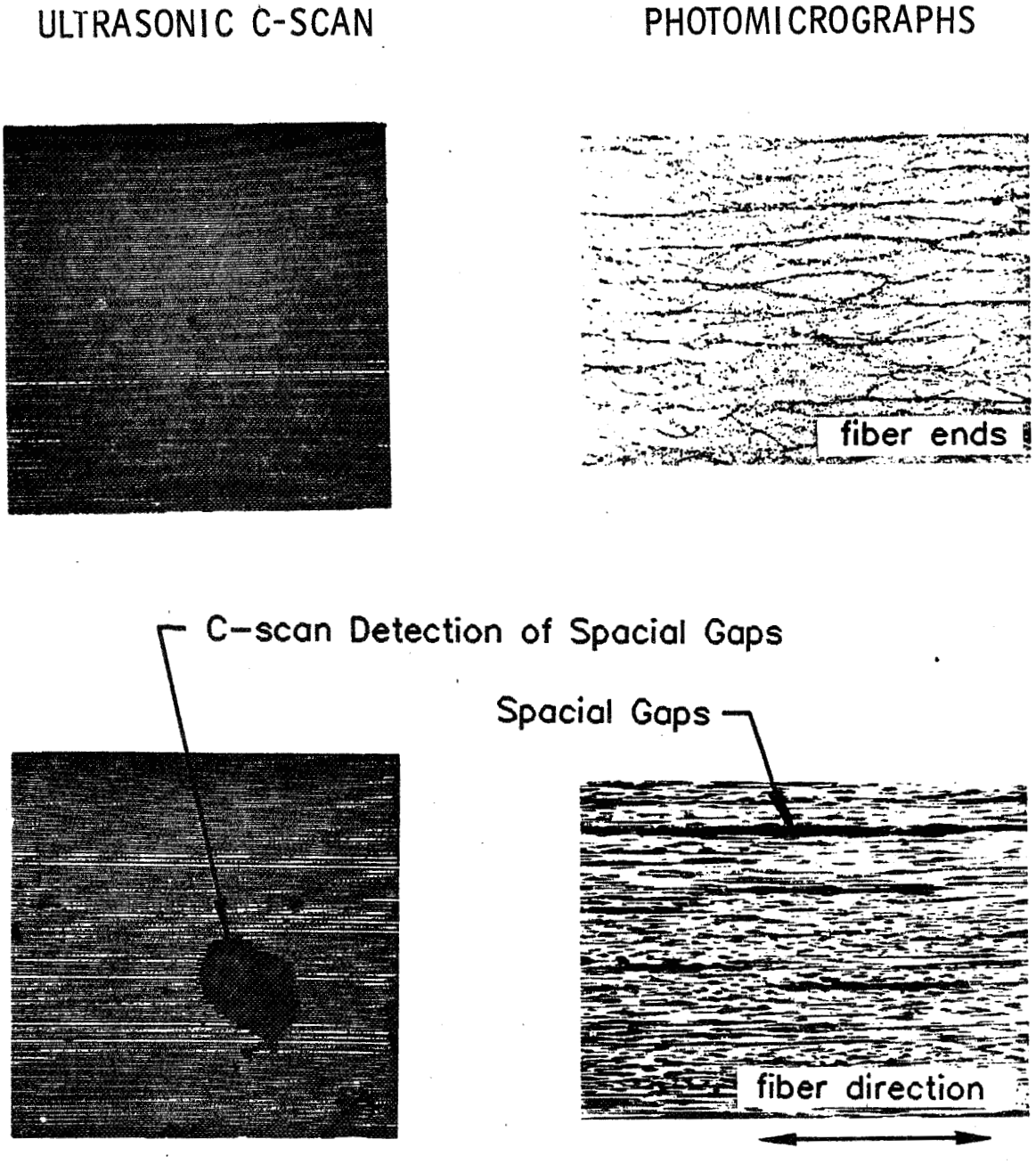

Figure 3.1 C-Scan Technique Detection of Spacial Gaps After Cure of Unidirectional Graphite/Epoxy Composite

The solvent was removed by vacuum stripping individual (i.e. not stacked) prepreg sheets at a temperature above the glass transition temperature of the resin for a 12 hour period of time. All materials were kept dry in a heated vacuum (102°C/215°F) desiccator until tested. The pertinent material properties are listed in Table 3.1.

The test samples were prepared in the following fashion:

1) Three 76.2 mm x 76.2 mm (3" x 3") square sheets of AS4/P1700 prepreg (solvent free and dry) were cut from a roll of prepreg. By matching the prepreg size with the mold cavity, fiber washout was prevented. Thus, only local deformation at the ply interfaces was allowed (i.e. global movement of resin and fibers through the thickness of the prepreg was inhibited.)
2) The prepregs $[0,90,0]_T$ were sandwiched between layers of Kapton film 0.0762 mm (0.003 inch) that had been treated with a release agent (Fig. 3.2a).
3) The specimen was placed in the mold cavity.
4) The punch was then placed in the mold cavity and the assembly placed between preheated press platens (at testing condition temperature) (Fig. 3.2b).
5) The temperature of the mold and prepreg were monitored during the test. The mold and prepreg were held at the desired temperature for a period of time sufficient to ensure a uniform temperature.
6) Pressure was then applied and the contact time was measured, starting when the desired pressure was reached.

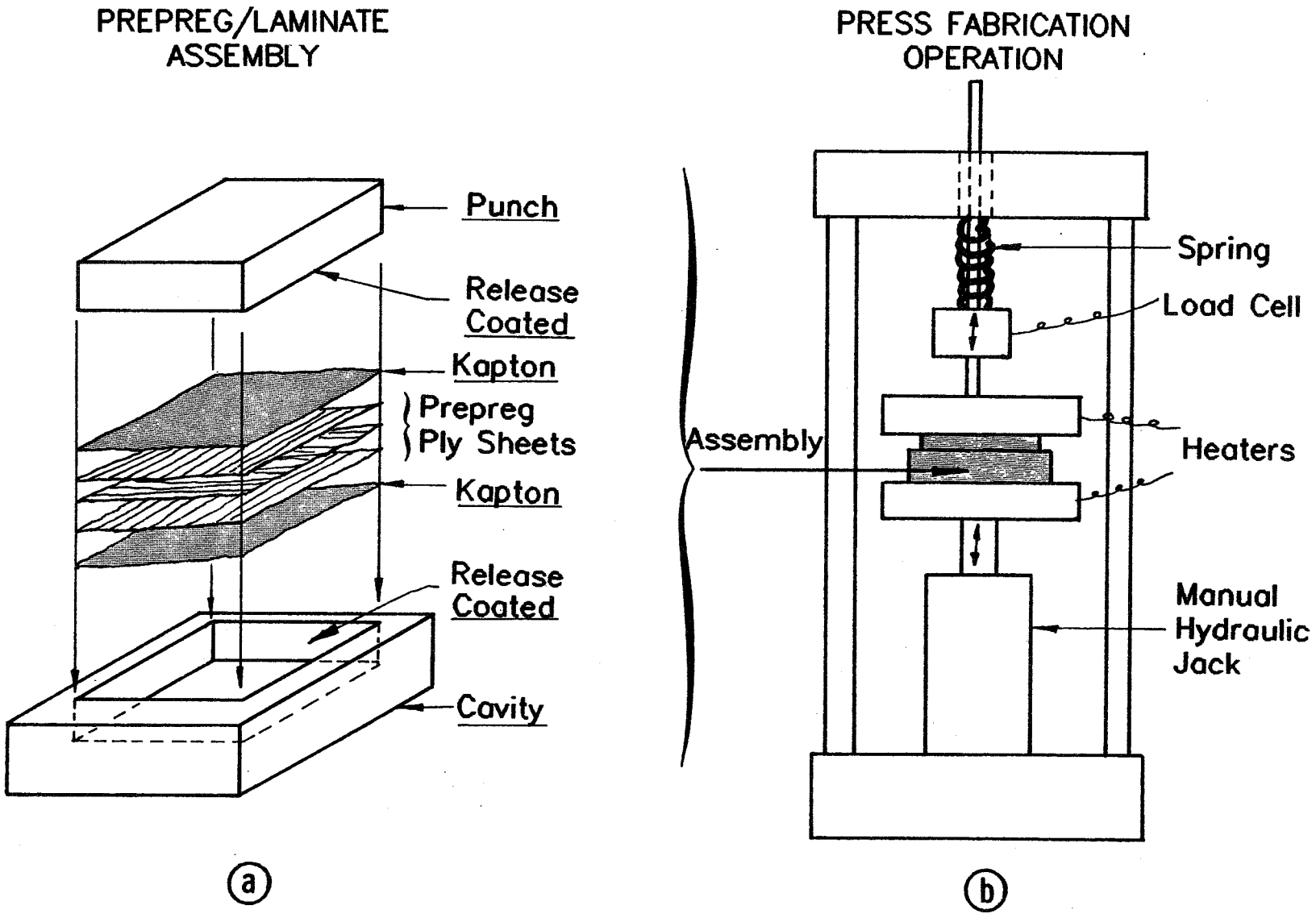

Figure 3.2 Intimate Contact Testing (a) Specimen Preparation, (b) Testing Apparatus

Table 3.1 Material Properties

	Property/Description	Value (ave.)
AS-4 graphite fiber	specific gravity	1.74
	number of fibers per tow	12,000
	fiber sizing	G
P1700 polysulfone (bead) resin	specific gravity	1.24
	glass transition temperature-Tg	194°C (381°F)
	structure of polymer	amorphous
solvent-cyclohexanone	boiling point	68.7°C (155.6°F)
prepreg	width	304.8 mm (12 in.)
	dry resin content by wt	32.3%
	volatile content by wt	19.05%
	areal fiber wt	148.8 gm/m^2

7) The pressure was released after the desired contact time had been attained.

8) The mold was removed and allowed to cool slowly to between 23.9°C - 37.8°C (75-100°F) below the T_g of the resin.

9) The sample was removed and C-scanned.

3.2.3 Testing Procedure

The C-scan data was obtained as a function of position over the top surface of each test specimen. The magnitude of the signals recorded were compared to the threshold (determined as showing spacial gaps in graphite/epoxy) indicating the locations of contact and spacial gaps at the interfaces over the entire width and length of the specimen. Plots of black and white profiles were made of each specimen reproducing the areas of contact as white and the areas of spacial gaps as black. This procedure works very well in showing the top areal view of contacting and non-contacting areas; however, it cannot be used to locate which of the two interfaces present in the $[0,90,0]_T$ laminate are not in contact, if not both. Thus, the C-scan provides only a qualitative measure of the true area of contact. A statistical interpretation of the black area is needed since it results when either of the two interfaces, or both are in contact.

The test matrix for determining the effect of the processing parameters on contact area is given in Table 3.2. The test matrix provides a temperature range from just above the T_g to a maximum allowable temperature before noticeable degradation in the properties of the prepreg are observed. The pressure range covers a range from

Table 3.2 Intimate Contact Test Matrix

		TEMPERATURE		
		240°C (465°F)	288°C (550°F)	330°C (625°F)
PRESSURE	172KPa (25 psi)	t_c = 20 min 10 5 2 1 1/2	t = 15 min 5 2 1/2	t_c = 10 min 5 2 1 1/2
	344KPa (50 psi)	t_c = 20 min 10 5 2 1 1/2	t_c = 15 min 5 2 1/2	t_c = 10 min 5 2 1 1/2
	688 KPa (100 psi)	t_c = 5 min 2 1 1/2	t_c = 15 min 5 2 1	t_c = 40 min 20 2 1 1/2

above vacuum bag pressures to a typical autoclave pressure.

3.3 Results and Discussion-IC

This section presents experimental data showing the variation of intimate contact area over the range of the processing parameters P, T, and t_c presented in Table 3.2. Also presented is a model of intimate contact area of a $[0,90,0]_T$ laminate as a function of the processing parameters. The IC model is comprised of three sub-models: 1) formulation of the viscoelastic deformation of a single tow; 2) a statistical distribution describing the prepreg geometric nonuniformity; and 3) experimental data of the neat resin viscosity is empirically extended to include the influence of the fiber on the viscoelastic response of the resin.

3.3.1 Original Data and Data Reduction

Black and white C-scans were taken of each of the specimens listed in Table 3.2. The specimens tested have two interfaces. One on each side of the middle ply in the $[0,90,0]_T$ laminate. The white areas of the C-scanned specimens are areas where intimate contact is achieved throughout the specimen thickness (i.e. both interfaces); however, the black areas do not define areas of total interfacial spacial gaps. Three conditions of spacial gaps are possible that will cause black areas to show up in the C-scan approach used. First, that both interfaces are not coalesced. Second, the top interface is not coalesced while the bottom is. Third, the bottom interface is not coalesced and the top is.

A statistical interpretation of the data will be required because the C-scanned data was obtained from specimens with two interfaces in series, and it is desired to obtain the outcome of the experiment as if one interface had been used. Intuitively, the occurrence of contact and no contact areas forming during processing will have an equal probability at either of the two interfaces. Further, one would also expect the two occurrences to be probabilistically independent and not mutually exclusive as a first approximation.

With these assertions the probability (Pr) of a contact event occurring at the top and bottom interfaces may be written as:

$$Pr_T(\text{top}) = Pr_B(\text{bottom}) \tag{3.1}$$

The joint probability of achieving contacts directly on top of one another of the two interface system may be written as:

$$Pr_J(\text{joint top and bottom}) = Pr_T \cdot Pr_B \tag{3.2a}$$

The joint probability is identically defined as the ratio of the white area to the total white and black areas of the C-scan data. The joint probability may then be written as:

$$Pr_J = \frac{WC}{WC + BC} \tag{3.2b}$$

where WC and BC denotes the white and black areas, respectively. Equation 3.3a may also be rewritten in terms of the fractions of the

white ($\overline{WC}$) and black ($\overline{BC}$) areas to a unit area such that:

$$Pr_J = \frac{\overline{WC}}{\overline{WC} + \overline{BC}} \tag{3.3a}$$

$$\overline{WC} = \frac{WC}{WC + BC} \tag{3.3b}$$

$$\overline{BC} = \frac{BC}{WC + BC} \tag{3.3c}$$

Therefore, the following relationship results:

$$\overline{BC} + \overline{WC} = 1.0 \tag{3.4a}$$

Since the C-scan data will allow the direct computation of the joint probability, Pr_J, the probability of contact occurrences of the top and bottom interfaces independent of one another can be evaluated by taking the square root of the joint probability. Thus, the degree of intimate contact for one surface, D_{IC}, may be written as:

$$Pr_B = Pr_T = D_{IC} = \sqrt{Pr_J} \tag{3.4b}$$

Table 3.3 reports the statistical degree of intimate contact D_{IC}. Plots of the data will not be presented here nor a discussion until after the model is presented. A thorough investigation and interpretation will then be made.

Table 3.3 Degree of Intimate Contact Data

PRESSURE	TEMPERATURE: 240°C (465°F)		288°C (550°F)		330°C (625°F)	
172 KPa (25 psi)	t_c = 20 min	D_{IC} = 65.5%	t_c = 15 min	D_{IC} = 73.9%	t_c = 10 min	D_{IC} = 96.2%
	10	55.8	5	65.9	5	68.8
	5	52.5	2	46.6	2	64.8
	2	24.8	1/2	21.0	1/2	36.2
	1	11.8				
	1/2	12.8				
344 KPa (50 psi)	t_c = 20 min.	D_{IC} = 95.2%	t_c = 15 min	D_{IC} = 98.6%	t_c = 10 min	D_{IC} = 86.8%
	10	83.4	5	93.5	5	99.2
	5	68.6	2	65.2	2	87.3
	2	43.0	1/2	53.2	1	93.3
	1	32.6			1/2	78.8
	1/2	24.8			1/2	78.4
688 KPa (100 psi)	t_c = 5 min	D_{IC} = 89.0%	t_c = 15 min	D_{IC} = 99.4%	t_c = 40 min	D_{IC} = 100%
	2	71.5	5	97.6	20	99.8
	1	71.6	2	91.6	2	99.8
	1/2	44.2	1	85.3	1	99.2
					1/2	86.3

3.3.2 Intimate Contact Sub-Models

An approximate model is presented for relating the processing parameters to the degree of intimate contact D_{IC}. This IC model incorporates the use of 3 sub-models:

1) a statistical distribution describing the prepreg geometric non-uniformity of tow heights;
2) a mechanics model similating the viscoelastic response of the fiber reinforced resin to the compressive loading typical of thermoplastic matrix composite processing; and
3) an assumed constitutive relationship for the viscosity of the resin, as well as, an assumed relationship simulating the fibers influence on the viscosity of the neat resin. These sub-models have been merged in a final IC model formulation.

The model has been constructed from physical reasoning of the observations made while processing, as well as, from some intuitive speculation.

No global flow (i.e. fiber washout or resin bleed) of the laminate was observed for the processing conditions tested; therefore, the coalescence must be occurring as a local deformation at the ply interfaces. Because the laminates were thin, (3 ply) the prepreg geometric non-uniformity showed up on the outer surfaces by scattering the ambient light nonuniformly when underprocessed. Increased areas of contact were observed to grow parallel to the fiber by C-scan and surface reflection methods. This resulted in a checkerboard pattern

in the case of cross-ply laminates. The formation of the checkerboard pattern occurred in a random piecewise manner over the areal surface of the laminate and not necessarily uniformly. For these reasons the IC model should incorporate for its foundation a sub-model that simulates the uniformly distributed compressive loading of a single unidirectional tow, normal to the top and bottom surfaces. The local deformation model must also be a function of the viscoelastic properties of the resin and fiber.

Intuitively, one would expect prepregs of greater or lesser tow uniformity to influence the quality of the laminate for a given set of processing parameters (i.e. prepregs of greater nonuniformity are expected to take longer to process to achieve quality laminates). For this reason the model should also include a description of the prepreg's tow geometry as input.

Figure 3.3 shows a flow chart of the model formulation. A detailed description of each sub-model follows.

3.3.2a Mathematical Description of Prepreg's Geometric Nonuniformity-Sub-Model

The importance of tow heights varying across the width of a prepreg has already been pointed out. Presented here is the method for obtaining the tow height distribution for the prepreg.

Figure 3.4 shows the assumed geometry of the prepreg tow cross-section. The cross-sectional area A_i of each tow is constant, while the subscript i denotes the tow number and q is the number of tows.

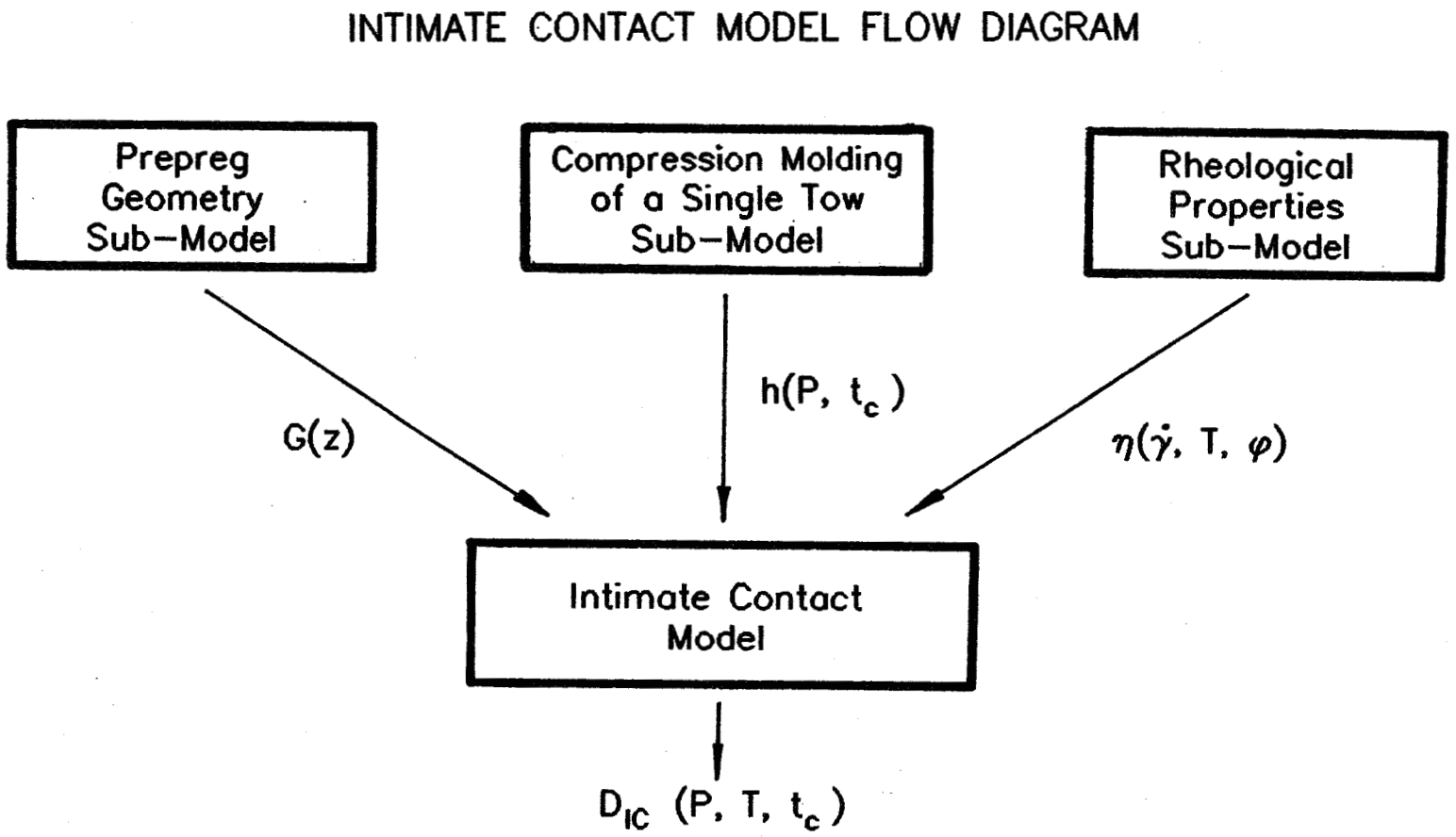

Figure 3.3 Model Formulation Flow Diagram

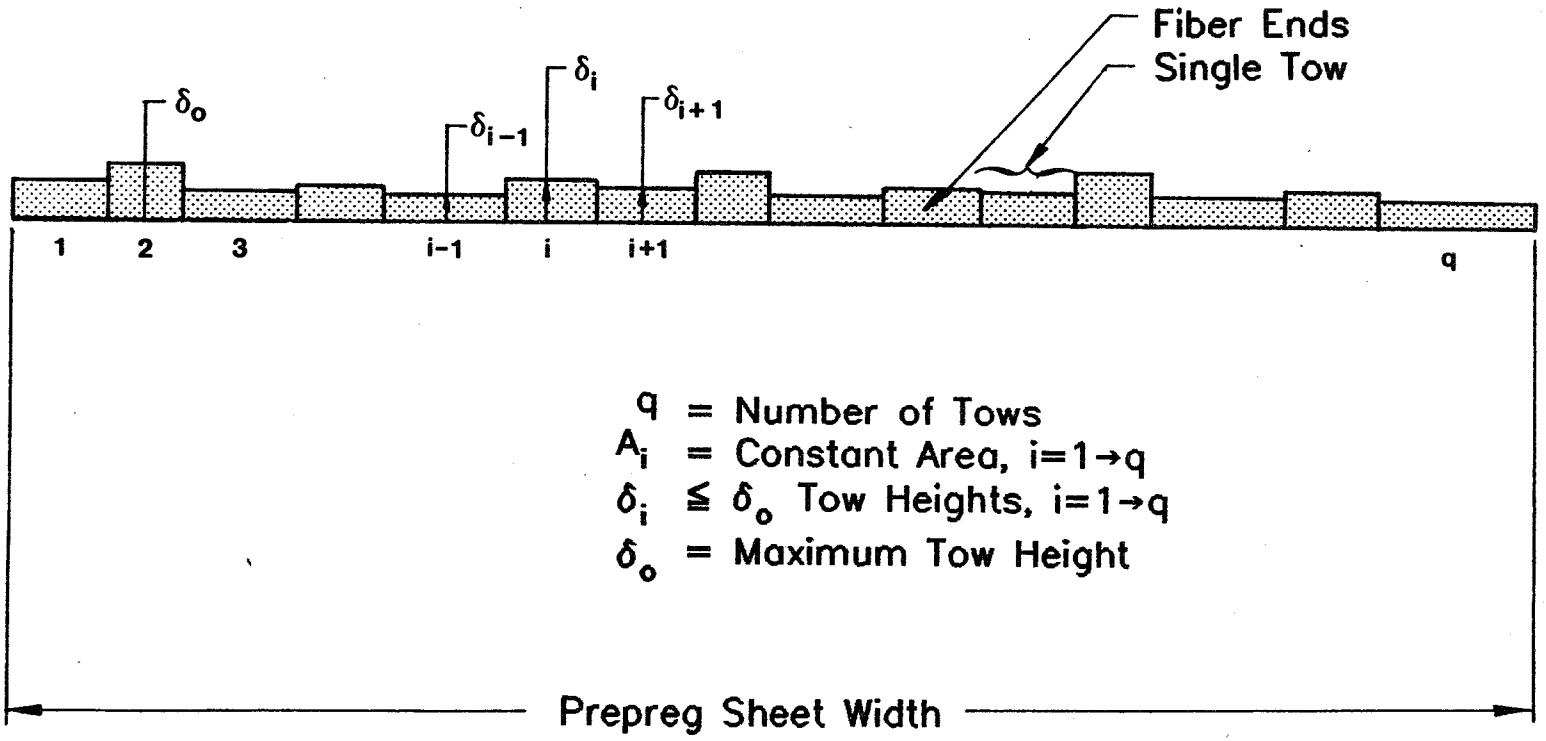

Figure 3.4 Schematic of Prepreg Geometry

The heights in the model are also assumed to be constant along each tow width although in reality this is not true.

The prepreg tow heights were measured with a micrometer to the nearest thousandth of an inch. Each tow height was measured across a twelve inch width prepreg sheet perpendicular to the fibers. Measurements were made once every foot over a five foot length of prepreg. No appreciable difference in tow height variation was observed along the length of a single tow. The tow heights, δ_i, were then normalized to the largest tow height δ_o according to Eq 3.5.

$$\bar{z}_i = - \frac{\delta_i - \delta_o}{\delta_o} \tag{3.5}$$

A histogram of the tow height data is shown in Fig. 3.5. This figure shows the percent tows within the interval of tow heights shown. A two parameter Weibull function was fit to the histogram shown as the solid line in Fig. 3.5. The Weibull density function, $g(\bar{z})$, is defined in Eq 3.6 along with the values of the constants used to fit the data

$$g(\bar{z}) = \left(\frac{\alpha}{\beta}\right) \left(\frac{\bar{z}}{\beta}\right)^{\alpha-1} \exp\left[-\left(\frac{\bar{z}}{\beta}\right)^{\alpha}\right] \tag{3.6}$$

where: $\alpha = 2.25$ shape parameter

$\beta = 0.1108$, scale parameter

The cumulative distribution (Eq 3.7) is defined as:

$$G(\bar{z}) = \int_0^{\bar{z}} g(s)ds \rightarrow 1 - \exp\left[-\left(\frac{\bar{z}}{\beta}\right)^{\alpha}\right] \tag{3.7}$$

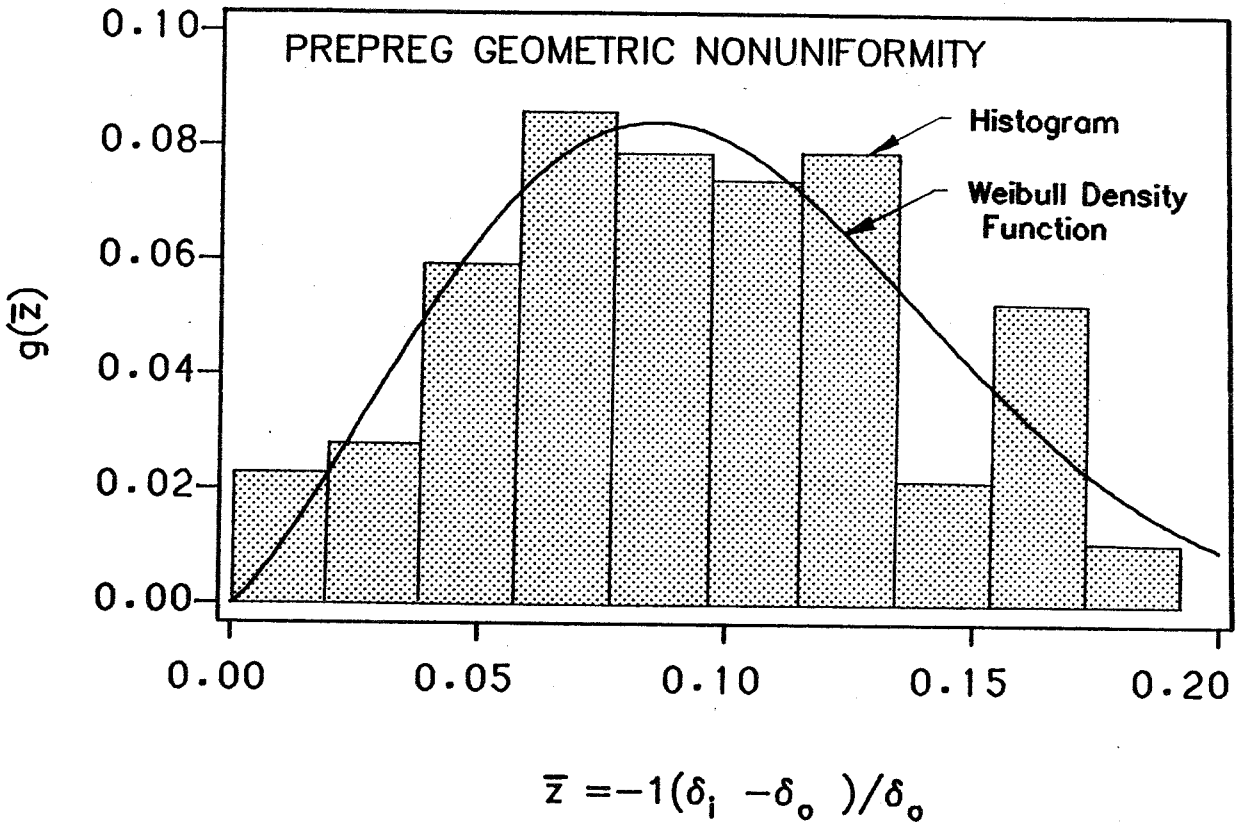

Figure 3.5 Weibull Density Model of Prepreg Geometric Nonuniformity with Histogram

The function $G(\bar{z})$ defines the total number of tows having height greater than or equal to δ_i. As will be pointed out later, $G(\bar{z})$ is the degree of intimate contact as a function of tow height or $\bar{z}$. The viscoelastic response of a single tow subjected to compression loading normal to the fiber direction will couple $G(\bar{z})$ with time through the time dependency of $\bar{z}(t)$.

3.3.2b Compression Molding of a Single Tow-Sub-Model

Presented here is the derivation of the viscoelastic flow response of a single tow subjected to compression molding as a function of the processing parameters, pressure, temperature ($>T_g$) and contact time. This sub-model is the foundation of the intimate contact model. It defines the rate at which the tow deforms (i.e. fiber/resin squeezes) between two parallel and uniformly distributed compressive loads through the inherent temperature sensitive viscoelastic material properties.

Figure 3.6 shows the coordinate system used for the sub-model. Based on experimental observations during compression molding of laminate samples, the following postulates were assumed in the derivation:

1) The combined fiber/resin deformation perpendicular to the fiber direction (x-direction) dominates any local resin flow taking place parallel to the fiber.
2) Negligible resin flow from the tow occurs in all directions, maintaining the same fiber/matrix distribution within a

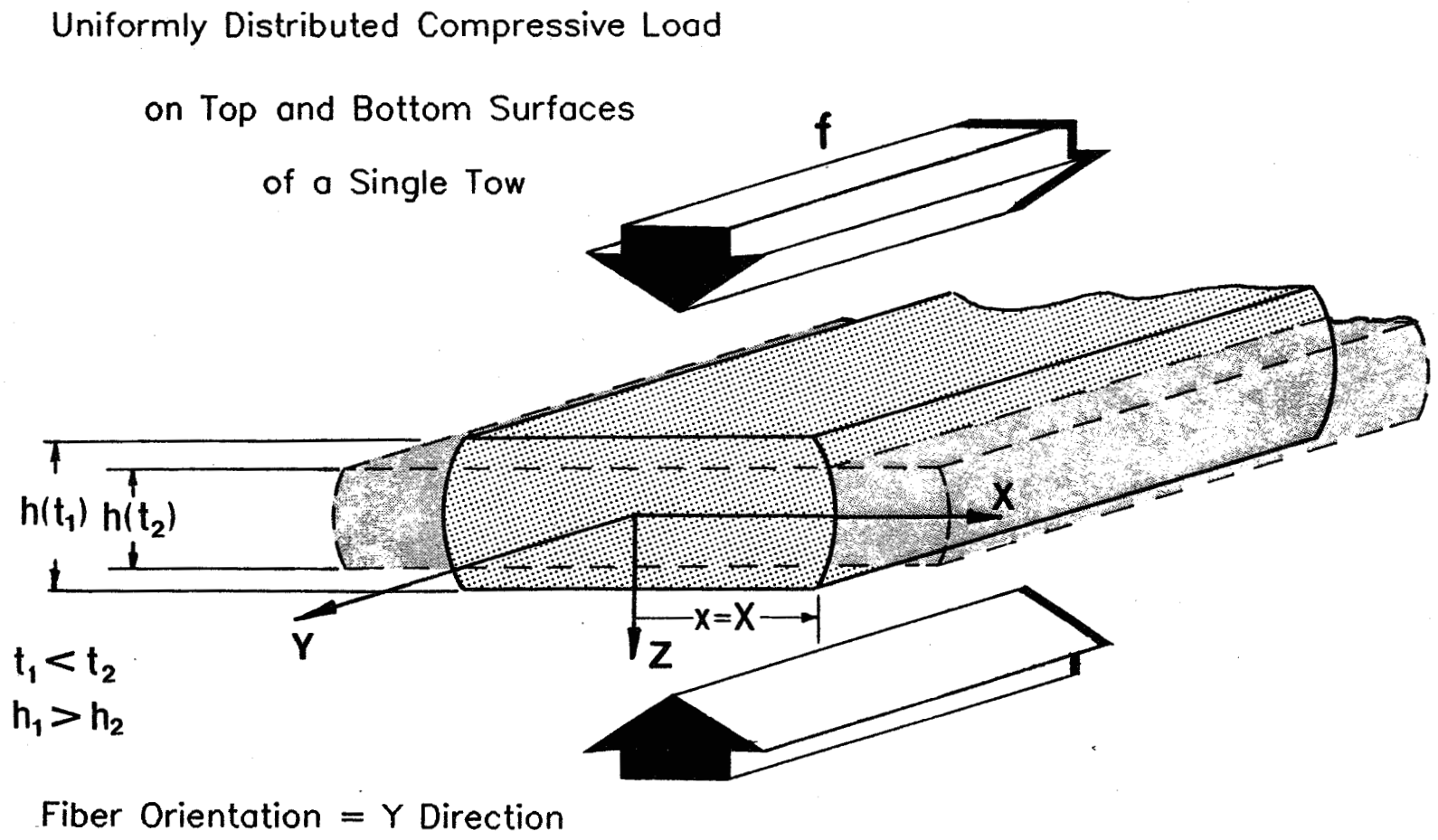

Figure 3.6 Geometry of a Single Tow Subject to Uniform Compressive Loading Normal to XY Planes of Top and Bottom Surfaces

ply. This is due to the high fiber volume fraction v_f = 68%, and the high viscosity of the resin.

These two observances are untypical for most thermosetting resin composites in that the lowest viscosity of the P1700 resin exceeds the gel point of an epoxy matrix composite.

The analysis that follows is based on the assumption that the problem can be treated as a viscometric flow. In viscometric flows time-dependent elastic effects are not considered. If the fluid relaxation time is small with respect to the time required for the fluid to deform around fibers, the fluid will accommodate quickly and no elastic effects would be observed [18].

In an analogous study of neat polymer flows under squeeze loading, (i.e. parallel plate plastometer) Grimm [19] has shown experimentally that by restricting the test to slow squeezes, the assumption of steady shear was found to be adequate, and that useful viscosity measurements could be obtained.

The derivation presented here parallels the derivation presented by Bird et. al. [20] in the study of the viscosity properties of polymers under squeeze loading between parallel plates. The coordinate system for that study was cylindrical. Dienes and Klemm [21] have derived the rheological equations for a Newtonian fluid subject to the parallel plate plastometer loading. Kataoka et. al. [22] derived rheological equations for a power-law fluid. Dealy [23] gives a good history in the development of squeezing flow rheology.

From the previously described observances, assumptions shown in Eq 3.8 are made regarding the velocity field and the pressure:

$$v_x = v_x(x,z)$$

$$v_z = v_z(z)$$

$$v_y = 0$$

$$p = p(x) \tag{3.8}$$

From the assumed velocity field the components of the rate-of-strain tensor are:

$$\dot{\underset{\approx}{\gamma}} = \begin{bmatrix} \dot{\gamma}_{xx} & \dot{\gamma}_{xz} & 0 \\ \dot{\gamma}_{xz} & \dot{\gamma}_{zz} & 0 \\ 0 & 0 & 0 \end{bmatrix} ; \quad \dot{\gamma}_{xx} = 2\frac{\partial v_x}{\partial x} , \ \dot{\gamma}_{zz} = 2\frac{\partial v_z}{\partial z} , \ \dot{\gamma}_{xz} = \frac{\partial v_x}{\partial z} \tag{3.9}$$

Also, assuming that the non-Newtonian effects result predominately from the shearing components rather than the elongational effects, the diagonal components in Eq 3.9 can be neglected. Therefore, the rate-of-strain tensor reduces to the following:

$$\dot{\underset{\approx}{\gamma}} = \dot{\gamma}_{xz} \begin{bmatrix} 0 & 1 & 0 \\ 1 & 0 & 0 \\ 0 & 0 & 0 \end{bmatrix} ; \quad \dot{\gamma}_{xz} = \frac{\partial v_x}{\partial z} \tag{3.10}$$

The equation of continuity is:

$$\underset{\sim}{\nabla} \cdot \underset{\sim}{v} = 0 \rightarrow \frac{\partial v_x}{\partial x} + \frac{\partial v_z}{\partial z} = 0 \tag{3.11}$$

The equations of motion are (neglecting inertia terms);

x-direction
$$\underline{\frac{\partial \tau_{xx}}{\partial x}} + \frac{\partial \tau_{zx}}{\partial z} + \frac{dp}{dx} = 0 \qquad (3.12)$$

z-direction
$$\underline{\frac{\partial \tau_{xz}}{\partial x}} + \underline{\frac{\partial \tau_{zz}}{\partial z}} = 0 \qquad (3.13)$$

The 1st dashed-underlined term in Eq 3.13 is dropped because the flow is assumed to be locally and instantaneously under steady shear between two fixed planes, (i.e. uniform x-dir.). The remaining dashed underlined terms in Eqs 3.12 and 3.13 are elongational stresses which are assumed to have minor importance compared to the shear stress.

The constitutive equation assumed is the power-law fluid. It is a 'generalized Newtonian fluid' (GNF) constitutive equation which assumes: 1) the viscosity is strain rate dependent, 2) only shear strain rate components exist, and 3) the shear strain rate is independent of time. The power-law equation is written as:

$$\tau_{ij} = - m\left(\frac{1}{2}\left[\dot{\gamma}_{xx}^2 + \dot{\gamma}_{zz}^2 + 2\dot{\gamma}_{xz}^2\right]\right)^{\frac{n-1}{2}} \dot{\gamma}_{ij} \qquad (3.14)$$

where m (units of shear viscosity-poise) and n (dimensionless) are constants used to describe the shear rate dependency of the polymer. Kataoka [22] has shown this approximation to be acceptable if a test does not span too wide a range of low shear rates. The value of n is evaluated from the constant slope of the log-log plot of η versus $\dot{\gamma}$.

An assumed velocity distribution given by Eq 3.15

$$v_x = xf(z) \tag{3.15}$$

will satisfy the equation of continuity. Integrating the equation of continuity (Eq 3.11) over the boundary from 0 to h/2 (tow height) and 0 to x (1/2 tow width), and observing quarter symmetry it is shown:

$$\int_0^{\frac{h}{2}} \int_0^x \frac{\partial v_x}{\partial x} \, dxdz + \int_0^{\frac{h}{2}} \int_0^x \frac{\partial v_z}{\partial z} \, dxdz = 0 \tag{3.16a}$$

$$\int_0^{\frac{h}{2}} v_x dz + x\dot{h} = 0 \tag{3.16b}$$

where; $\dot{h} = v_z$ at $z = h/2$.

Substituting the power-law Eq 3.14 in to the x-direction equation of motion yields:

$$\frac{\partial(-m\dot{\gamma}_{xz}^n)}{\partial z} + \frac{dp}{dx} = 0 \; . \tag{3.17}$$

Substituting $\frac{\partial v_x}{\partial z}$ for $\dot{\gamma}_{xz}$ from Eq 3.10, integrating with respect to z, and imposing the boundary conditions $\frac{\partial v_x}{\partial z} = 0$ at $z = 0$ and $v_x = 0$ at $z = h/2$ it is shown:

$$v_x = \frac{(h/2)^{\left(\frac{n+1}{n}\right)}}{\left(\frac{n+1}{n}\right)} \left(-\frac{1}{m}\frac{dP}{dx}\right)^{\frac{1}{n}} \left[1 - \left(\frac{z}{h/2}\right)^{\left(\frac{n+1}{n}\right)} \right] \tag{3.18}$$

Substituting Eq 3.18 into Eq 3.16b it is shown:

$$\left(-\frac{1}{m}\frac{dP}{dx}\right)^{\frac{1}{n}} = \frac{-\dot{h}\, x}{\left(\frac{h}{2}\right)\left(\frac{2n+1}{n}\right)} \left(\frac{2n+1}{n}\right) \tag{3.19}$$

Substituting Eq 3.19 into Eq 3.18 it is shown:

$$v_x = \frac{-2\dot{h}}{h}\left(\frac{2n+1}{n+1}\right)\left[1 + \left(\frac{z}{h/2}\right)^{\left(\frac{n+1}{n}\right)}\right]X \tag{3.20}$$

Integrating Eq 3.19 for pressure with the boundary condition $p = p$ at x, $p = p_a$ at $x = X$ (X = 1/2 tow width) it is shown:

$$p(x) - p_a = \frac{(-\dot{h})^n}{\left(\frac{h}{2}\right)^{2n+1}}\left(\frac{2n+1}{2n}\right)^n \frac{mX^{n+1}}{n+1}\left[1 - \left(\frac{x}{X}\right)^{n+1}\right] \tag{3.21}$$

Evaluating the force f applied to the tow shown in Fig. 3.6, and integrating over the top and bottom surfaces of the tow it is shown:

$$f = 2\int_0^X \left[(p - p_a) + \tau_{zz}\right]\Big|_{z = \frac{h}{2}} dx\ , \tag{3.22}$$

where τ_{zz} was determined to be zero at $z = h/2$ by previous assumptions, as well as, mathematically by substitution of the constitutive equation (Eq 3.14) into the equation of continuity (Eq 3.11). Thus τ_{zz} at $z = h/2$ can be written as:

$$\tau_{zz}\Big|_{z = \frac{h}{2}} = 0 \tag{3.23}$$

Substituting Eqs 3.21 and 3.23 into Eq 3.22 and evaluating f it is shown:

$$f = 2m\left(\frac{1 + 2n}{n}\right)^n \left(\frac{(-\dot{h})^n}{\left(\frac{h}{2}\right)^{(2n + 1)}}\right) X^{(n+2)} \left(\frac{1}{n + 2}\right) \tag{3.24}$$

Although the applied force is constant over time, X(t) is not. However, noting that the cross-sectional area A_i of the tow remains constant with time Eq 3.25 can be substituted into Eq 3.24 to eliminate X(t) as a function of time.

$$2h(t) \cdot X(t) = A; \quad A = \text{constant for } t \geq 0 \tag{3.25}$$

Therefore,

$$f = 2^n m \left(\frac{1 + 2n}{n}\right)^n \frac{(-\dot{h})^n}{h^{(3n + 3)}} A^{(n + 2)} \left(\frac{1}{n + 2}\right) \tag{3.26}$$

Equation 3.26 describes the compression of a tow as a function of the strain rate dependent viscosity, the applied force, the tow height, and time. Thus, all processing parameters are now related through the rheological flow phenomena and the viscoelastic properties of the resin.

3.3.2c Rheological Material Properties

This section presents the shear viscosity data of the neat P1700 resin data as a function of shear rate. The temperature effects on viscosity are presented by the WLF Eq 3.27. Also presented is an assumed relationship for viscosity, simulating the effects of fiber reinforcement on the polymer observed by investigators in the field of rheology [24]. A detailed explanation addressing the experiment, and data reduction scheme is given in Appendix A.

Figure 3.7 presents the steady $(\eta(\dot{\gamma}))$, and complex $(\eta^*(\omega))$ viscosity as a function of the rate-of-strain $(\dot{\gamma})$ or frequency (ω). As a first approximation, use of the Cox-Merz Law allows a direct relationship between the complex viscosity and steady shear viscosity with the frequency and the rate of shear strain, respectively. The viscosity/temperature relationship for the P1700 resin is expressed by the WLF equation given by Eq 3.27

$$\log\left(\frac{\eta}{\eta_{ref}}\right) = -\frac{C1(T - T_{ref})}{C2 + (T - T_{ref})} \qquad (3.27)$$

$$C1 = 5.714$$

$$C2 = 54.309$$

where; T is the temperature being observed, T_{ref} is the reference temperature (220°C(428°F)), and η_{ref} is the viscosity at the reference temperature and η is the viscosity at temperature T.

Various researchers [24,25,26] have studied the influences of particle and fiber reinforcements on the viscosity of the neat resin. The shear rate dependence of the viscosity of the reinforced polymer is additionally complicated because the non-Newtonian property of the resin is superposed on the non-Newtonian effect due to the reinforcement. Bartenev and Zakharenko [27] have observed that higher concentrations of carbon black in polyisobutylene resulted in approaching infinite shear viscosity at low shear stresses and exhibiting a yield value. However, White et. al. [26] reported that yield values are not present in all reinforced systems as Chapman

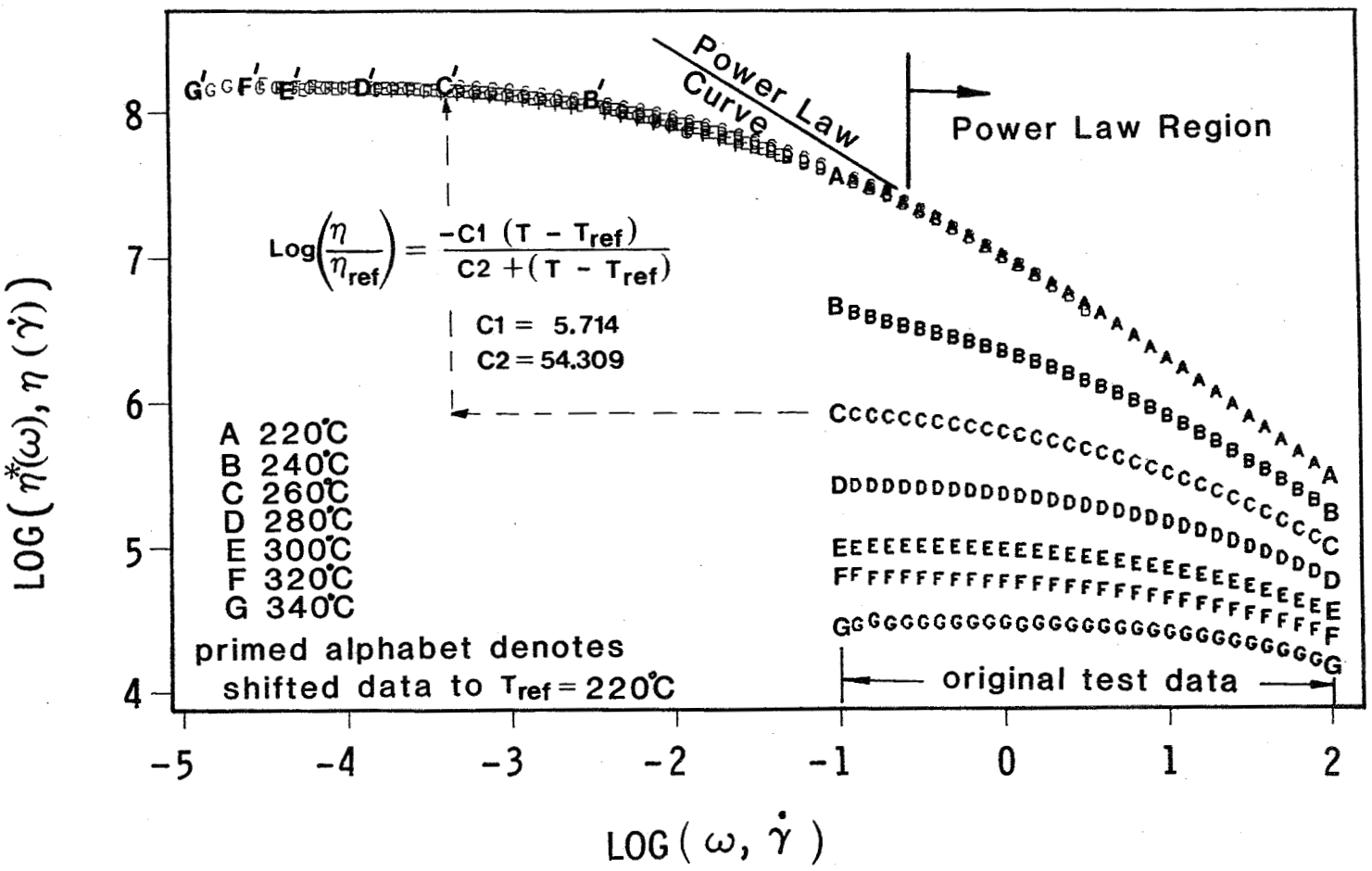

Figure 3.7 Complex Viscosity versus Frequency and Steady Shear Viscosity Versus Rate of Strain Using Cox-Merz Rule

and Lee [28] have observed with glass fiber and bead reinforced high polymers. Matsumoto [29] reported that the concentration effects on viscosity may be temperature sensitive. Kataoka et. al. [24] has experimentally shown that the viscosity of fiber (length to dia. ratio of carbon fiber = 600) and particle reinforced polymers increases and acts more non-Newtonian (i.e. more strain-rate dependent) at lower shear rates relative to the neat polymer. Also shown, was that higher concentrations of reinforcement of the polymer ϕ resulted in higher magnitudes of viscosity. Defining, η_r as the ratio of the fiber reinforced resin viscosity to the neat resin viscosity, Kataoka et. al. [24] have shown good superposition of viscosity versus shear rate data at increasing concentrations of reinforcement ($0 < \phi < 0.65$).

From the above cited works, the effects of fiber reinforcement on the neat resin viscosity (Fig. 3.7) are assumed to take the following form as a first approximation. For a power-law fluid defined in Eq 3.14 the curves in Fig. 3.7 shift to higher viscosities at lower shear rates for the higher fiber concentration present in the study (v_f = 68%). This shift is shown as the temperature (T) and concentration (ϕ) dependent variable c (reinforcement/viscosity influence factor) in Eq 3.28 which is analogous to the reduced viscosity defined earlier.

$$c(T,\phi) = \frac{\eta(T,\dot{\gamma},\phi)}{\eta(T,\dot{\gamma},0)} \quad \begin{matrix}\text{(fiber filled resin)} \\ \text{(neat resin)}\end{matrix} \tag{3.28}$$

This model will be taken as is. Its use in the intimate contact model is only for illustrating viscoelastic tendencies for model

justification. Obviously, future work in the area is needed to obtain a better understanding of the influence of fiber reinforcement on the resin viscosity.

3.3.3 Intimate Contact Model

3.3.3.a Problem Formulation

Presented here is a physical interpretation by which prepregs coalesce at the interfaces during the processing of a thermoplastic matrix composite laminate. Recalling the three sub-models that make up the intimate contact model (refer to Fig. 3.3) construction can now begin.

Figure 3.8 shows the geometry of the prepreg as applied to the intimate contact model, and implies the following: 1) all tows are not in contact initially, but progressively increase with time, 2) the tows act independently concerning the disruption of flow, however, not independently concerning the input of loading, and 3) only slow, steady, and small deformations exist.

The first assertion seems justified from the non-uniformity of coalesced interfacial surfaces observed from the C-scan data. The first statement of the second assertion was assumed to allow for a closed form solution as a first approximation. Its justification lies in the already assumed existence of slow, steady, small deformations as stated in the third assertion. The later statement of the second assertion seems justified on the grounds that only shear thinning viscosity reponses were experimentally observed on the neat resin,

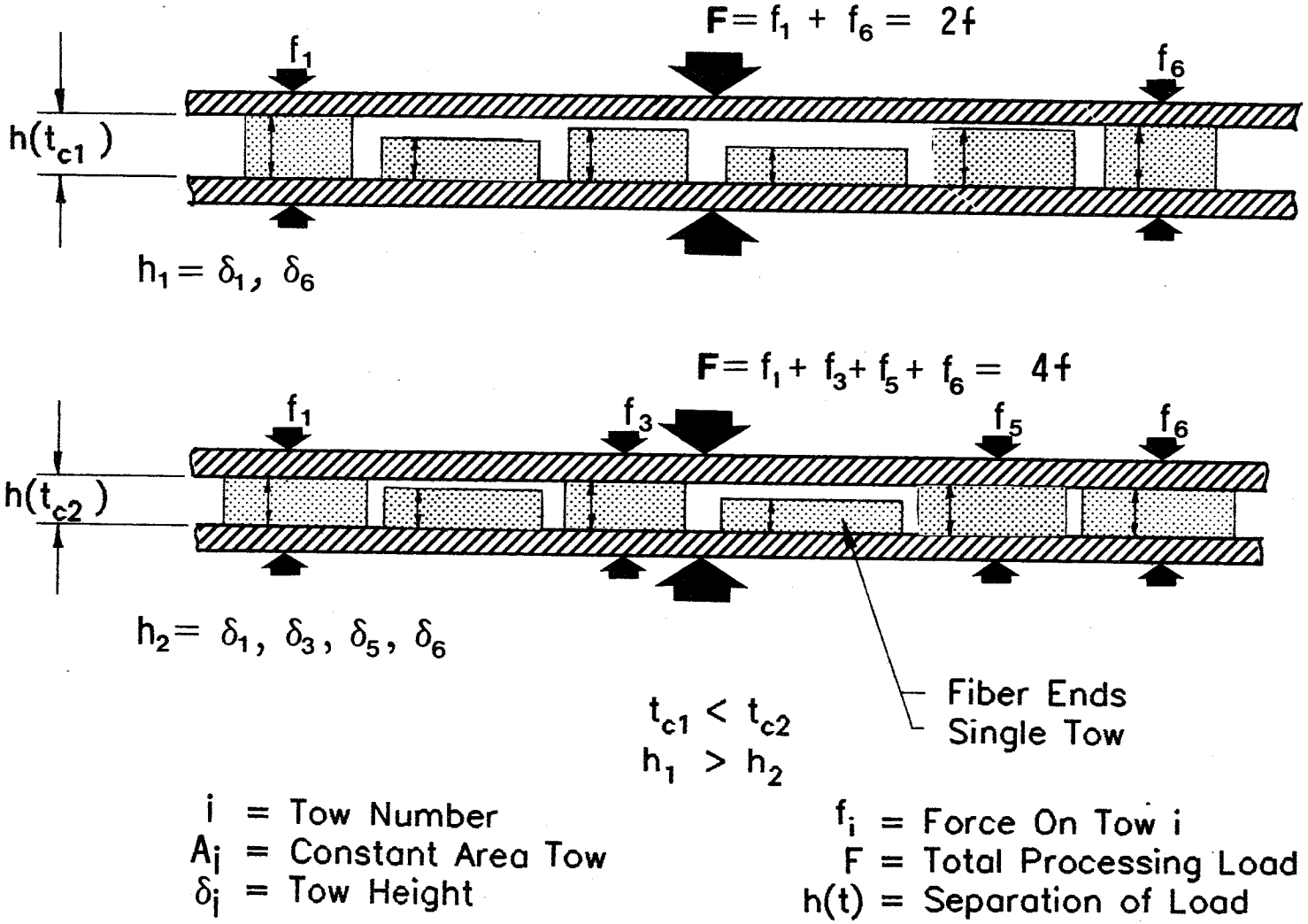

Figure 3.8 Intimate Contact Model Formulation of Prepreg Geometry

(Fig. 3.7) (also expected of fiber reinforced viscosity [24,26,29]) and that, if the force per tow was kept constant with time then dilatent viscosity responses would be the result.

3.3.3b Mathematical Model

Figure 3.8 shows the progressive nature of the distribution of the applied force F (constant in time) to the individual force per tow, f, as a function of time. It is assumed that F is distributed evenly to those tows in contact only. Thus, the following definition is given in Eq 3.29 where the viscosity coefficient m (Eq 3.14) will now be premultiplied by the c (the reinforcement/viscosity influence factor given in Eq 3.28) to simulate the tow's viscosity:

$$F = \sum_{i=1}^{q} f(h(t),\delta_i) \; ; \text{ if } \begin{cases} \delta_i < h(t) & f = 0 \\ \delta_i \geq h(t) & f = \text{finite} \end{cases} \qquad (3.29)$$

where;

$f \equiv$ is the load per tow,

$\delta_i \equiv$ is the individual tow height,

$h(t) \equiv$ is the spacing between the plates as a function of time,

$q \equiv$ is the total number of tows across the specimen width

Knowing that the cumulative distribution function $G(\bar{z})$ discerns between tows in contact and tows not in contact Eq 3.29 can be written as:

$$F = G' \, [G(\bar{z}(t))f \tag{3.30}$$

where;

$$G' \equiv \frac{G(\bar{z}(t)) + N1}{1 + N1}$$

$$N1 = \frac{NI}{1 - NI}$$

NI = initial fraction of tows in contact (3% for all test)

G = Eq 3.7

$\bar{z}$ = Eq 3.5

f = Eq 3.26

Writing Eq 3.30 in full form we have:

$$F = 2^n \{ \frac{1 - \exp[-(\frac{\bar{z}}{\beta})^{\alpha}] + N1}{1 + N1} \} \; c \; m \; (\frac{1 + 2n}{n})^n \; \frac{(-\dot{h})^n}{h^{(3n+3)}} \; A^{(n+2)} \; (\frac{1}{n + 2}) \tag{3.31}$$

Equation 3.31 is the intimate contact formulation relating the processing parameters, and the viscosity to the degree of intimate contact D_{IC} via the squeeze flow phenomenon of a prepreg. The pressure P enters into the solution through F, the temperature T enters into the solution through its influence on the viscosity, the viscosity $\eta(\dot{\gamma},T,\phi)$ enters into the solution through the parameters m, $c(\phi,T)$, and n, and the prepreg's geometry enters into the solution

in the form of G'. G' is the degree of intimate contact numerically solved for as a function of time (Eq 3.32).

$$G'(t) = D_{IC}(t) \tag{3.32}$$

3.3.4 Intimate Contact Model/Experimental Correlation

3.3.4a Discussion

This section presents a comparison of the intimate contact model (Section 3.3.3) with the experimental data (Section 3.3.1). The following discussions are addressed: 1) the method by which the model was fitted to the data through the assumed viscosity relationships, 2) the validity of the observed viscoelastic responses of the viscosity relationships with those responses expected by rheological theory, 3) the influences of the processing parameters on the degree of intimate contact, and 4) the influences of the prepreg's geometric nonuniformity on the degree of intimate contact.

Because of the lack of experimental data for the shear viscosity of the fiber reinforced P1700 resin, the values of c and n were determined by fitting the model's response to the intimate contact test data over the range of the processing parameters. The viscosity coefficient m, represents the viscosity of the neat resin, which is a function of temperature. The values of c and n cannot be uniquely determined from one set of pressure and temperature processing conditions. However, certain expected trends should be observed for the relative values of c and n when comparing whole sets of

experimental data at different temperature and pressure processing conditions.

The variable c is expected to be a function of temperature [26]. The value of n is expected to be a function of the pressure since increasing pressure results in expanding the range of shear rates present during the testing period. Kataoka et. al. [24] has shown that n may be a function of test time depending on the pressure and material tested. This assertion seems justified in that the power-law constitutive equation, Eq 3.14, describes only the straight portion of the viscosity data shown in Fig. 3.7, and does not allow for zero shear rate viscosity or characteristic time (i.e. horizontal portion of curve and transition region respectively [19,22]). Nevertheless, the power-law relationship will be used for the current study.

Since the absolute values of c and n are not deterministic from the intimate contact data for the present model (i.e. two unknown constants for every set of processing P and T conditions) the power-law exponent n was arbitrarily set to one (i.e. Newtonian n = 1) for the lowest pressure studied (P = 172 KPa (25 psi)) for each temperature condition.

The choice of n = 1 for the P = 172 KPa (25 psi) data allows the higher processing pressures to be evaluated in a relative sense for non-Newtonian shear thinning responses. The higher pressure data should exhibit a more non-Newtonian response.

With the selection of n = 1 for each set of intimate contact data having a specified temperature and an applied pressure of 172 KPa (25

psi), the value of c was then obtained by fitting the model to the data. This was repeated for each set of temperature data with P = 172 KPa (25 psi). Also, because c is a function of T, the values were kept constant for each processing temperature while the value of n was used to fit the data for the higher processing pressures.

Figure 3.9 plots the degree of intimate contact versus the processing contact time at the various pressure and temperature conditions listed in Table 3.1. Shown on each plot are the power-law exponent n and the reinforcement/viscosity influence factor c used to fit the data, and the power-law viscosity coefficient m obtained from the neat resin data. The statistical distribution defining the prepreg's geometric non-uniformity, $g(\bar{z})$, was held constant for all the tests. The effects of pressure (holding temperature constant) can be observed by comparing the plots forming a vertical column. The effects of temperature (holding pressure constant) can be observed by comparing the plots forming a horizontal row. The better fit to data is observed at higher pressures when a greater shear rate dependent viscosity is used. This is to be expected. Good correlation exists between theory and experiment over the entire spectrum of contact time for each set of pressure and temperature conditions. It is observed that both pressure and temperature have a dramatic influence on the time required to achieve 100% intimate contact.

The values of n and c were determined by fitting the data, and cannot be obtained using the present model and testing method. However, the relationships between the power law exponent, n with P,

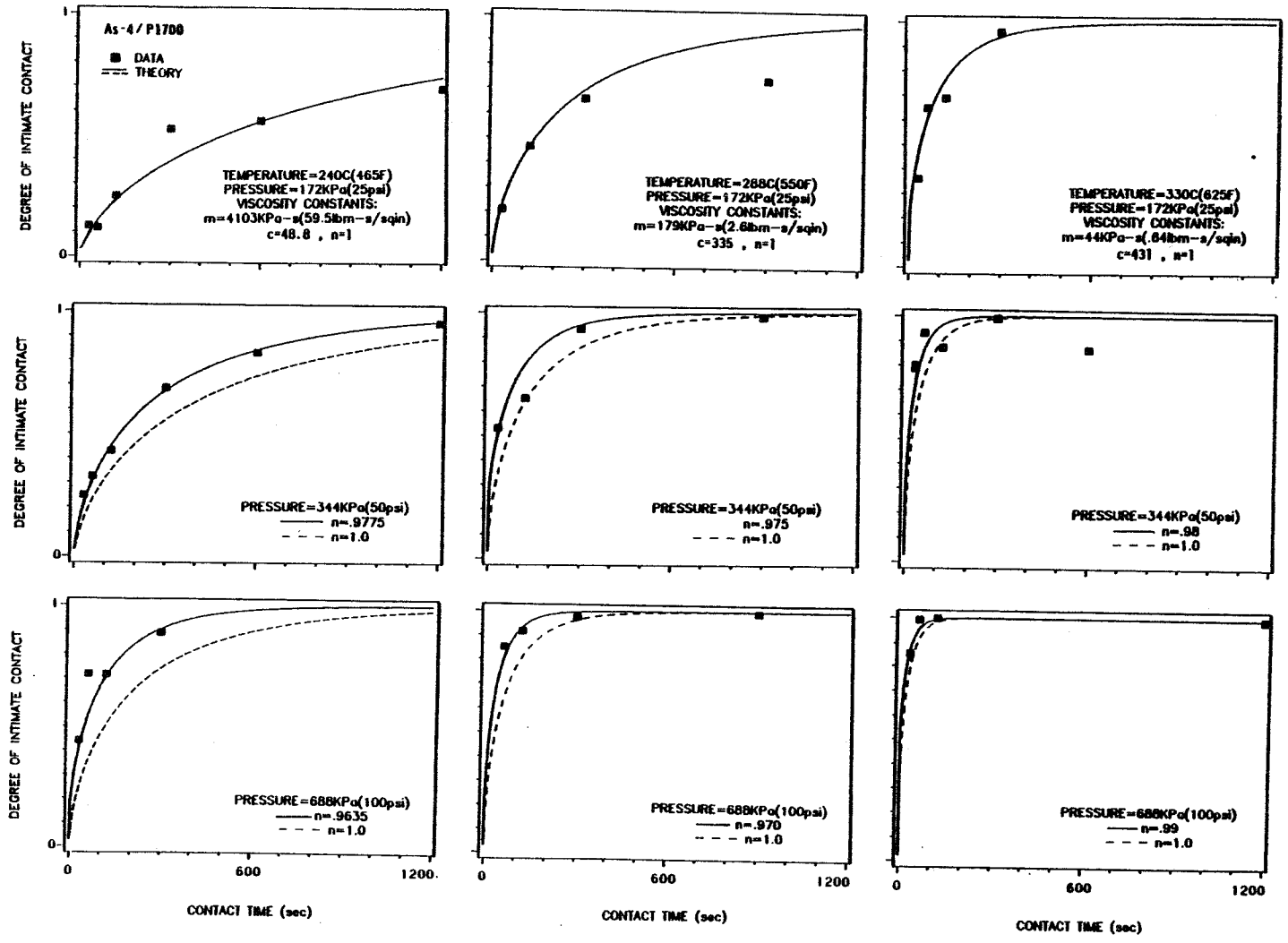

Figure 3.9 Comparison Between Intimate Contact Theory and Test Data

and the reinforcement/viscosity influence factor, c with T have viscoelastic significance.

Concentrating on the values of n first, it is noted that within the realm of experimental error n decreases with increasing pressure for each set of temperature data, exhibiting increasing shear thinning with P [24]. This is expected if too large a range of shear rates is covered over the test period, as observed by Kataoka. Also, because n is not constant among the three applied processing pressures tested, the tests were not in the typical power-law region shown in Fig. 3.7, but extended into the transition zone (i.e. knee portion of the curve separating Newtonian responses from non-Newtonian). Thus, correct viscoelastic responses are observed in the pattern of the values of n with pressure, with higher pressures exhibiting greater non-Newtonian response than the lower pressures. Remembering that the selection of $n = 1$ at the lowest applied pressure was arbitrary, nothing can be said as to where the response lies within the transition zone, as n is bounded by $n = 1$ to 0.07 where $n = 0.07$ is the value for the neat resin.

Addressed here are the observed values of c for similating the influence the fiber has on the neat resin viscosity. Figure 3.10a plots the values of c as a function of temperature. The effective viscosity ($c \cdot m$) is plotted against temperature in Figure 3.10b where it is shown that although c increases with temperature the effective viscosity does not, as would be expected. However, is the response of c to temperature realistic? No reports in literature were found that addressed the temperature effects over such a large range; however,

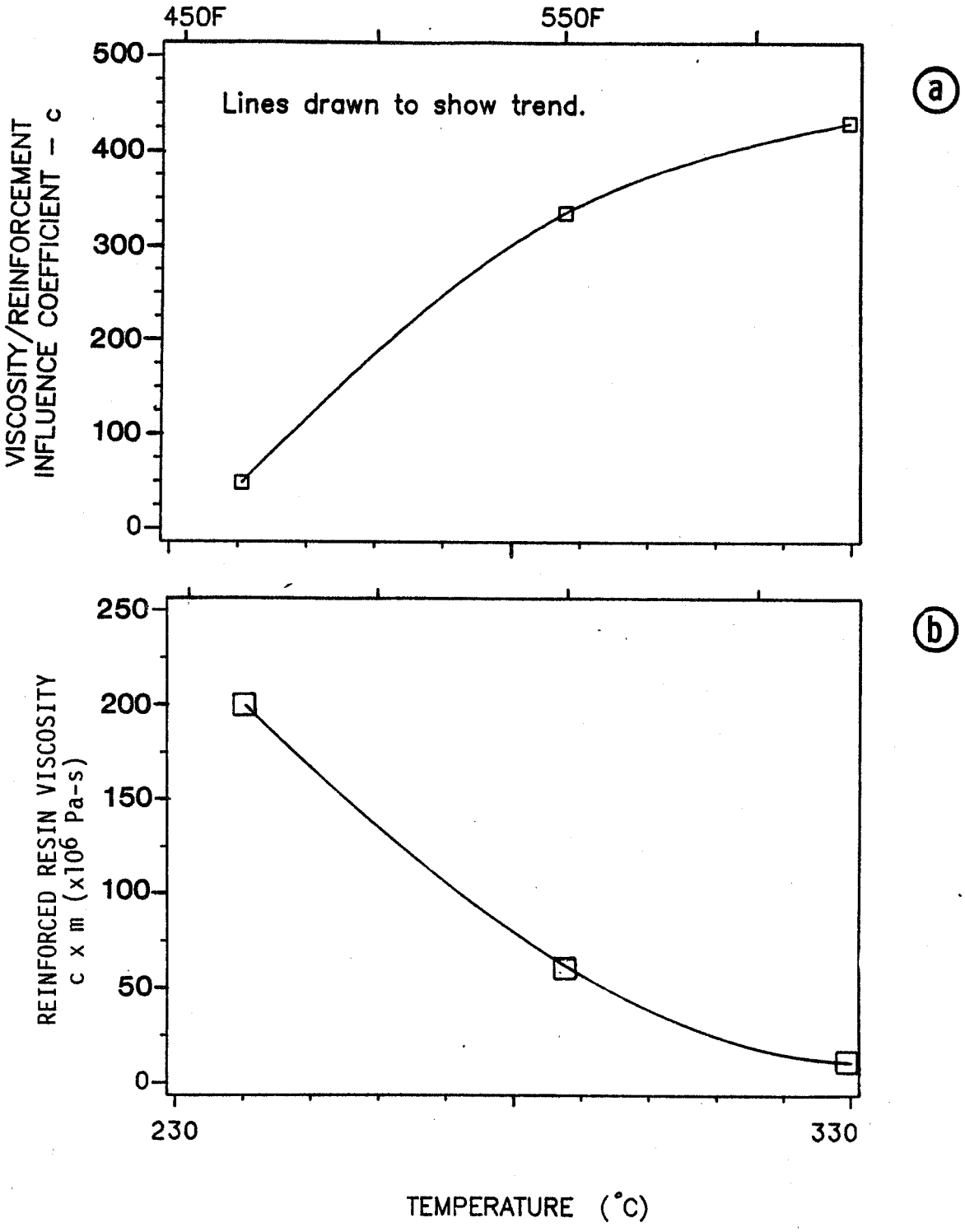

Figure 3.10 Effects of Temperature on Fiber Reinforced Resin Viscosity Parameters

Pisipati [30] has shown c to increase at the lower shear rates (as assumed here) but reverses at the high shear rates for a 20% glass fiber-reinforced nylon. As stated in the previous sections, the theory and experimental work are still in their developmental stages. Interested readers are referred to the work by Pisipati.

In summary, the values of c and n seem arbitrary when correlated to single sets of pressure and temperature data; however, when the responses of c with T, and n with P are observed over an entire spectrum of applied pressures and temperatures, viscoelastic material responses are observed. Further work is needed if the values of c and n are to be quantified, as well as their responses.

3.3.4b Influences of the Prepreg Geometric Nonuniformity on D_{IC}

Intuitively, the greater the nonuniformity of the prepreg (i.e. the greater the difference between tow heights) the greater the contact time required to achieve a given state of D_{IC}. The following study was made addressing the effects of tow nonuniformity on the degree of intimate contact. This study was divided into two parts: 1) the effects of statistically skewed distributions (i.e. heavily populated thin or thick tows) and 2) the effect of statistically deviated tow uniformity (i.e. greater or lesser tow height uniformity). The processing conditions used for this study were chosen as P = 172 KPa (25 psi) and T = 240°C (465°F).

Statistically Skewed Tow Nonuniformity

Shown in Fig. 3.11a are three conditions of skewness of tow

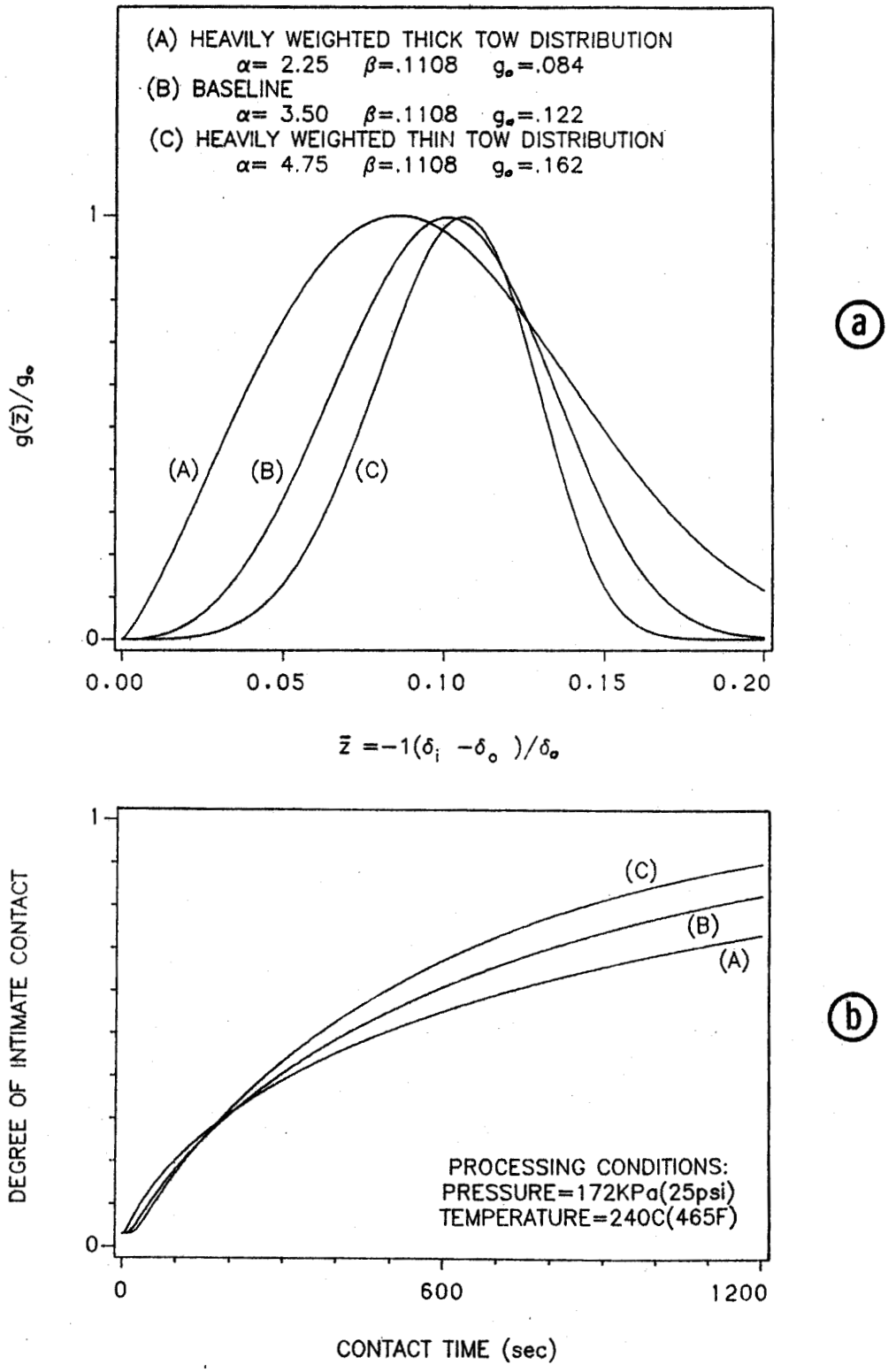

Figure 3.11 Effects of Probabilistically Skewed Distributions of Tow Height Nonuniformity Across the Width of a Prepreg with the Degree of Intimate Contact

nonuniformity: 1) curve A is the tow distribution in the present study which simulates a heavily populated thick tow distribution, 2) curve B is the normal distribution of curve A by setting $\alpha = 3.50$, and is used as the baseline in both the skewness and deviated tow nonuniformity studies, and 3) curve C simulates a heavily populated thin tow distribution.

Figure 3.11b shows that a heavily populated thin tow prepreg results in a faster initial growth of D_{IC} followed by a slower growth as 100% contact is approached. The opposite is true of prepregs being heavily populated with thick tows.

Statistically Deviated Tow Nonuniformity

Shown in Fig. 3.12a are two conditions of deviated normal distributions of tow nonuniformity: 1) curve D is the baseline curve B used in Fig. 3.11 simulating a large deviation in tow uniformity, and 2) curve E is a normally distributed prepreg simulating greater tow uniformity.

Comparing curves D and E in Fig. 3.12b, it is found, as expected, that the smaller the standard deviation (curve E) the shorter the contact time required to achieve the same D_{IC}.

3.3.4c Observations of the Model

As a final word about the intimate contact results, reference is made to Figs. 3.13a and 3.13b. Had plate separation been monitored as

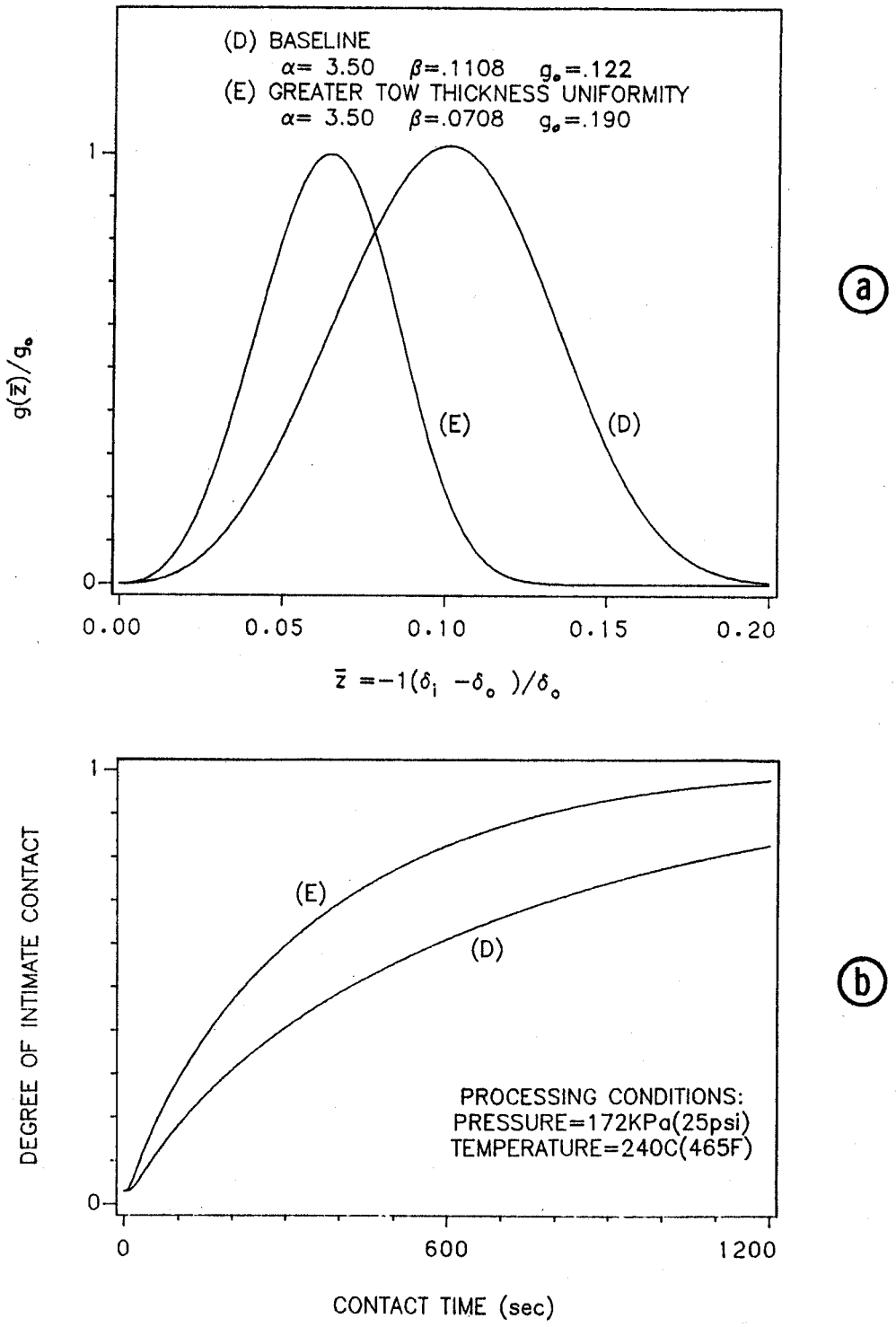

Figure 3.12 Effects of Probabilistically Deviated Normally Distributed Tow Height Nonuniformity Across the Width of a Prepreg with the Degree of Intimate Contact

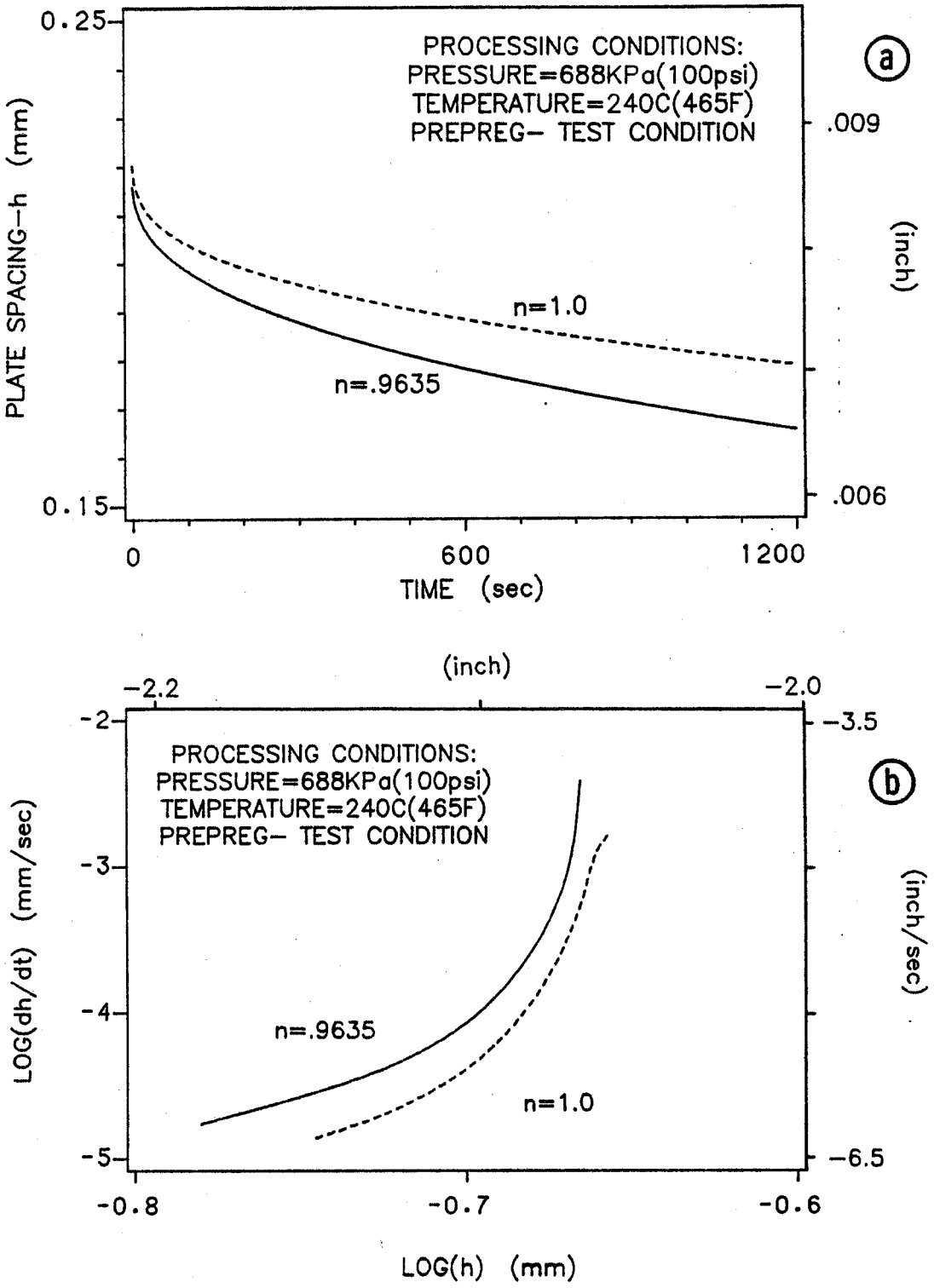

Figure 3.13 Observations of Model Concerning (a) Tow Height versus Contact Time, and (b) the Rate of Decreasing Tow Height due to Compression Loading versus Tow Height

a function of time in lieu of C-scanned area as a function of time, then the following responses would have been realized according to the model. Plate separation h versus t_c is shown in Fig. 3.13a while log (dh/dt) versus log (h) is shown in Fig. 3.13b. The rate at which the plates approach each other (Fig. 3.13b) has two physically distinct regions.

The first region has the characteristics of a decreasing plate separation rate. This similates the force per tow decreasing with time (i.e. the area of contact increasing with time as the force is kept constant). Whether or not this response is valid must still be evaluated. The model cannot predict transient conditions, only steady state conditions as assumed in the formulation. In other words, the stress overshoot typical of viscoelastic materials cannot be predicted as new tows come into contact and start their flow process.

The second region is the steady state region where 100% contact has been achieved at the interfaces and a global squeeze flow occurs. The slope of this portion of the curve is 1/6 for Newtonian fluids. If other than 1/6 the material is non-Newtonian where the slope of the power-law region can be evaluated. Because of the mold cavity, no global squeeze was allowed nor would this region be possible to evaluate using the C-scan technique.

4.0 Computer Model

A computer code was developed which can be used to calculate the degree of autohesion, D_{Au}, and the degree of intimate contact, D_{IC}, at the interface of a thermoplastic matrix composite during processing. The model is limited to constant temperature (greater than the T_g of the resin) and constant pressure conditions throughout the laminate. With the pressure and temperature conditions specified, of major interest are the states of autohesion and intimate contact as a function of the processing time, t_p (i.e. total elapsed time) and more specifically the processing time required to achieve full intimate contact and cohesive strength of the interface.

Intuitively, coalescence at the interfaces of stacked plies is expected to be quicker for unidirectional laminates, than for angle ply and cross-ply laminates due to the nesting of tows. Thus, because the intimate contact model was formulated using data obtained from cross-ply laminates, the computer model presented here is expected to give conservative results for laminates other than cross-ply.

The computer code provides the user with the following information about processing:

1) the degree of intimate contact (i.e. fraction of interfacial area in contact) as a function of processing time,

2) the distribution of the degree of autohesion over the interfacial area in contact, and

3) the minimum degree of autohesion of a total interfacial area in contact as a function of processing time.

Up to now, the autohesion and intimate contact models were formulated independently. However, during the processing of

thermoplastic matrix composites, the two time dependent phenomena occur simultaneously.

The computer code couples the autohesion model with the intimate contact model through the observation that autohesive bonding cannot begin until intimate contact is achieved. As processing time progresses the total area in contact increases (i.e. D_{IC}). Because the total area in contact (i.e. D_{IC}) is the cumulation of smaller areas, d_{IC}, achieving contact previous to the processing time in question, the set of d_{IC}'s at a given processing time will each have a unique degree of autohesion. This is due to the differences in the length of time that each d_{IC} has been in contact. The model distinguishes between the length of time (t_{IC}) required for each successive element of area to come into contact, and the length of time (t_{Au}) each successive element has been in contact. Thus, the following equation was used in the computer model formulation:

$$t_p = t_{IC} + t_{Au} \tag{4.1}$$

where t_p, t_{IC}, and t_{Au} are defined previously.

Solution of the autohesion model (Section 2) and intimate contact model (Section 3) requires that the input parameters be specified. The input parameters are shown in Table 4.1, and are grouped in the following catagories: I) Processing Cycle, II) Prepreg Properties, and III) Resin Properties.

The input parameters describing the temperature and pressure conditions are specified by the user. The parameter denoted by a

Table 4.1 Input Parameters

I) Processing Cycle

a) Constant temperature condition

b) Constant pressure condition

II) Prepreg Properties

c) Initial distribution of geometric nonuniformity of tow heights* (see Eq 3.7)

d) Fiber volume fraction of composite v_f = 68%

e) fiber reinforced resin viscosity parameters** (see Eq 3.28)

f) Cross-sectional area of a single tow

g) Glass transition temperature - T_g

III) Resin Properties

h) Resin dynamic viscosity $\eta'(T,\omega)$ (see Appendix A)

i) Autohesion parameters (K(T), or K_0' and $a_T(T)$)*** (see Eqs 2.11, 2.14, and 2.15)

* measured by user

** empirically determined by fitting IC theory to experimental data

*** material property experimentally measured

single astrisk (*) must be measured by the user. The method used to obtain this parameter can be found in Section 3.3.2a. The parameter denoted by a double asterisk (**) was determined by fitting the theory to experimental data as described in Section 3.3.4. The material property denoted by a triple asterisk (***) was determined experimentally as described in Section 2.0. All other parameters are either specified by the manufacturer or can be found in the open literature.

With the input parameters specified, Eqs 2.10 (or 2.15) and 3.31 are solved numerically.

Three cases were run on the computer to show the relationship between the degree of intimate contact and the degree of autohesion for various processing conditions. The computer model was used to calculate the degree of intimate contact, the degree of autohesion, and the total processing time of a fiber-reinforced thermoplastic matrix composite under different processing conditions. The material properties of AS4/P1700 prepreg were used as input data to the model.

Case I - P = 172 KPa (25 psi), T = 240°C (465°F), t_p = 0 → 3000 sec

Case II - P = 344 KPa (50 psi), T = 240°C (465°F), t_p = 0 → 3000 sec

Case III - P = 172 KPa (25 psi), T = 227°C (440°F), t_p = 0 → 3000 sec

The degree of intimate contact was calculated as a function of the processing time for cases I, II, and III, independent of the autohesion phenomenon. However, at each processing time a whole distribution of D_{Au} values exist because of the progressive nature of intimate contact with time. By plotting the degree of autohesion versus the percent of contacted area (i.e. d_{IC}, density of contacted

area) shown in Fig. 4.1, the distribution of autohesion over the area in contact is obtained for all three cases. The solid curves represent the distributions of autohesion (for 1% intervals of D_{Au}) at different processing times up to but not including, a degree of autohesion of 1.0. The table on the graph shows the values of the percent of contacted area having a degree of autohesion equal to 1.0. For case I, at short processing times (i.e. t_p = 10 sec) it is shown that no areas in contact have occurred that have a D_{Au} greater than ≈0.63, and that at point "A" approximately 0.8% of the contacted area has a D_{Au} between .395 and .405. As expected, at longer processing times greater percentages of contacted area coexist with the higher degree of autohesion. This observation is obvious for curves "a" and "b" but somewhat disquised for curves "c" through "j". This is because at the long processing times an increasing percentage of the contacting area has a degree of autohesion equal to one. These values are shown in the tables on Fig. 4.1.

The effects of pressure and temperature on the distribution of autohesion over the contacted area are shown in Fig. 4.1 by comparing the top and center graphs and top and bottom graphs, respectively. By comparing the results from Case I and Case II, the effect of a 50% increase in pressure (holding temperature constant) can be observed. It is shown that the distribution of autohesion is skewed upward for the higher pressure condition indicating a more rapid growth in areas coming into contact and a less uniform distribution of autohesion at any one processing time. However, this observation on the skewness is somewhat insensitive at long processing times. Also, the increase in

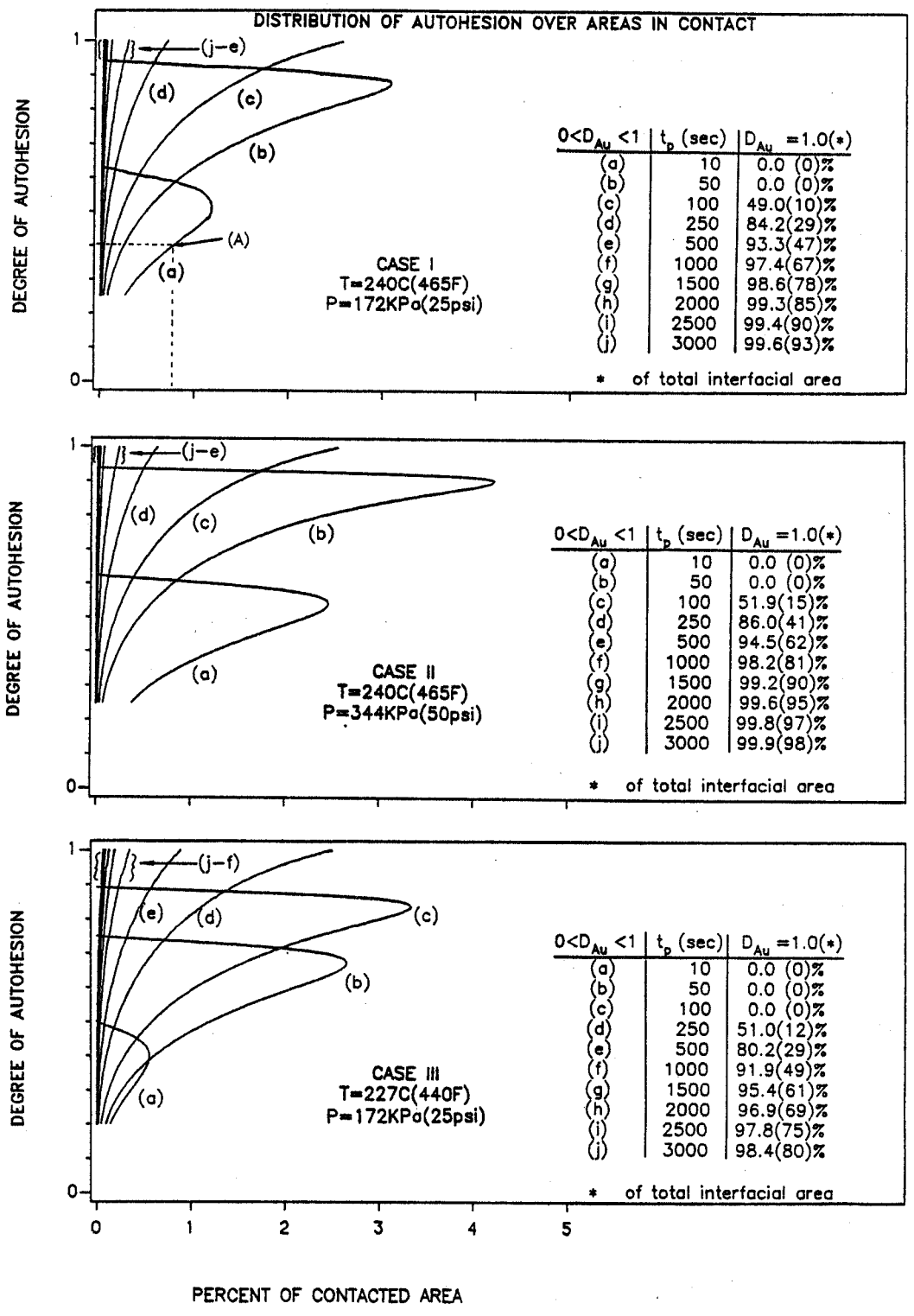

Figure 4.1 Distribution of the Degree of Autohesion Over the Area in Intimate Contact for Several Processing Times

pressure results in greater percentages of contacting area having a D_{Au} = 1 at long processing times.

The effect of temperature on the distribution of autohesion can be observed by comparing Case I with Case III (holding pressure constant) where Case III is 13°C (25°F) lower as shown in Fig. 4.1. The 13°C (25°F) decrease in temperature results in suppressing the distribution to lower degrees of autohesion, as well as, lower percentages of contacted areas. This is a result of temperature affecting both the viscosity and autohesive properties of the resin thereby influencing the growth of contacting area, and the growth of autohesion.

Shown in Fig. 4.2 is a plot of the minimum degree of autohesion versus the degree of intimate contact at several processing times. This curve was obtained by integrating the curves in Fig. 4.1 at each processing time. The curves show the coexistence of D_{Au} and D_{IC} at a given processing time. This cumulative distribution will provide the user with the minimum degree of autohesion expected for a given area in intimate contact (i.e. D_{IC}) at any processing time. These curves show the cumulative distribution of contacted area to the total area up to a given D_{Au}. Thus, using t_p = 100 seconds as an example point "B" shows that ≈20% of the total interfacial area is in intimate contact, point "C" shows that ≈10% of the interfacial area is in intimate contact with a D_{Au} = 1.0, and point "D" shows that approximately 17% of the interfacial area in contact has a value of D_{Au} of 0.70 or greater. At very long processing times the lines

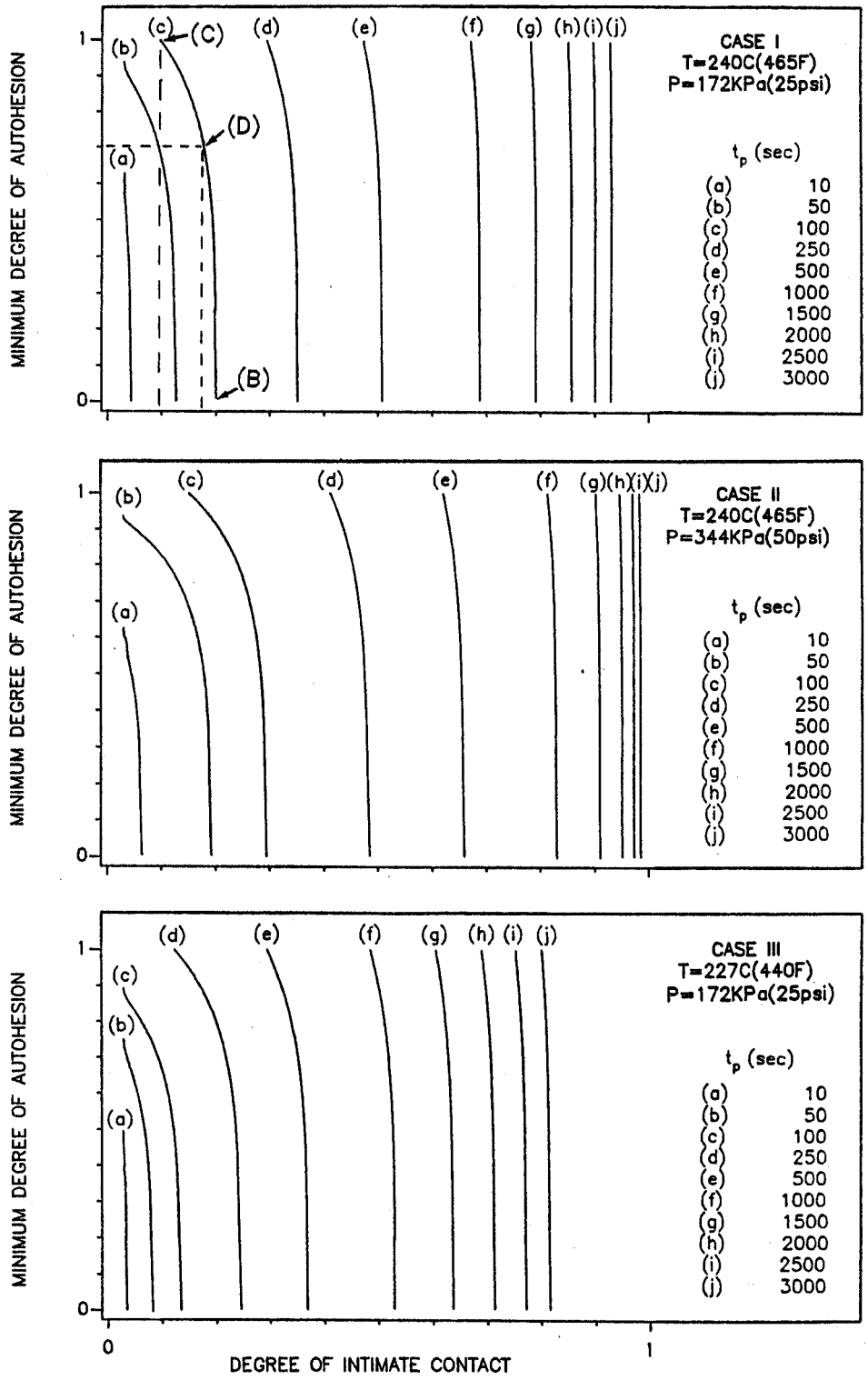

Figure 4.2 Cumulative Distribution of Areas in Intimate Contact Having a Minimum Degree of Autohesion at Several Processing Times

appear more vertical because of the compressing time scale with increasing D_{IC} (i.e. D_{IC} does not increase linearly with time).

The effect of pressure is shown in Fig. 4.2 by comparing the top and center graphs. It is shown that the higher pressure results in higher degrees of intimate contact for any one processing time. No pressure effects were expected nor observed on the autohesive values as observed by the intercepts of curves "a" and "b" with D_{Au} at the initial contact area.

The effects of temperature are shown in Fig. 4.2 by comparing the top and bottom graphs. It is shown that the lower temperature results in smaller degrees of intimate contact at any given processing time. This result is expected since the viscosity increases with a decrease in temperature thus suppressing the rate of deformation and the growth of intimate contact. Also observed, is the influence of temperature on the degree of autohesion. At the lower temperature and at any processing time a greater percentage of the areas in contact have a degree of autohesion less than 1.0. This is because a decrease in temperature decreases the molecular mobility of the diffusing molecular chains thus suppressing the degree of autohesion for any unit of time.

Figure 4.3 summarizes cases I through III showing the effects of temperature and pressure on D_{IC} and D_{Au} at t_p equal to 50 and 1000 seconds. More easily seen than in Fig. 4.2 is the increasing range of D_{IC} values as processing time is increased, The effect of pressure on D_{IC} and D_{Au} can be observed by comparing cases I and II. For the same temperature, a 172 KPa (25 psi) pressure increase results in

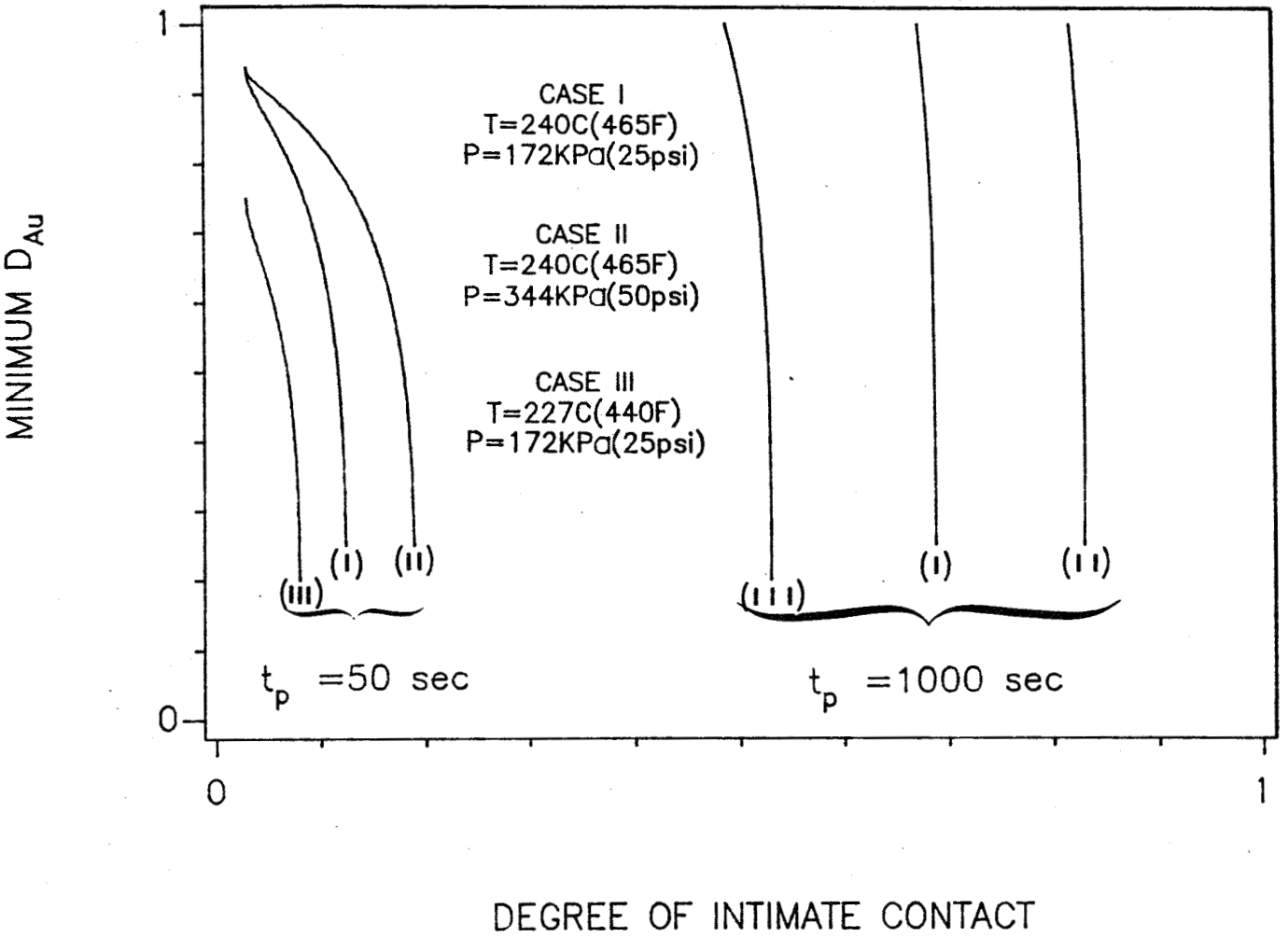

Figure 4.3 Summary Plot of the Minimum Degree of Autohesion Versus the Degree of Intimate Contact at Processing Times of 50 and 1000 sec.

higher values of D_{IC} with no observed effects on D_{Au} as expected.

In summary, the length of processing time required to achieve full intimate contact and cohesive strength of the interfacial area is subjected to the processing temperature and processing pressure conditions selected. The time frames of the intimate contact model and autohesion model are related to the processing time frame by Eq 4.1. Figure 4.4 shows the length of processing time required to achieve $D_{Au} = 1.0$, and $D_{IC} = 1$ for a given temperature and pressure. Because the temperatures tested for intimate contact are well above the T_g of the resin the influence of autohesive time to the overall processing time played a very minor role (refer to Eq 4.1). While the increase in pressure may decrease the time required to achieve 100% intimate contact the effect on the final processing time may not be as dramatic at temperatures lower than those tested. As pointed out in Section 2.0, at temperatures just above the T_g of the resin a degree of autohesion equal to one could only be obtained only after long autohesive contact times ($\approx$20 minutes). The nonlinearity of these curves shows the importance of just minor changes of the processing conditions with the final processing time.

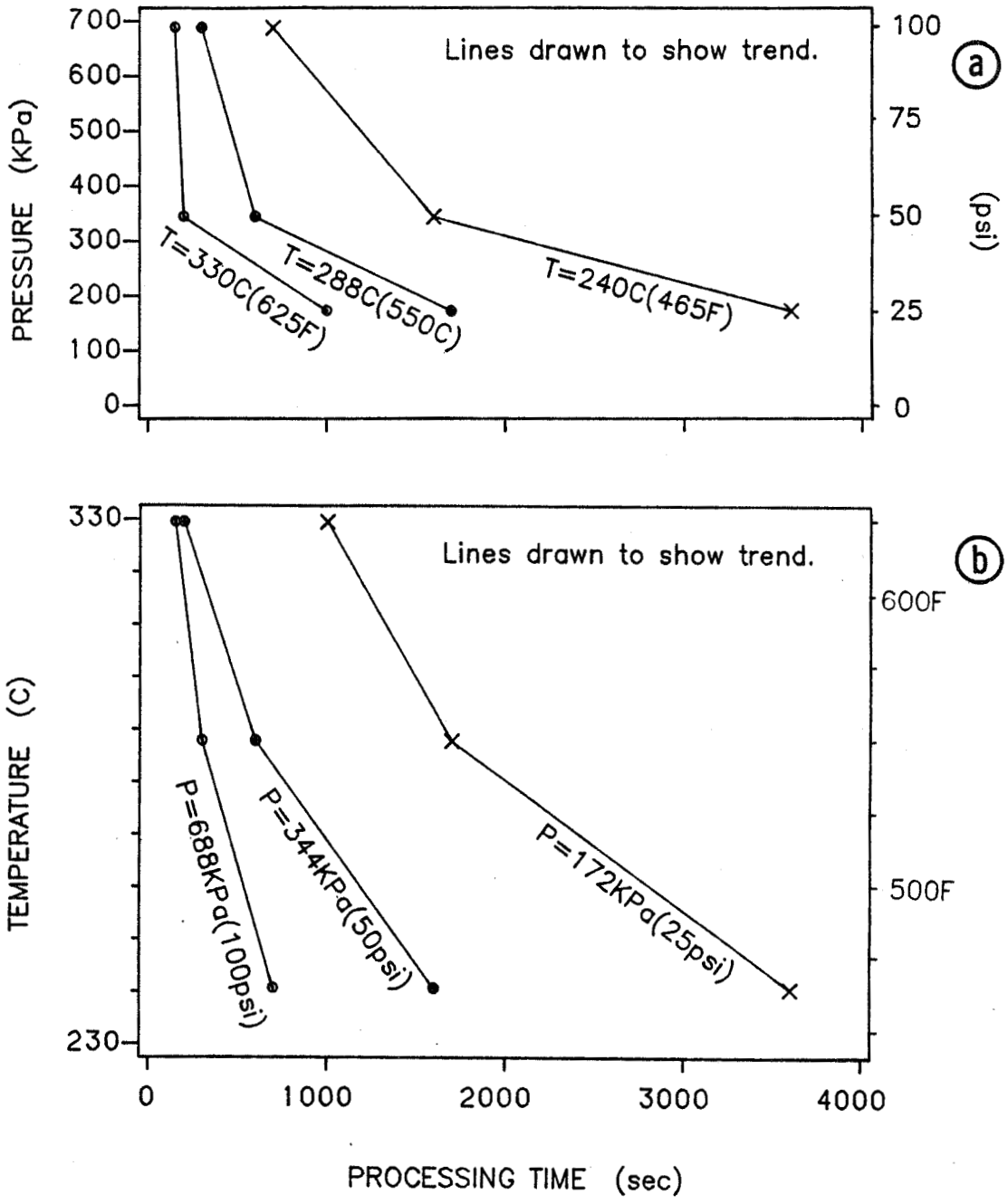

Figure 4.4 Effects of Temperature and Pressure on the Final Processing Time Required to Achieve Full Intimate Contact and Cohesive Strength

5.0 Conclusions

The following major tasks were completed during the course of this investigation:

1) Models were developed to simulate the processing of continuous fiber (AS4 graphite) reinforced thermoplastic matrix (P1700 polysulfone) composites. The models successfully describe the ply interfacial bonding phenomenon (consolidation) and the ply interfacial deformation (coalescence) phenomenon through mechanisms attributed to autohesion and squeeze flow, respectively.

Autohesion Model/Experiment

a) The autohesion model predicts the experimentally determined autohesion strength of the neat resin to be proportional to the fourth root of contact time.

b) A testing method for obtaining autohesive strength data at the same elevated temperature that the autohesion phenomenon occurred was successfully developed. The test method reduces the overall testing time required for room temperature testing.

c) Time-temperature superposition of the experimentally determined autohesive strength data was successfully applied in an empirical Arrhenius format and also in a

WLF method thereby coupling testing time to testing temperature.

Intimate Contact Model/Experiment

a) Black and white C-scans were obtained of $[0,90,0]_T$ laminates processed at several pressures, temperatures and times. The C-scan settings were set to indicate spacial gaps at the ply interfaces. The theory of probabilistics was applied to the C-scan data to distinguish between areas in contact and spacial gaps at the top and bottom interfaces.

b) A model was developed to simulate the growth of interfacial areas obtaining intimate contact.

- The model accounts for; 1) the extent of tow height nonuniformity across the width of a prepreg, and 2) the viscoelastic response of the deformation of a single tow subjected to a uniformly distributed compressive load over the top and bottom surfaces.

- The results of the model fits the experimental data quite well because of an assumed empirical formulation to indicate the fiber's influence on the neat resin viscosity. Further work is needed

to eliminate the experimetally determined constants for complete model verification. However, the expected viscoelastic response was observed between the processing parameters and the formation of intimate contact areas.

c) Experimentally measured dynamic viscosity data was obtained for the P1700 polysulfone neat resin over the temperature range from 220°C to 400°C in 20°C intervals. The frequency range was 0.1 to 100.0 rad./sec.

- Steady shear viscosity results were obtained by applying the Cox-Merz rule to the dynamic viscosity data.

- A master curve of the original viscosity data was constructed in the WLF manner. The results are an expanded frequency (or shear rate range) from 3.0E-06 to 100. rad/sec at 220°C.

2) A computer code was developed from the autohesion and intimate contact models. This code can be used to generate the following information for flat plate composites:

a) the degree of intimate contact, D_{IC}, as a function of processing time,

b) the degree of autohesion, D_{Au}, as a function of the length of time certain percentages of the interface have been in contact and the processing time.

3) The following input parameters required in the computer code for the solution of the models were specified:

a) shear viscosity of the neat resin, η, was obtained experimentally as a function of shear strain rate, $\dot{\gamma}$, and temperature, T,

b) shear viscosity parameters of the fiber reinforced resin, c and n, were obtained experimentally as a function of temperature, T, and pressure, P, respectively,

c) the autohesion diffusion coefficient, K_o, was obtained experimentally as a function of temperature,

d) the prepreg's geometric non-uniformity, $g(\bar{z})$, was measured and defined statistically.

4) The computer model quantitatively confirms the intuitive speculation that decreased processing time can be realized by either increasing temperature, or pressure, or both. With the user defining any two of the three processing parameters (P, T, and t) the computer model will define the third parameter required to achieve a completely contacted and bonded interface.

5) A parametric study was performed on the extent of tow height nonuniformity to illustrate how the models and the

associated computer code can be used to determine the appropriate processing parameters for achieving a uniformly processed composite in the shortest time.

Normally Distributed Tow Height Nonuniformity

Prepregs having greater or lesser extents of tow height nonuniformity have been shown to greatly influence the final processing time required to achieve full intimate contact and full bond strength.

Skewed Distribution of Tow Height Nonuniformity

Prepregs having a greater number of tows that are thick require longer processing times than prepregs having a greater number of thin tows due to the changing load per tow distribution of the constant applied processing pressure.

The following recommendations are made concerning the outcome of this study:

1) that autohesive strength be measured on actual laminates at room temperature in order to observe any differences in the development of the degree of autohesion and the contact time with the neat resin test,
2) that the effects of strain rate and shear strain on the cohesive strength be obtained at temperatures just above glass transition temperature,

It has been observed that if a steep thermal gradient through the thickness in the three ply laminate ($[0,90,0]_T$) is imposed, greater or lesser extents of warpage (out of plane curvature) of a symmetric lay-up can be obtained. It is the extent of warpage that leads one to believe that varying shear strains are taking place during this transitory period (also resulting in varying thermal stresses). This can be explained since the material is still capable of motion during the transition period when cooling from the processing temperature to the Tg of the resin (unlike thermosets which solidify).

It is the varying extent of shear strain and its rate that can place areas of reduced autohesive strength at the 0°/90° ply interface as the fibers contract or expand to different extent. It is believed that the varying amounts of shear strain will also result in a varying loss of autohesion strength and a different initial condition from which autohesion formation is to restart. The autohesion process occurs very slowly at temperatures just above the Tg of the resin leading one to believe that a limiting factor may be this cooling down period if the shortest processing time is desired.

3) Lastly, that a faster and more accurate means of measuring the degree of intimate contact, than the C-scan method used here,

may be realized through the measurement of processing plate separation as a function of time. Also, the use of dielectrics may be very useful in monitoring the formation of intimate contact by monitoring the change in signal with the increasing area of contact.

References

1. May, L. C., and Goad, R. C., "Manufacturing Methods for Fabrication and Assembly of Advanced Composite Primary Structure," U.S. Air Force Materials Laboratory Report Nr. AFML-TR-75-111, July, 1975.

2. Hoggatt, J. T., and VonVolki, A. D., "Evaluation of Reinforced Thermoplastic Composites and Adhesives," Naval Air Systems Command Final Report - Contract N00017-7A-C-0026, March, 1975.

3. Hill, S. G., et. al., "Advanced Thermoplastic Composite Development," Final Report on Contract N00019-77-C-0561, Boeing Aerospace Company, Seattle, Washington, May, 1979.

4. Husman, and Hartness, J., "Polyphenyl Sulfone Matrix Composites," 24th National SAMPE Symposium and Exhibition, Volume 24, Book 2, p. 21 (1979).

5. Hartness, J., "Polyphenylene Sulfide Matrix Composites," 25th National SAMPE Symposium and Exhibition, Volume 25, pg. 376 (1980).

6. Voyutskii, S. S., Autohesion and Adhesion of High Polymers, Volume 4, Polymer Reviews, Interscience Publishers, New York, (1963).

7. Bothe, L., and Rehage, G., "Autohesion of Elastomers," Rubber Chemistry and Technology, 55, 1308 (1981).

8. De Gennes, P. G., "Reptation of a Polymer Chain in the Presence of Fixed Obstacles," Journal of Chemical Physics, 55, 572 (1971).

9. De Gennes, P. G., "Entangled Polymers," Physics Today, pp. 33-39, June, 1983.

10. Wool, R. P., "Molecular Aspects of Tack," Rubber Chemistry and Technology, 57, 307 (1983).

11. Wool, R. P., and O'Connor, K. M., "Theory of Crack Healing in Polymers," Journal of Applied Physics, 52, 5953 (1981).

12. Wool, R. P., "Relations for Healing, Fracture, Self-Diffusion, and Fatigue of Random Coil Polymers," ACS Polymer Preprints, 23 (2), 62 (1982).

13. Jud, K., Kausch, H. H., and Williams, J. G., "Fracture Mechanics Studies of Crack Healing and Welding of Polymers," Journal of Materials Science, 16, 204 (1981).

14. Skewis, J. D., "Self-Diffusion Coefficients and Tack of Some Rubbery Polymers," Rubber Chemistry and Technology, 39, 217 (1966).

15. Hamed, G. R., and Shieh, C. H., "Relationship Between the Cohesive Strength and the Tack of Elastomers," Journal of Polymer Science, Polymer Physics Edition, 21, 1415 (1983).

16. Ling, F. F., "The Properties of Random Surfaces in Contact," Surface Mechanics, ASME Winter Annual Meeting, p. 36, November, 16-21, 1969.

17. Blakely, J. M., Surface Physics of Materials, Volume 2, pp. 475-487, Academic Press, New York, (1975).

18. Sadowski, T. J., and Bird, R. B., "Non-Newtonian Flow Through Porous Media I. Theoretical II. Experimental," Transactions of the Society of Rheology, 9(2), 243 (1965).

19. Grimm, R. J., "Squeezing Flows of Polymeric Liquids," AIChE Journal, 24(3), 427 (1978).

20. Bird, R. B., Armstrong, R. C., and Hassager, O., Dynamics of Polymeric Liquids, Vol. 1, pp. 223-226, John Wiley and Sons, New York, (1977).

21. Dienes, G. J., and Klemm, H. F., "Theory and Application of the Parallel Plate Plastometer," Journal of Applied Physics, 17, 458 (1946).

22. Kataoka, T., Kitano, T., and Nishimura, T., "Utility of Parallel-Plate Plastometer for Rheological Study of Filled Polymer Melts," Rheologica Acta, 17 (6), 626 (1978).

23. Dealy, J. M., Rheometers for Molten Plastics, pp. 174-177, Van Nostrand Reinhold Company, New York, (1982).

24. Kataoka, T., Kitano, T., Sasahara, M., and Nishijima, K., "Viscosity of Particle Filled Polymer Melts," Rheologica Acta, 17(2), 149 (1978).

25. Mooney, M., "The Viscosity of a Concentrated Suspension of Spherical Particles," Journal of Colloid Science, 6, 162 (1951).

26. White, J. L., Czarnecki, L., and Tanaka, H., "Experimental Studies of the Influence of Particle and Fiber Reinforcement on the Rheological Properties of Polymer Melts," Rubber Chemistry and Technology, 53, 823 (1980).

27. Bartenev, G. M., and Zakharenko, N. V., "The Viscosity and Flow Mechanism of Polymer-Filler Mixtures," Kolloidn. ZH., 24, 121 (1962).

28. Chapman, F. M., and Lee, T. S., "Effect of Talc Filler on the Melt Rheology of Polypropylene," SPE Journal, 26(1), 37 (1970).

29. "A Modified Casson Equation for Dispersion," Transactions of the Society of Rheology, 14(4), 617 (1970).

30. Pisipati, R. M., "A Rheological Characterization of Particle and Fiber Filled Nylon 6,6 Melts and Its Application to Weld-Line Formation in Molded Parts," Ph.D. Thesis, VPI&SU, 1983.

Appendix A

Rheological Properties of UDEL® P1700 Resin

A.1 Introduction

Experimentally obtained dynamic viscosity data was obtained for neat P1700 polysulfone resin using a parallel plate testing fixture within the frequency range from 0.1 to 100.0 radians per second at temperatures from 200°C to 400°C in 20°C intervals. The viscosity data was tested to be linearly viscoelastic over the test spectrum. Also, the viscosity data was evaluated for time-temperature superposition in the WLF manner. All temperature conditions fit quite well with the WLF theory except for the temperature conditions above the 360°C data, where prolonged exposure to a nitrogen purged atmosphere was found insufficient to prevent degradation of the polymer.

Presented here are the experimental procedure (Section A.2), the original test data (Section A.3), application of the Cox-Merz rule to obtain steady shear viscosity from the dynamic viscosity data (Section A.4.1), and the construction of a master curve from the WLF theory relating time and temperature with viscosity (Section A.4.2).

A.2 Experiment

The dynamic viscosity data were taken using the Rheometrics System Four rheometer (Fig. 2.5) using a parallel plate test fixture (Fig. 2.6). The dynamic viscosity, $\eta'(\omega)$, shear storage modulus, $G'(\omega)$, and shear loss modulus, $G''(\omega)$, were obtained from

amplitudes of oscillation of the driven top plate and the non-driven bottom plate and the phase angle between the oscillations of the two plates. The equations relating η', G', and G'' with the measured quantities of torque, M, frequency, ω, and phase angle, θ for the parallel plate plastomer are as follows:

$$\eta' = \frac{G''}{\omega} \quad \text{Poise} \tag{A.1a}$$

$$\eta'' = \frac{G'}{\omega} \quad \text{Poise} \tag{A.1b}$$

$$\eta^* = \sqrt{(\eta')^2 + (\eta'')^2} \tag{A.1c}$$

$$G' = K \cdot [\text{Real } M/\theta] \quad \text{Dynes/cm}^2 \tag{A.2}$$

$$G'' = K \cdot [\text{Imag } M/\theta] \quad \text{Dynes/cm}^2 \tag{A.3}$$

where; $K = \frac{(2H/10) \cdot 980.7}{\pi(R/10)^4}$

ω = frequency

η'' = is the out of phase component of η^*

η^* = is the complex viscosity

H = is the plate spacing (mm)

R = is the radius of the plates (mm) (12.5 mm)

θ = is the phase angle (radians)

M = is measured torque

All P1700 sample disks used in the test were prepared in a similar fashion to the thick film preparation used for autohesion sample

preparation described in Section 2.3.2. All viscosity measurements were made in a nitrogen purged oven. At temperatures of 360°C and greater, nonrepeatable data were observed with the same specimen. This was attributed to the degradation of the polymer as greater discoloration of the polymer was observed with prolonged times at higher temperatures. Using several different specimens all other temperature data showed good repeatability. No effects of plate separation from 1.0 mm to 1.70 mm were observed in the viscosity response.

Shown in Table A.1 are the conditions of the dynamic viscosity test and the conditions used to verify the test as being linear viscoelastic.

A.3 Test Data Results and Discussion

A.3.1 Dynamic Testing

Shown in Fig. A.1, A.2, and A.3 are the linear viscoelastic complex viscosity, (η^*), the shear storage modulus, $G'(\omega)$, and the shear loss modulus, $G''(\omega)$ for the test conditions shown in Table A.1, respectively. Smooth and continuous data curves are obtained at all temperatures over the entire frequency range except at the very low frequencies and high temperature data. This slight fluctuation is attributed to the very low torque output signals produced at these conditions. The greater fluctuations are present in the measurement of G' because of the magnitude difference with G''. As expected there is a greater shear dependent response of viscosity with frequency

Table A.1 Viscosity Test Matrix

Dynamic Test

Oven Temp.	Frequency	% Strain	Plate Spacing	N_2 Purge	Linear Check
220°C	0.1-100. rad/sec	1.0%	1.145 mm	Yes	--
240°C	0.1-100.	1.0	1.145	Yes	--
260°C	0.1-100.	5.0	1.145	Yes	Yes
280°C	0.1-100.	10.0	1.145	Yes	--
300°C	0.1-100.	15.0	1.145	Yes	--
320°C	0.1-100.	10.0	1.700	Yes	Yes
340°C	0.1-100.	20.0	1.700	Yes	--
360°C	0.1-100.	20.0	1.700	Yes	Yes
380°C	0.1-100.	20.0	1.700	Yes	--
400°C	0.1-100.	20.0	1.700	Yes	--

Linear Check

Oven Temp.	Frequency	% Strain	Plate Spacing	N_2 Purge
260°C	0.5 rad/sec	1-20%	1.145 mm	Yes
	5.0	1-20	1.145	Yes
	50.	1-20	1.145	Yes
320°C	0.5	1-20%	1.693 mm	Yes
	5.0	1-20	1.693	Yes
	50.	1-20%	1.693	Yes
360°C	0.5 rad/sec	1-40%	1.145 mm	Yes
	5.0	1-40	1.145	Yes
	50.	1-40	1.145	Yes

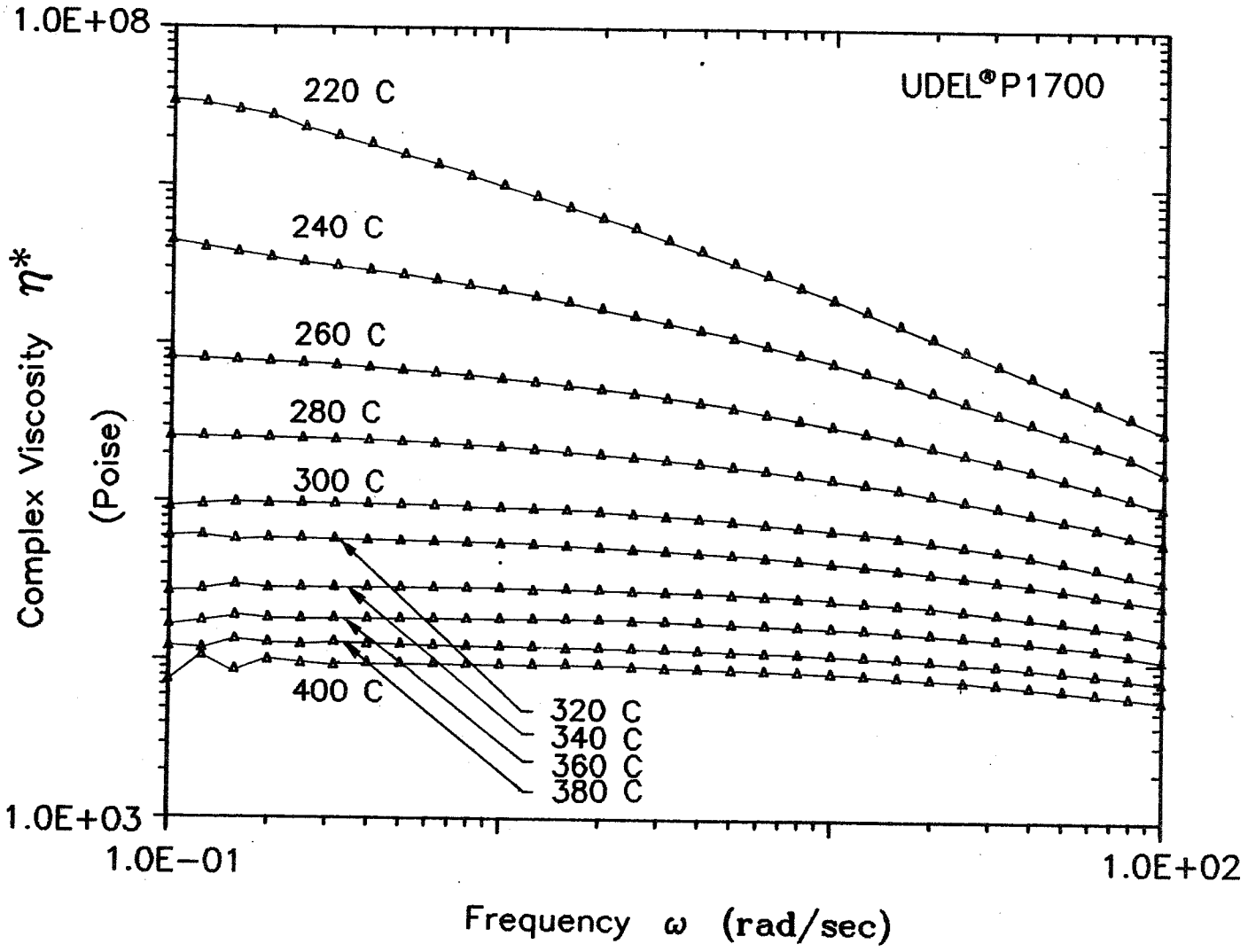

Figure A.1 Linear Viscoelastic Complex Viscosity Data of UDEL® P1700 Resin

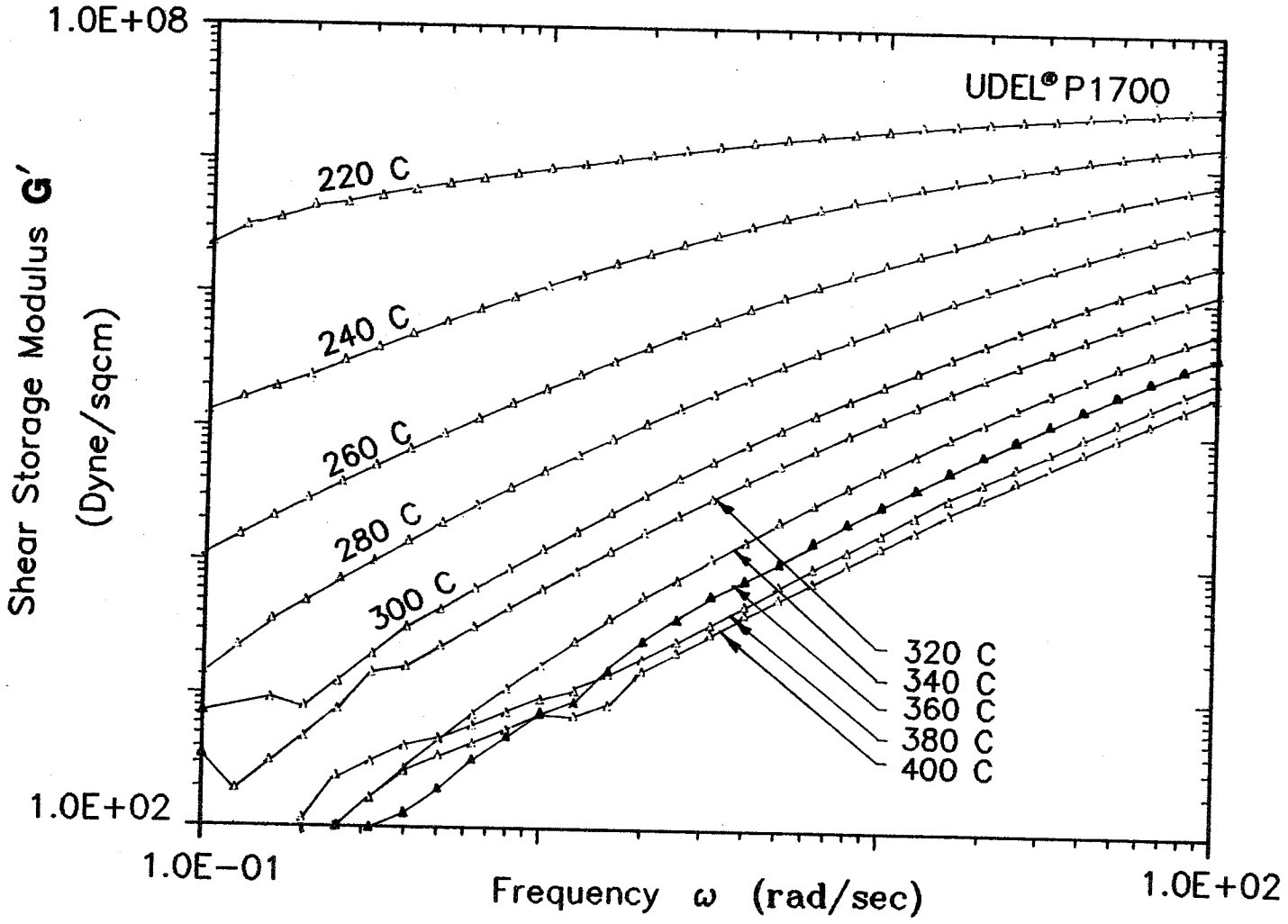

Figure A.2 Linear Viscoelastic Shear Storage Modulus of UDEL® P1700 Resin

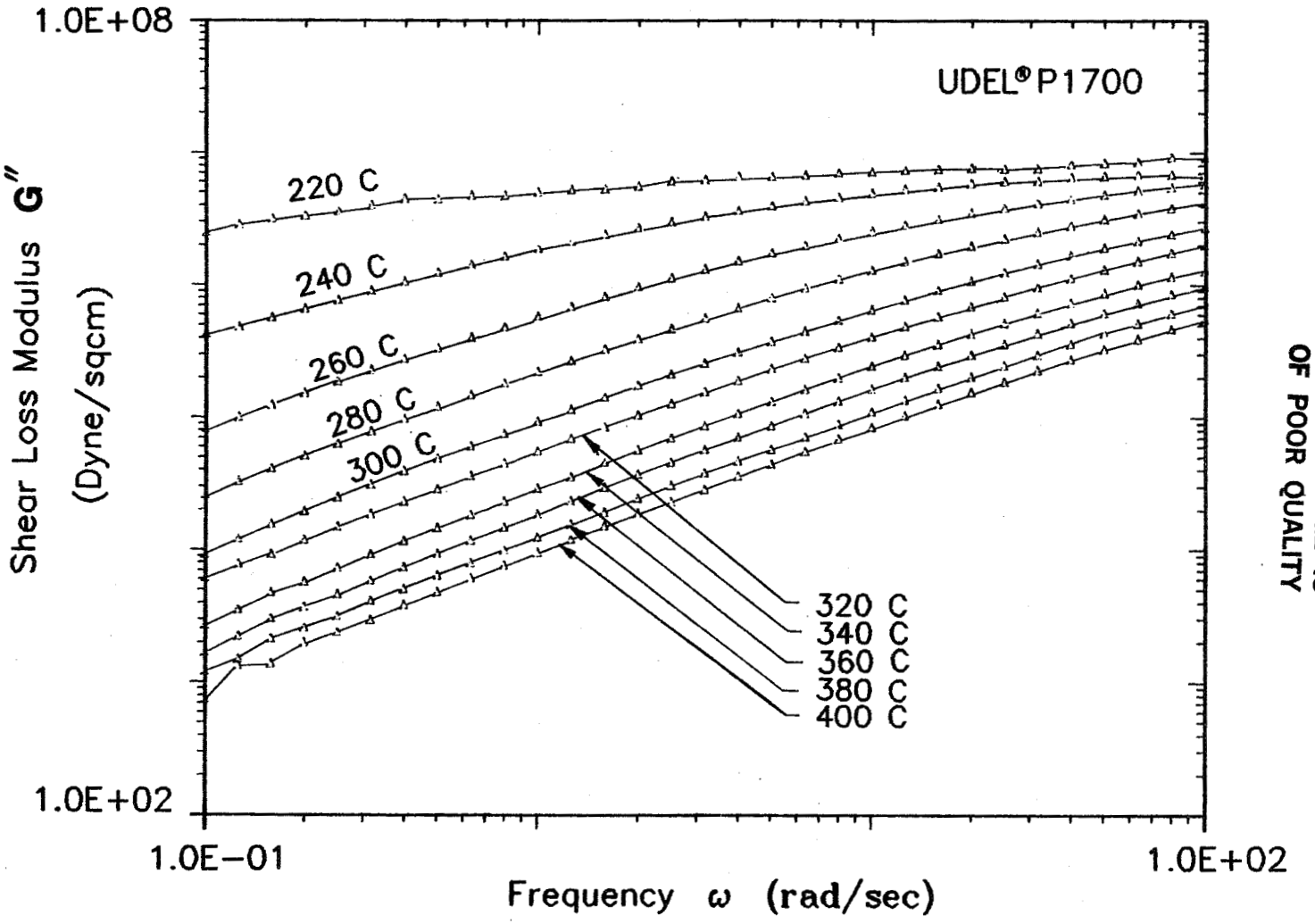

Figure A.3 Linear Viscoelastic Shear Loss Modulus of UDEL® P1700 Resin

(i.e. shear rate) at the lower temperatures and a greater extent of the Newtonian domain over the frequency range tested at high temperatures.

A.3.2 Linear Check

Checks for linear viscoelastic material response of the dynamic viscosity data were made at temperatures of 260°C, 320°C and 360°C and are shown in Figs. A.4, A.5, and A.6, respectively. These linear checks involved measuring the viscosity response at a given frequency (i.e. time) and varying the percent of strain. Theoretically, as shear strain is increased for a given shear rate, a greater entanglement density is realized resulting in increased material resistance to deformations. This results in fracture on the molecular level and a further decrease in resistance. The test was repeated for three frequencies spanning the range of frequencies tested. The linear portion of the viscosity versus percent strain response separates the domains of the linear and nonlinear viscoelastic material responses. The percent strain value indicating the transition provided the limit of strain in the dynamic testing procedure. Once again, some scatter is observed at the start up of the test at the low shear strain. Further limitations of the test, not present in any theory for linear viscoelasticity, are the capacity of the torque load cell being exceeded at higher shear strains and rates and the material being extruded from between the plates at large strains and frequencies.

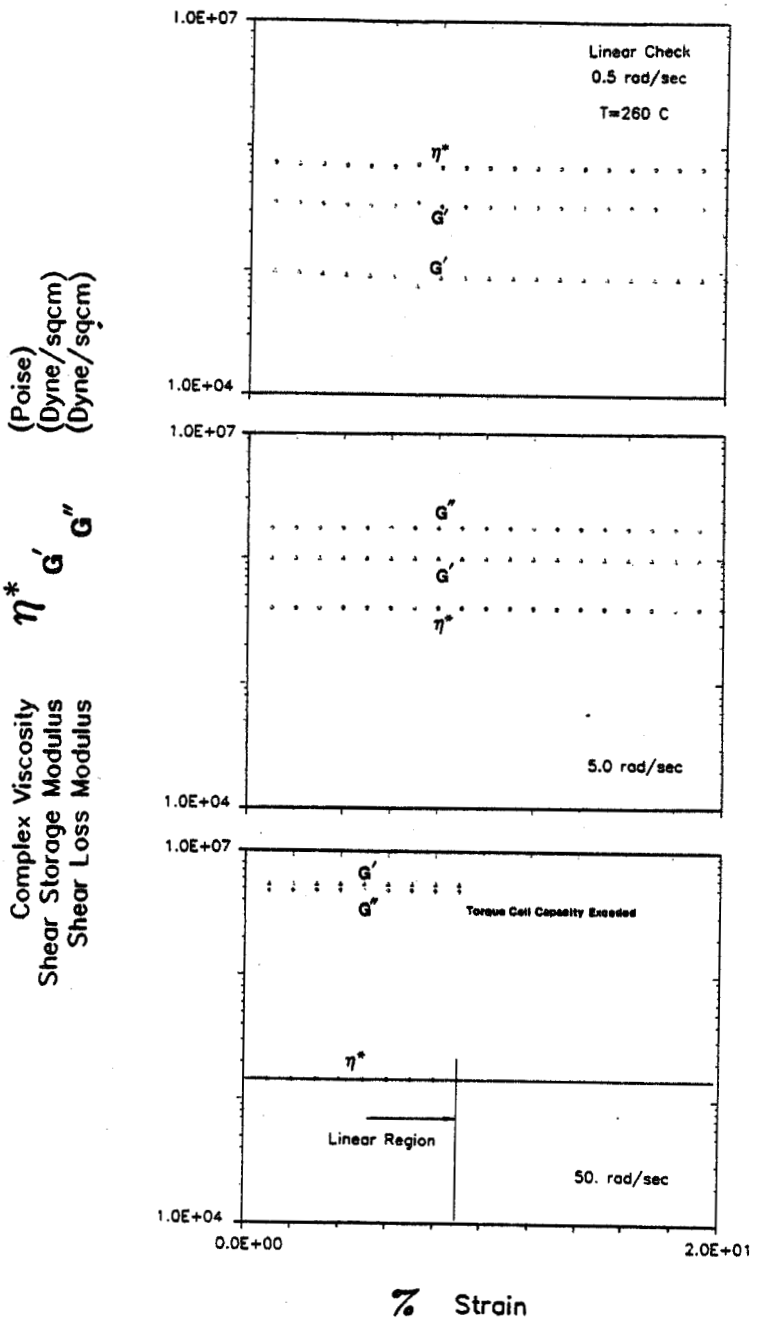

Figure A.4 Linear Check of Viscosity Data of UDEL® P1700 Resin at T = 260°C, Plots of η^*, G', and G'' versus Percent Strain at Frequencies 0.5 rad/sec (top graph), 5.0 rad/sec (center graph), 50.0 rad/sec (bottom graph)

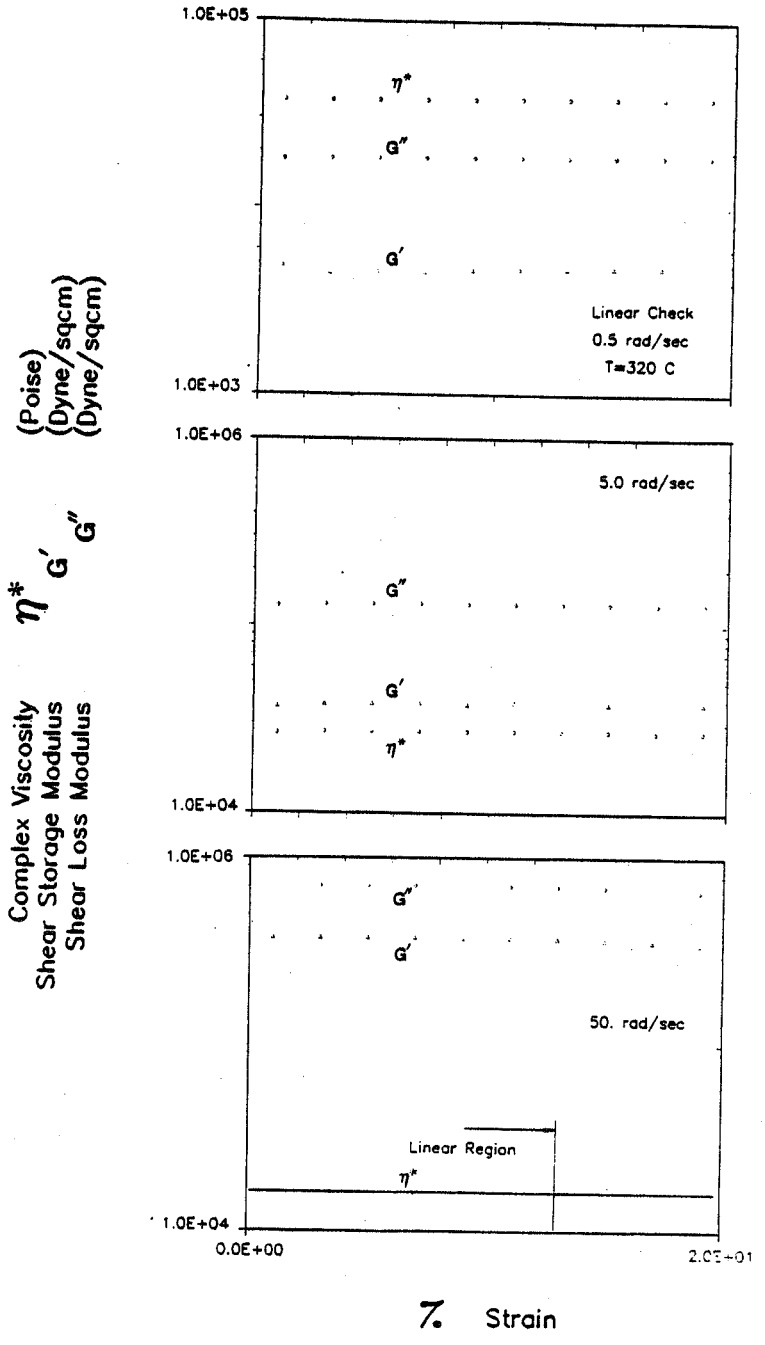

Figure A.5 Linear Check of Viscosity Data of UDEL® P1700 Resin at T = 320°C, Plots of η*, G′, and G″ versus Percent Strain at Frequencies 0.5 rad/sec (top graph), 5.0 rad/sec (center graph), 50.0 rad/sec (bottom graph)

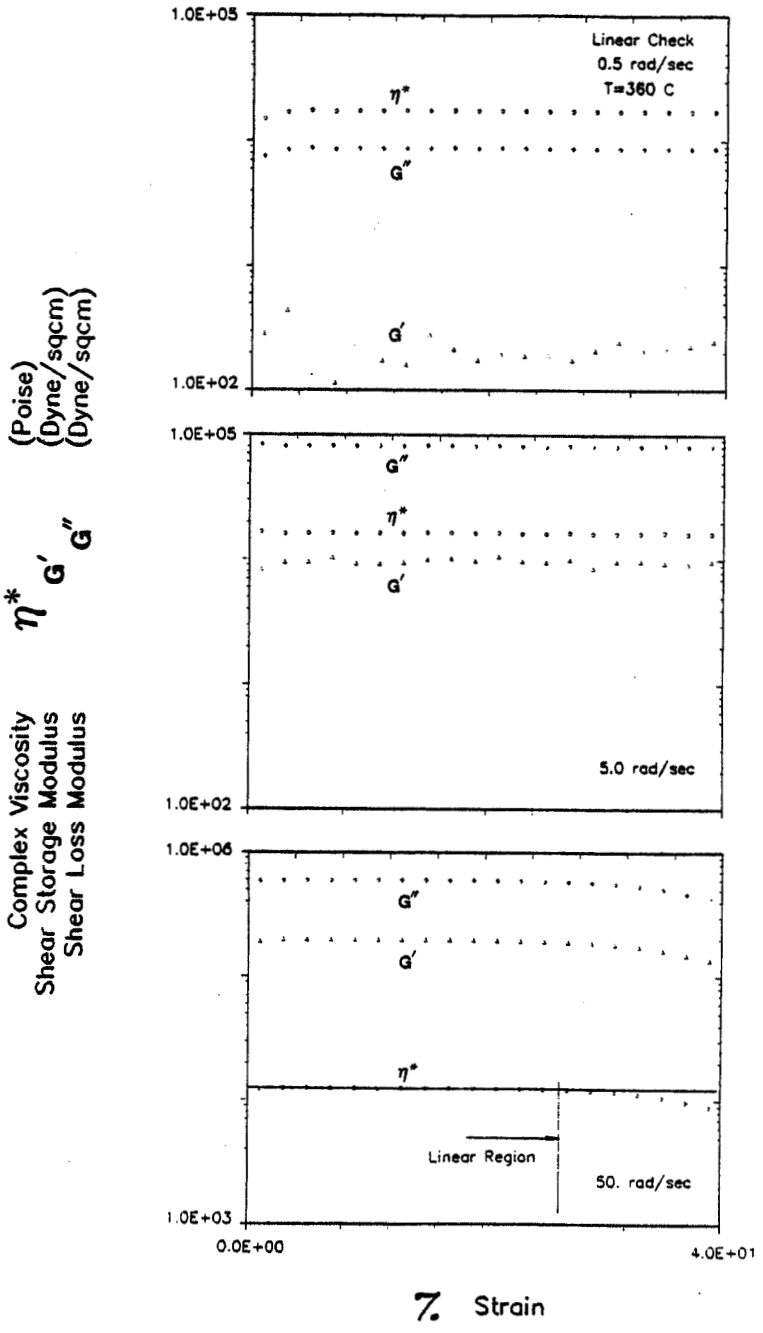

Figure A.6 Linear Check of Viscosity Data of UDEL® P1700 Resin at T = 360°C, Plots of η*, G', and G" versus Percent Strain at Frequencies 0.5 rad/sec (top graph), 5.0 rad/sec (center graph), 50.0 rad/sec (bottom graph)

A.4 Viscoelastic Theory

Presented here are the application of the Cox-Merz rule allowing the approximation of steady shear viscosity from the dynamic viscosity and the application of the WLF theory of time-temperature superposition to the dynamic viscosity data. In both instances the theory is well developed and will be used to evaluate its usefulness to the P1700 material response.

A.4.1 Cox Merz Rule

The empirical rule of Cox and Merz [20] has been used to approximate the steady shear viscosity from dynamic viscosity data in the absence of actual steady shear viscosity by the use of the complex viscosity. It has been observed experimentally that both the steady shear viscosity and dynamic viscosity converge to the same value as the shear rate and frequency respectively go to zero. However, at the high shear rates and frequencies it is found that the steady shear viscosity exceeds the value of that of the dynamic viscosity. This is expected since a greater degree of chain entanglements will be realized for continuous shear conditions in lieu of an oscillating one.

The Cox-Merz rule is shown as Eq A.4 where the relationship empirically predicts that the magnitude of the complex viscosity is equal to the steady shear viscosity at equal values of frequency and shear rate:

$$|\eta^*(\omega)| \equiv \sqrt{(\eta'(\omega))^2 + (\eta''(\omega))^2} = \eta(\dot{\gamma})\Big|_{\dot{\gamma}=\omega} \qquad (A.4)$$

where; η^* = Eq A.1c, the complex viscosity

η' = Eq A.1a, the dynamic viscosity

η'' = Eq A.1b, the out of phase component of η^*

This rule has been shown to be very useful in the accurate prediction of steady shear viscosity with dynamic viscosity data.

A.4.2 WLF Theory - Master Curve

Using the WLF theory of time-temperature superposition the shear rate dependent viscosity data at the higher temperatures can be used to simulate the shear rate dependent viscosity at another shear rate and lower temperature. To illustrate this, Fig. A.7 has been plotted with the original viscosity data shown in Fig. A.1 and the shifted viscosity data, to the reference temperature (T_{ref} = 220°) data. Remembering that the frequency is the reciprocal of time; the high temperature data at short times simulate the response of lower temperature and long time conditions. The magnitudes of the shifted data to the data at some reference temperature (T_{ref} = 220°C) has resulted in the following experimentally determined WLF constants for the WLF equation (Eq A.5):

$$\log \left(\frac{\eta}{\eta_{ref}}\right) = - \frac{C1(T - T_{ref})}{C2 + (T - T_{ref})} \qquad (A.5)$$

where; T = temperature in question

T_{ref} = 210°C

η = viscosity in question

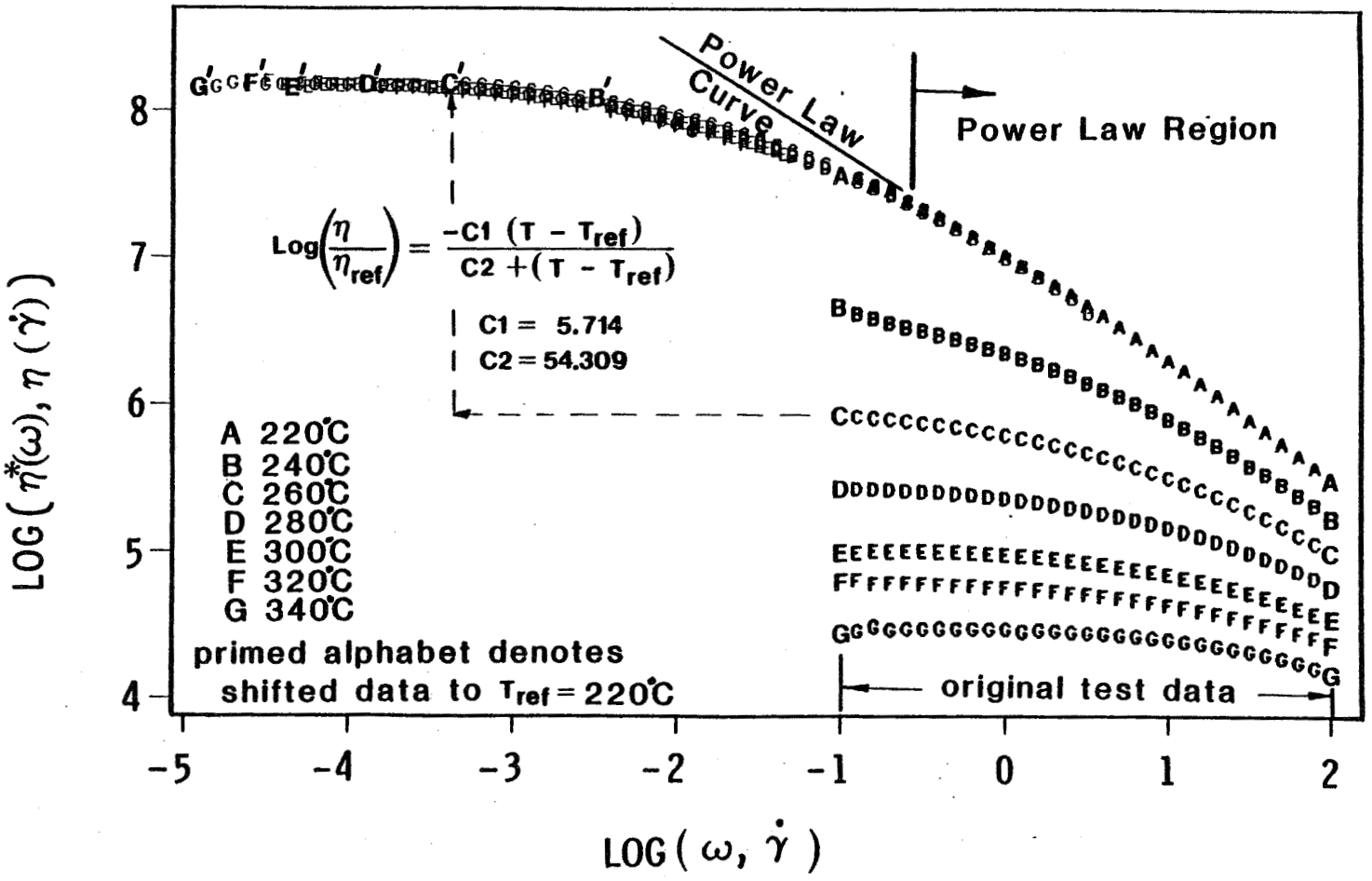

Figure A.7 Master Curve of Complex Viscosity Data Using WLF Time-Temperature Superposition at a Reference Temperature, T_{ref} = 220°C

η_{ref} = reference viscosity

C1 = 5.714 experimetally determined constant

C2 = 54.309 experimentally determined constant.

BIBLIOGRAPHIC DATA SHEET	1. Report No. CCMS-85-10	2. VPI-E-85-21	3. Recipient's Accession No.

4. Title and Subtitle

Thermoplastic Matrix Composite Processing Model

5. Report Date September, 1985

6.

7. Author(s)

Philip H. Dara and Alfred C. Loos

8. Performing Organization Rept. No. CCMS-85-10 VPI-E-85-21

9. Performing Organization Name and Address

Virginia Polytechnic Institute & State University
Engineering Science and Mechanics
Blacksburg, Virginia 24061

10. Project/Task/Work Unit No.

11. Contract/Grant No. NAG-1-343

12. Sponsoring Organization Name and Address

National Aeronautics and Space Administration
Langley Research Center
Hampton, Virginia 23665

13. Type of Report & Period Covered

14.

15. Supplementary Notes

16. Abstracts

The effects the processing parameters pressure, temperature, and time have on the quality of continuous graphite fiber (AS4) reinforced thermoplastic matrix (UDEL® P1700) composites have been quantitatively accessed by defining the extent to which intimate contact and bond formation has occurred at successive ply interfaces. Two models are presented predicting the extents to which the ply interfaces have achieved intimate contact and cohesive strength. The models are based on experimental observation of compression molded laminates and neat resin conditions, respectively. Identified as the mechanism explaining the phenomenon by which the plies bond to themselves is the theory of autohesion (or self diffusion). Theoretical predictions from the "Reptation Theory" between autohesive strength and contact time are used to explain the effects of the processing parameters on the observed experimental strengths. The application of a time-temperature relationship, in the WLF manner, for autohesive strength predictions is evaluated. A viscoelastic compression molding model of a tow was developed to explain the phenomenon by which the prepreg ply interfaces develop intimate contact. The intimate contact model contains submodels defining the degree of nonuniformity of tow heights across the width of a prepreg, viscoelastic mechanics model simulating the response of tows to a compressive load, and an empirical relationship of the influence of fibers on the neat resin viscosity.

17. Key Words and Document Analysis. 17a. Descriptors

17b. Identifiers/Open-Ended Terms

17c. COSATI Field/Group

18. Availability Statement	19. Security Class (This Report)	21. No. of Pages
Distribution Unlimited	UNCLASSIFIED	137
	20. Security Class (This Page) UNCLASSIFIED	22. Price

VIRGINIA TECH CENTER FOR COMPOSITE MATERIALS AND STRUCTURES

The Center for Composite Materials and Structures is a coordinating organization for research and educational activity at Virginia Tech. The Center was formed in 1982 to encourage and promote continued advances in composite materials and composite structures. Those advances will be made from the base of individual accomplishments of the thirty-four founding members who represent ten different departments in two colleges.

The Center functions by means of an Administrative Board which is elected yearly. The general purposes of the Center include:

- collection and dissemination of information about composites activities at Virginia Tech,
- contact point for other organizations and individuals,
- mechanism for collective educational and research pursuits,
- forum and mechanism for internal interactions at Virginia Tech.

The Center for Composite Materials and Structures is supported by a vigorous program of activity at Virginia Tech that has developed since 1963. Research expenditures for investigations of composite materials and structures total well over five million dollars with yearly expenditures presently approaching two million dollars.

Research is conducted in a wide variety of areas including design and analysis of composite materials and composite structures, chemistry of materials and surfaces, characterization of material properties, development of new material systems, and relations between damage and response of composites. Extensive laboratories are available for mechanical testing, nondestructive testing and evaluation, stress analysis, polymer synthesis and characterization, material surface characterization, component fabrication and other specialties.

Educational activities include eight formal courses offered at the undergraduate and graduate levels dealing with the physics, chemistry, mechanics, and design of composite materials and structures. As of 1982, some 33 Doctoral and 37 Master's students have completed graduate programs and several hundred Bachelor-level students have been trained in various aspects of composite materials and structures. A significant number of graduates are now active in industry and government.

Various Center faculty are internationally recognized for their leadership in composite materials and composite structures through books, lectures, workshops, professional society activities, and research papers.

FOUNDING MEMBERS OF THE CENTER

Aerospace and Ocean Engineering
Raphael T. Haftka
William L. Hallauer, Jr.
Eric R. Johnson

Chemical Engineering
Donald G. Baird

Chemistry
James E. McGrath
Thomas C. Ward
James P. Wightman

Civil Engineering
Raymond H. Plaut

Electrical Engineering
Ioannis M. Besieris
Richard O. Claus

Engineering Science and Mechanics
Hal F. Brinson
John C. Duke, Jr.
Daniel Frederick
Robert A. Heller
Edmund G. Henneke, II
Carl T. Herakovich
Michael W. Hyer
Robert M. Jones
Manohar P. Kamat
Alfred C. Loos
Don H. Morris
Daniel Post
J. N. Reddy
Kenneth L. Reifsnider
C. W. Smith
Wayne W. Stinchcomb

Industrial Engineering and Operations Research
Joel A. Nachlas

Materials Engineering
David W. Dwight
D. P. H. Hasselman
Charles R. Houska
M. R. Louthan, Jr.

Mathematics
Werner E. Kohler

Mechanical Engineering
Norman S. Eiss, Jr.
Charles E. Knight
S. W. Zewari

Inquiries should be directed to:

Center for Composite Materials & Structures
College of Engineering
Virginia Tech
Blacksburg, VA 24061
Phone: (703) 961-4969

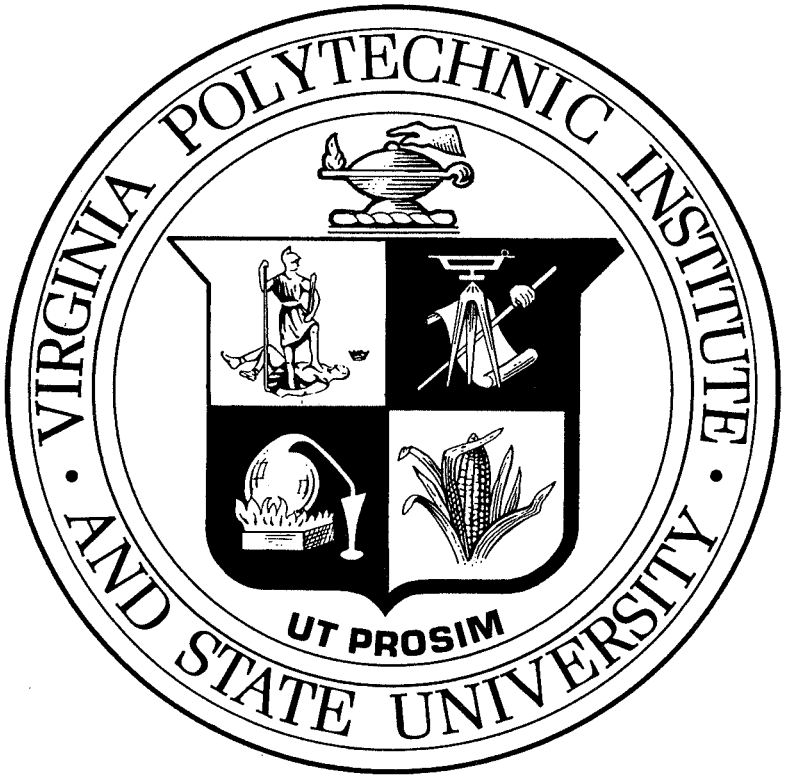
VIRGINIA POLYTECHNIC INSTITUTE
AND STATE UNIVERSITY
UT PROSIM